RNA involvement during non-homologous end joining of resected DNA double-strand breaks in G1

TECHNISCHE UNIVERSITÄT DARMSTADT

Vom Fachbereich Biologie
der Technischen Universität Darmstadt

zur Erlangung des Grades
Doctor rerum naturalism
(Dr. rer. nat.)

Dissertation
von M.Sc. Na Wei

Erstgutachter: Prof. Dr. Markus Löbrich

Zweitgutachter: Prof. Dr. Alexander Löwer

Darmstadt 2022

Na Wei: RNA involvement during non-homologous end joining of resected DNA double-strand breaks in G1
Darmstadt, Technische Universität Darmstadt
Jahr der Veröffentlichung der Dissertation auf TUprints: 2022
URN: urn:nbn:de:tuda-tuprints-215655
Tag der mündlichen Prüfung: 24.08.2022
Veröffentlicht unter CC BY-SA 4.0 International
https://creativecommons.org/licenses/

For my parents and friends,

my success would not be possible without their supports.

Ehrenwörtliche Erklärung

Ich erkläre hiermit ehrenwörtlich, dass ich die vorliegende Arbeit entsprechend den Regeln guter wissenschaftlicher Praxis selbstständig und ohne unzulässige Hilfe Dritter angefertigt habe.

Sämtliche aus fremden Quellen direkt oder indirekt übernommenen Gedanken sowie sämtliche von Anderen direkt oder indirekt übernommenen Daten, Techniken und Materialien sind als solche kenntlich gemacht. Die Arbeit wurde bisher bei keiner anderen Hochschule zu Prüfungszwecken eingereicht. Die eingereichte elektronische Version stimmt mit der schriftlichen Version überein.

Darmstadt, 17.06.2022

.....

Na Wei

Table of Contents

Abbreviations

4-OHT	4-hydroxytamoxifen
53BP1	P53 binding protein 1
Ab	Antibody
alt-NHEJ	Alternative non-homologous end-joining
APS	Ammonium persulfate
ATM	Ataxia telangiectasia mutated
ATR	Ataxia telangiectasia and Rad3-related protein
bFGF	Basic fibroblast growth factor
β-ME	Beta-mercaptoethanol
bp	Base pair
BrdU	5-bromo-2'-deoxymuridine
BSA	Bovine serum albumin
c-NHEJ	Classical non-homologous end-joining
Cas9	CRISPR associated protein 9
CDKs	Cycline-dependent kinases
Chk1	Checkpoint kinase 1
Chk2	Checkpoint kinase 2
CRISPR	clustered regularly interspaced short palindromic repeats
CtIP	C-terminal binding protein-interacting protein
DAPI	4', 6-diamidino-2-phenylindole
DDR	DNA damage response
DMEM	Dulbecco's Modified Eagle Medium
DMSO	Dimethyl sulfoxide
DNA	Deoxyribonucleic acid
DNA-PK	DNA-dependent protein kinase
DNA-PKcs	DNA-dependent protein kinase catalytic subunit
DRB	5,6-dichloro-1-b-D-ribofuranosyl benzemidazol
DSB	Double-strand break
dsDSB	Double stranded DSB
EDTA	Ethylene diamineter traacetic acid
EdU	5-ethynyl-2'-deoxyuridine
EGF	Epidermal growth factor
EXO1	Exonuclease1

EXD2	Exonuclease 3'-5' domain-containing protein 2
FA	Formaldehyde
FACS	Fluorescence activated cell scanning
FCS	Fetal calf serum
GAPDH	Glyceraldehyd-3-phosphat-hehydrogenase
GFP	Green fluorescent protein
Gy	Gray
h	hour
γH2AX	Phosphorylated histone 2AX
HR	Homologous recombination
HRP	Horseradish peroxidase
i	Inhibitor
IF	Immunofluorescence
IR	Ionizing radiation
IRIF	Irradiation induced foci
kDa	Kilo Dalton
kV	Kilo volt
LIF	Leukemia inhibitory factor
Lig I	Ligase I
Lig III	Ligase III
Lig IV	Ligase IV
mA	Milli ampere
mESC	Mouse embryonic stem cell
MiliQ water	Purified water
min	Minutes
Mre11	Meiotic recombination 11
MRN	Mre11-Rad50-Nbs1
Nbs1	Nijmegen breakage syndrome 1
NEAA	Non-essential amino acids
NHEJ	Non-homologous end-joining
nt	Nucleotide
OH	Hydroxyl
p	Phosphate
PAGE	Polyacrylamide gel electrophoresis
PAR	Poly (ADP-ribose)

PARP1	Poly (ADP-ribose) polymerase-1
PBS	Phosphate buffer saline
PI	Propidium iodide
PIKK	Phosphoinositide-3-kinase-related protein kinase
Plk3	Poli-like kinase 3
PVDF	Polyvinyldifluorid
Rad51	Radiation repair protein 51
R-loop	RNA loop
RNA	Ribonucleic acid
RNase A	Ribonuclease A
RNAPII	RNA polymerase II
RPA	Replication protein A
RPM	Rotation per minute
RT	Room temperature
SDS	Sodium dodecyl sulfate
siRNA	Small interfering RNA
SSB	Single-strand break
ssDNA	Single stranded DNA
TBS	Tris buffered saline
V	Volt
WB	Western blot
X-IR	X-ray irradiation
XLF	XRCC4-like factor
XRCC1	X-raycrosscomplementingprotein1
XRCC4	X-raycrosscomplementingprotein4

Figure list

Table list

1 Summary

DNA damage caused by physical or chemical mutagens threatens genomic integrity and the survival of living organisms. Particularly, DNA double-strand breaks (DSBs), the most hazardous lesions, arise when both DNA strands in the double helix are broken simultaneously, thus enhancing the risk of genome rearrangements. To revert the damaged genetic information and minimize the impact of damages in the genome, two major DSB repair pathways exist: non-homologous end joining (NHEJ) and homologous recombination (HR). In NHEJ, the two DSB ends are directly rejoined by DNA ligase IV complex and guided by short homologous DNA sequences in single-stranded overhangs at DSB ends. NHEJ accurately repairs DSBs only when these overhangs are perfectly matched, otherwise it can possibly lead to small insertions/deletions and translocations. Conversely, HR, only occurring during S/G2, utilizes the homologous sister-chromatid as a template to recombine the resected strands, thereby avoiding the loss of any information at DSBs.

In fact, DSB repair kinetics consist of two components: the fast repair process which resolves most of the breaks within a few hours upon DSB induction, and the slow repair process that repairs the rest of breaks. Previous published work has characterized that the fast repair process in G1 and G2 both relies on resection-independent NHEJ, whereas the slow repair process represents resection-dependent NHEJ in G1 and HR in G2. However, why resection is required for the slow DSB repair in G1 remains unillustrated. Indeed, emerging evidence highlights that persistent DSBs in G1, when HR is unavailable, preferentially cluster at actively transcribed genes during the delayed repair. Besides, recent studies propose that transcription repression caused by DSB damage can be resumed at later times in actively transcribed regions. Therefore, it can be speculated that a correlation between transcription and resection may exist in the slow repair component in G1, thus being the main focus of this work.

For this purpose, mouse embryonic stem cells (mESCs) were used, as they were found to be an interesting system to study resection. In fact, consistent with previous work, the co-immunostaining analysis of pRPA and γH2AX foci showed that resection also occurs in G1-mESCs at some X-ray irradiation (X-IR) and restriction enzyme-induced DSBs. Meanwhile, the reduction of pRPA foci formation when resection is inhibited by the PLK inhibitor (PLKi) and siCtIP, further confirms that a distinctive resection process arises in G1-mESCs, unlike the resection step in HR. Besides, inhibition of resection causes a repair defect, indicating that resection-dependent NHEJ is required for the repair of some DSBs in G1-mESCs.

In addition, transcription inhibition reduces pRPA foci as well as DNA-RNA hybrid formation, and causes a repair defect in G1. However, the reduction of pRPA foci formation and the repair defect

were both rescued when transcription was only inhibited before X-IR and resumed after X-IR. Taken together, these results suggest that transcription promotes DSB resection and is probably required for the slow DSB repair in G1.

To investigate how resection affects transcription during DSB repair in G1, different EU pulse labeling methods were used to distinguish pre-existing RNA before DSB induction or damage-induced RNA. The results showed that resection inhibition diminishes the accumulation of damage-induced RNA but does not affect the pre-existing RNA, suggesting that resection may contribute to the resuming of transcription post DSB induction. Furthermore, DNA-RNA hybrid formation at DSBs was also observed in a resection-dependent manner. Finally, chromatin immunoprecipitation-quantitative polymerase chain reaction (ChIP-qPCR) analysis suggests that DSBs which undergo resection in G1 are located in intragenic regions and that resection is required for the repair of those DSBs.

Recent studies have also involved RAD52 in RNA-mediated DSB repair and showed that it was recruited to transcriptionally active damage sites during G0/G1 phase. Accordingly, we also observed that RAD52 is required for DNA-RNA hybrid formation at DSB sites. Strikingly, both immunofluorescence and ChIP-qPCR analysis showed that RAD52 deficiency does not affect the level of resection and does not cause a defect in the repair of intragenic DSBs in G1. This indicates that RAD52 is dispensable for initiating resection, but is likely to be a downstream factor that regulates DNA-RNA hybrid formation at DSBs.

Collectively, these results suggest that resection-dependent NHEJ in G1 may preferentially arise in genes and be regulated by transcription. Moreover, RAD52 supports DNA-RNA hybrid formation at resected DSBs arising in genes which we hypothesize may enhance the repair fidelity.

Zusammenfassung

Durch physikalische oder chemische Mutagene verursachte DNA-Schäden bedrohen die genomische Integrität und das Überleben lebender Organismen. Insbesondere DNA-Doppelstrangbrüche (DSB), die gefährlichsten Läsionen, die entstehen, wenn beide DNA-Stränge in der Doppelhelix gleichzeitig gebrochen werden, erhöhen das Risiko von Genomumlagerungen. Um die geschädigte genetische Information zu reparieren und die Auswirkungen von Schäden im Genom zu minimieren, gibt es zwei wichtige DSB-Reparaturwege: die Nicht-homologe Endverknüpfung (NHEJ) und die Homologe Rekombination (HR). Beim NHEJ werden die beiden DSB-Enden durch den DNA-Ligase-IV-Komplex unter Zuhilfenahme kurzer homologer DNA-Sequenzen in einzelsträngigen Überhängen an den DSB-Enden direkt wieder zusammengefügt. Das NHEJ repariert DSBs nur dann korrekt, wenn diese Überhänge perfekt aufeinander abgestimmt sind, andernfalls kann es zu kleinen Insertionen/Deletionen und Translokationen kommen. Im Gegensatz dazu nutzt die HR, die nur während S/G2 stattfindet, das homologe Schwesterchromatid als Vorlage für die Rekombination der resektierten Stränge und vermeidet so den Verlust von genetischen Informationen an den DSBs.

Die Kinetik der DSB-Reparatur besteht aus zwei Komponenten: einem schnellen Reparaturprozess, der die meisten Brüche innerhalb weniger Stunden nach der DSB-Induktion beseitigt, und einem langsamen Reparaturprozess, der den Rest der Brüche repariert. Aus früheren Veröffentlichungen geht hervor, dass der schnelle Reparaturprozess in G1 und G2 auf dem resektionsunabhängigen NHEJ beruht, während der langsame Reparaturprozess einen resektionsabhängigen NHEJ-Weg in G1 und die HR in G2 darstellt. Warum die Resektion jedoch für die langsame DSB-Reparatur in G1 erforderlich ist, ist unklar. Es gibt Hinweise darauf, dass persistierende DSBs in G1, wenn keine HR zur Verfügung steht, vermehrt an aktiv transkribierten Genen auftreten. Außerdem legen neuere Studien nahe, dass eine durch DSBs verursachte Transkriptionsunterdrückung in aktiv transkribierten Regionen zu einem späteren Zeitpunkt wieder aufgenommen werden kann. Daher kann spekuliert werden, dass eine Korrelation zwischen Transkription und Resektion in der langsamen Reparaturkomponente in G1 bestehen könnte. Die Überprüfung dieser Theorie stellt den Schwerpunkt dieser Arbeit dar.

Zu diesem Zweck wurden embryonale Stammzellen der Maus (mESCs) verwendet, da sie sich als interessantes System zur Untersuchung der Resektion erwiesen haben. In Übereinstimmung mit früheren Arbeiten zeigten Kolokalisationsstudien von pRPA- und γH2AX-Foci, dass auch in G1-mESCs an einigen X-IR- und Restriktionsenzym-induzierten DSBs Resektion stattfindet. Die Beobachtung einer geringeren Zahl an pRPA-Foci, wenn die Resektion durch PLKi und siCtIP gehemmt wird, bestätigt, dass in G1-mESCs ein besonderer Resektionsprozess stattfindet, der sich von dem Resektionsschritt der HR unterscheidet. Außerdem führt eine Hemmung der Resektion zu

einem Reparaturdefekt, was darauf hindeutet, dass das Resektions-abhängige NHEJ für die Reparatur einiger DSBs in G1-mESCs erforderlich ist.

Darüber hinaus reduziert eine Transkriptionshemmung die Bildung von pRPA-Foci sowie von DNA-RNA-Hybriden und verursacht einen Reparaturdefekt in G1. Die Verringerung der Bildung von pRPA-Foci und der Reparaturdefekt traten jedoch nicht auf, wenn die Transkription nur vor X-IR gehemmt und nach X-IR wieder aufgenommen wurde. Zusammengenommen deuten diese Ergebnisse darauf hin, dass die Transkription die DSB-Resektion fördert und wahrscheinlich für die langsame DSB-Reparatur in G1 erforderlich ist.

Um zu untersuchen, wie sich die Resektion auf die Transkription während der DSB-Reparatur in G1 auswirkt, wurden verschiedene EU-Pulsmarkierungsmethoden verwendet, um zwischen der bereits vorhandenen RNA vor der DSB-Induktion und der durch die Schädigung induzierten RNA zu unterscheiden. Die Ergebnisse zeigten, dass die Hemmung der Resektion die Anhäufung der RNA verringert, welche erst nach der DSB-Induktion gebildet wird. Die zuvor bereits vorhandene RNA wurde von einer Hemmung der Resektion dagegen nicht beeinflusst. Dies deutet darauf hin, dass die Resektion zur Wiederaufnahme der Transkription nach der DSB-Induktion beitragen kann. Darüber hinaus wurde auch für die Bildung von DNA-RNA-Hybriden an DSBs eine Abhängigkeit von der Resektion beobachtet. Schließlich legen Analysen mittels Chromatin-Immunpräzipitation und quantitativer Polymerase-Kettenreaktion (ChIP-qPCR) nahe, dass DSBs, die in G1 resektiert werden, in Genen liegen und dass die Resektion für die Reparatur dieser DSBs erforderlich ist.

Jüngste Studien haben eine Rolle von RAD52 bei der RNA-vermittelten DSB-Reparatur postuliert und gezeigt, dass RAD52 während der G0/G1 Phase zu transkriptionell aktiven Schadensstellen rekrutiert wird. Konsistent hiermit konnte in dieser Arbeit beobachtet werden, dass RAD52 für die Bildung von DNA-RNA-Hybriden an DSB-Stellen erforderlich ist. Bemerkenswerterweise zeigten sowohl die Immunfluoreszenz- als auch die ChIP-qPCR-Analyse, dass ein RAD52-Mangel keine Auswirkungen auf das Ausmaß der Resektion hat und keinen Defekt bei der Reparatur von DSBs in Genen in G1 verursacht. Dies deutet darauf hin, dass RAD52 für die Einleitung der Resektion entbehrlich ist, aber wahrscheinlich ein nachgeschalteter Faktor ist, der die Bildung von DNA-RNA-Hybriden an DSBs reguliert.

Insgesamt deuten die Ergebnisse dieser Arbeit darauf hin, dass das von der Resektion abhängige NHEJ in G1 vorzugsweise in Genen auftritt und durch Transkription reguliert wird. Darüber hinaus unterstützt RAD52 die Bildung von DNA-RNA-Hybriden an resektierten DSBs, die in Genen entstehen, was – so unsere Hypothese – zu einer höheren Genauigkeit der Reparatur beitragen kann.

2 Introduction

2.1 DNA damage

2.1.1 Origins of DNA damage

DNA, the carrier of genetic information in all organisms, undergoes millions of damaging events per day which can trigger the generation of mutations and genomic instability. DNA, as an intrinsically reactive molecule, is vulnerable to chemical modifications caused by DNA damaging agents. DNA damage can be classified into two types: endogenous damage arising for example from metabolism and replication[1], and exogenous damage for example induced by ionizing radiation (IR), ultraviolet (UV) radiation, and chemotherapy[2].

IR is a form of high energy which is capable of detaching electrons from atoms or molecules of materials including living organisms, and cause breaks in chemical bonds[3]. The origins of IR include radioactive materials (such as uranium and radium in the earth) and radiation-generating machines, such as X-ray machines[4]. The dose of IR is measured in an international unit called Gray (Gy), which is equivalent to one Joule of energy absorbed per kilogram of a substance[5].

Gamma rays, X-rays, alpha particles, beta particles, neutrons and cosmic rays are considered major sources of IR. Among these, X-rays are commonly applied for medical diagnosis and radiotherapy, as they can penetrate into the body and are absorbed in different amounts depending on the radiological densities of various tissues. However, accumulating evidence also showed that high exposure to X-rays is related to the risk of developing cancer and dying, since X-rays can induce DNA strand breaks and mutations by generating free radicals within cells[6].

2.1.2 Impacts of DNA damage on the genomic context

It has been estimated that DNA damage may occur in the human body at the rate of 10,000 to 1,000,000 lesions per day, including base lesions, single-stranded beaks (SSBs) and double-stranded breaks (DSBs)[7]. With the accumulative disruption on the basic structure of DNA, various factors including chromatin conformation, sequence specificity, G-quadruplex secondary structures, strand-specific repair in genes, and transcription can affect the distribution of DNA damage (Fig. 2.1)[8]. Meanwhile, all these influences can result in mutations, microsatellite instability, altered methylation patterns and replication stress[8]. Importantly, DNA damage also interferes with the transcription machineries by impeding RNAPII progression and triggering transcription stress[9]. Moreover, DNA damage-induced transcription stress can generate mutant transcripts and perturb the integrity of the genome.

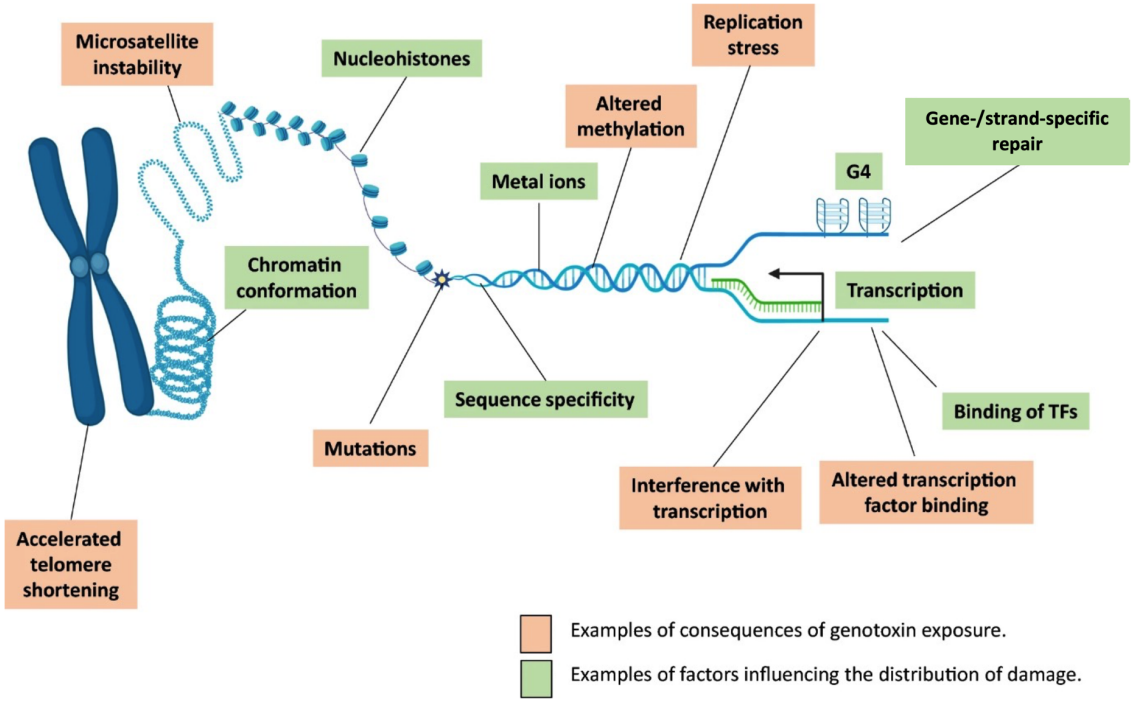

Figure 2.1 Examples of factors influencing the distribution of DNA damage and their potential impacts on the genomic context

The potential consequences of genotoxin exposure are shown in orange. The factors affecting the distribution of DNA damaged is shown in green (modified from Amente *et al*., 2021).

2.1.3 Global DNA damage response

To combat the threats caused by DNA damage and preserve genomic stability, a complex network of responses evolved in cells. These are called the DNA damage response (DDR) and include the activation of signaling pathways and cell cycle checkpoints, DNA repair mechanisms, and induction of cell death[10]. Upon the induction of DNA damage, members of the phosphatidylinositol 3-kinase-related kinases (PIKK) family, including DNA-dependent protein kinase catalytic subunit (DNA-PKcs), ataxia telangiectasia mutated (ATM) and ataxia telangiectasia and Rad3-related protein (ATR), facilitate the recognition of lesions, initiating a signaling cascade and regulating further downstream responses. DNA-PKcs can sense DSBs and engage the non-homologous end joining (NHEJ) machinery[11,12], which is required for the repair of most of DSBs in mammalian cells, except for those occurring at replication forks where homologous recombination (HR) is predominantly used (see further information of the usage of NHEJ versus HR in section 2.2). In addition, DNA-PK coordinates ATM and ATR to regulate the DNA damage checkpoints[13]. ATM mainly responds to DSBs and is recruited by the MRN complex so as to initiate cell cycle arrest and trigger DNA repair[14,15]. In contrast to ATM, ATR can be activated by replication protein A (RPA)-coated ssDNA, and plays crucial roles in response to replication stress[16].

2.2 DSB repair in G1 versus G2

DSBs are usually considered the most lethal DNA lesions since they can result in chromosome rearrangements and deletions. DSB repair is therefore essential to maintain genomic stability and is tightly regulated in a cell cycle-dependent manner. There are two main DSB repair pathways: NHEJ and HR. Owing no requirement of a sister chromatid, NHEJ, which directly ligates two broken ends, can occur throughout the cell cycle, but predominantly does so in G0/G1 and G2. Canonical NHEJ (c-NHEJ) refers to a specific NHEJ pathway which is mainly dependent on KU 70/80 heterodimer, DNA-PKcs, p53-binding protein 1 (53BP1), X-ray repair cross-complementing protein 4 (XRCC4), DNA ligase IV (DNA Lig IV) and XRCC4-like factor (XLF)[17]. Nevertheless, in contrast to NHEJ which occurs throughout all stages of cell cycle, HR only arises in late S and G2 and is considered to be error-free, since it demands a sister homologue as a template to retrieve the lost information[18–20]. In addition, another homology-independent repair which does not require these proteins but relies on DNA ligases I or III, XRCC1, PARP1 and DNA Polymerase θ is defined as backup NHEJ, microhomology-mediated end joining (MMEJ) or alternative NHEJ (alt-NHEJ)[21–23].

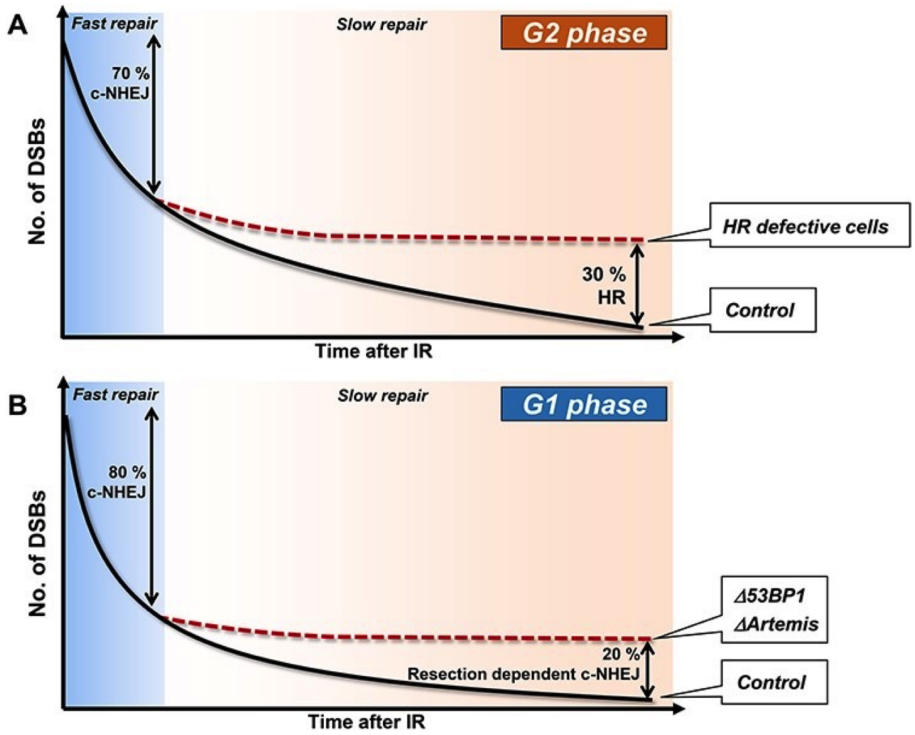

Figure 2.2 DSB repair kinetics and pathway usage after IR in G1 and G2

A. In G2, 70% of DSBs are repaired by the fast repair process of c-NHEJ, while 30% of DSBs are repaired by HR representing the slow repair component. **B.** In G1, 80% of IR-induced DSBs are repaired by cNHEJ in the fast repair process which is resection-independent, while the 20% of DSBs undergo repair *via* the slow repair component in a resection-dependent manner. Artemis and c-NHEJ proteins are required for the slow process and 53BP1 also affects the slow component kinetics (from Shibata and Jeggo 2020).

In respect of DSB repair pathway choices, several studies have revealed two-component kinetics of DSB repair, including the fast and the slow component (Fig. 2.2)[24,25]. Most of IR-induced DSBs in G1 and G2 undergo the fast repair process *via* c-NHEJ[24]. However, the remaining 20-30% of DSBs are repaired with slow repair kinetics *via* resection-dependent c-NHEJ in G1 and HR in G2[24,26].

2.2.1 Fast DSB repair process

The fast repair process utilizes resection-independent NHEJ to repair DSBs in both G1 and G2, and mainly comprises of three stages: recognition, DNA end processing and ligation (Fig. 2.3). In eukaryotes, the initial step of c-NHEJ is to recognize DSBs by the binding of Ku70/80 heterodimer which recruits and activates DNA-PKcs to form the DNA-PK complex. Then, DNA ends which are incompatible for ligation are trimmed by nucleases and resynthesized by DNA polymerases. Last, DNA-PK phosphorylates downstream factors, such as XRCC and DNA Lig IV[27,28], to promote the ligation of break ends. In the ligation step, the DNA Lig IV complex including DNA Ligase IV, XRCC4 and XLF, contributes to joining the DNA ends.

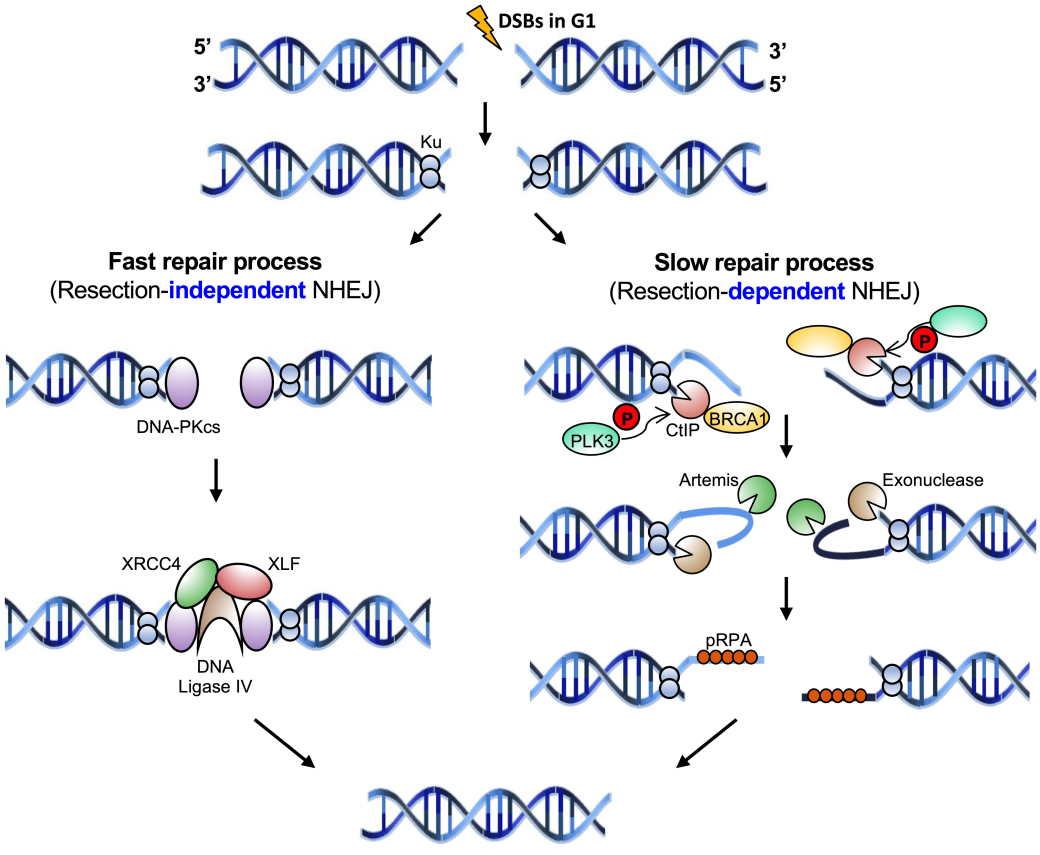

Figure 2.3 Model for the fast and slow DSB repair components in G1.

Left panel: Upon DSB induction in G1, the Ku70/80 heterodimer immediately detects DSB ends. During the fast repair process, DNA-PKcs is recruited after Ku binding. Following DNA end-processing, DSBs are rejoined

by DNA Lig IV, XRCC4 and XLF. **Right panel:** During the slow repair process, resection after DSB induction is initiated by PLK3 which phosphorylates CtIP, mediating the CtIP-BRCA1 interaction. Then, exonucleases execute the resection and Artemis completes the process, allowing the loading of pRPA onto the resected breaks. The repair process is then completed using the c-NHEJ machinery including DNA Lig IV, XRCC4 and XLF.

2.2.2 Slow DSB repair process

Following the fast NHEJ repair, the remaining unrepaired DSBs undergo repair by the slow component involving DNA-end resection (Fig. 2.3). The notion of resection-dependent NHEJ pathway in G1 which requires the Artemis nuclease was consolidated under three different approaches (Fig. 2.4)[29]. First, an indirect approach was taken to evaluate the repair defect levels through quantification of γH2AX foci number after X-ray IR (X-IR)-induced DNA damage. The result showed a repair defect after depletion of Artemis, confirming the utilization of resection-dependent c-NHEJ in G1. However, depletion of upstream resection factors such as CtIP and PLK3 does not cause such repair defect in HeLa and human fibroblasts. In fact, depletion of CtIP or PLK3 rescues the repair defect in Artemis-deficient cells after X-IR, suggesting that cells can switch between resection-dependent and independent repair processes. Moreover, resection in G1 was also monitored directly by detecting pRPA foci after α-particle irradiation[30]. The results indicate that the initial step of resection in G1 involves CtIP, BRCA1, Exonuclease 1 (EXO1), exonuclease 3'-5' domain-containing protein 2 (EXD2) and Mre11 exonuclease[31]. Finally, an assay developed by the Lopez's laboratory was applied to evaluate the rejoining of DSBs involving deletions and microhomology usage[32,33]. Moreover, repair events causing deletions or using microhomologies are observed after irradiation. Using this method, reduced rejoining events were observed in Artemis-deficient cells or in cells after inhibition of resection factors (CtIP and PLK3). These findings also unveil that CtIP and Artemis are required for resection in G1[31].

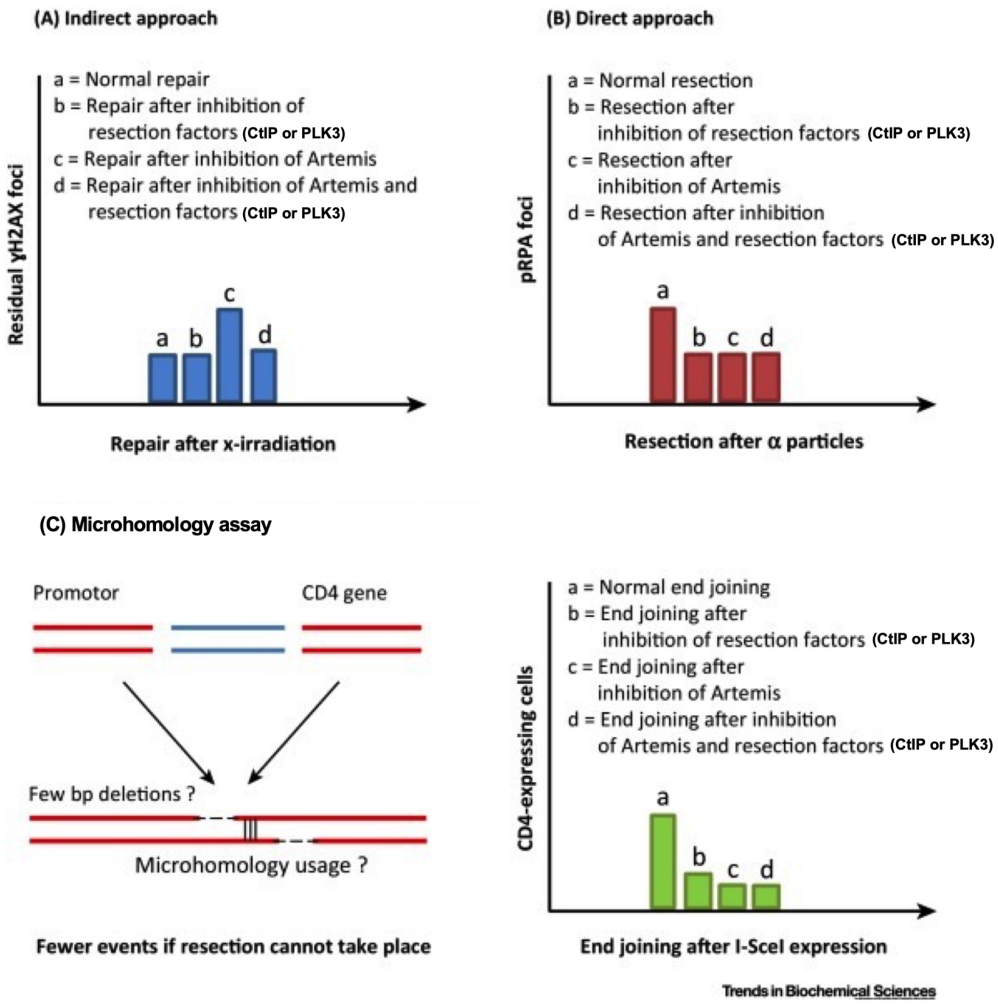

Figure 2.4 Approaches to monitor resection-dependent c-NHEJ

A. An indirect approach evaluates the rescue of the Artemis repair defect after X-IR-induced DNA damage. Absence or inhibition of upstream resection factors alleviates this repair defect. **B.** A direct approach assesses resection levels by numerating pRPA foci after α-particle irradiation. Inhibition of resection reduces pRPA foci numbers. **C.** Microhomology assay involving an integrated construct is used to monitor the rejoining of two closed I-SceI DSBs. The promoter and the CD4 gene in this construct are separated by an intervening sequence which can prevent transcription of CD4[32]. Rejoining involving junctional deletions and short microhomologies can lead to loss of the intervening fragment to generate CD4-expressing cells (modified from Löbrich and Jeggo, 2017).

However, the slow repair process in NHEJ is distinct from that in HR (Fig. 2.5)[31]. First, resection in G1 during NHEJ is much shorter than that in G2 during HR since Ku may remain in the DSB vicinity by inward translocation to restrict the exonuclease activity[34–36]. Ku as a resection barrier has been reported to strongly colocalize with pRPA in G1, but not with RAD51 in G2[31]. Meanwhile, another recent study observed the loss of Ku from long resected DSBs in G2[37]. Following Ku binding to DSB ends, resection in G1 is initiated by PLK3 which phosphorylates CtIP at Ser327 to promote the CtIP-

BRCA1 interaction[30]. On the other hand, resection in G2 is regulated by the phosphorylation of CtIP by cyclin-dependent kinases (CDKs) and ATM[38]. In addition, different nuclease activities of Mre11 are needed for each process. While Mre11 exonuclease activity is required for executing resection in G1, it is the Mre11 endonuclease which is essential for resection in G2[39]. Last, during the resection step in G2, the large region of ssDNA restrains the re-binding of DNA-PK to DSBs after the removal of DNA-PK[40]. In contrast, DNA-PK binding to DSBs is maintained during G1-resection which also likely lead to limited resection in G1[31,40].

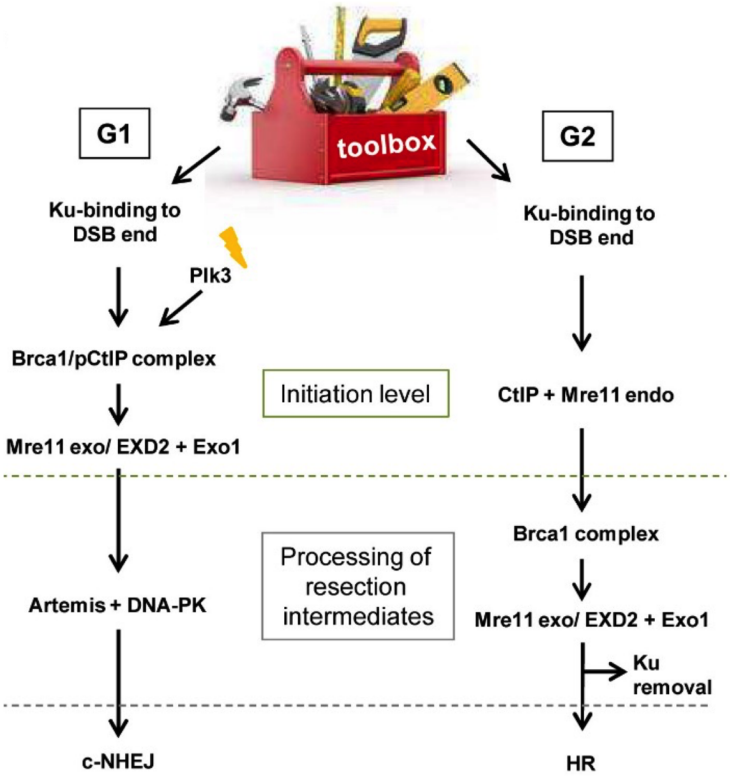

Figure 2.5 Model comparing the resection step between the slow repair components in G1 (c-NHEJ) and G2 (HR)

The scheme characterizes distinctive investigated factors involved in resection-dependent repair process in G1 and G2 (from Biehs *et al*., 2017).

2.2.3 DSB repair at active genes

Apart from the tight regulation of DSB repair choice during the cell cycle, emerging evidence supports the notion that the balance between DSB repair pathways is also modulated by chromatin which encodes for epigenetic information[41–45]. DSB repair at active genes is a pivotal process to maintain genomic stability. Over the past decade, a fair number of tools have been developed to decipher how the chromatin landscape at damaged locus influences DSB repair pathway choice across the genome. These include site-specific enzyme-induced DSB systems, such as AsiSI, I-PpoI, CRISPR/Cas9 and

zinc finger proteins (ZFN)[46].

The Legube's lab developed the AID-AsiSI-ER-U20S (AID-DIvA) cell system, which enables AsiSI expression under the control of auxin in U2OS cells, an inducible system that allows the generation of sequence-specific DSBs at annotated positions in the genome[43,47,48]. Based on the genome-wide mapping of RAD51 and XRCC4 in this cell system, it was first shown that DSBs in actively transcribed genes are preferentially repaired in G2 by HR, while DSBs induced in intergenic or silent regions are likely repaired in a fast manner by NHEJ throughout the cell cycle[43]. In addition, another recent study demonstrates that Cas9-induced specific DNA breaks at centromeres, which are highly specialized genomic loci, recruit RAD51 in G1 to activate the HR pathway in order to preserve centromeric integrity[49]. Expectedly, in order to preserve genetic information intact, DSB repair at active genes is more prone to HR since it is a well-known error-free pathway.

Strikingly, in G1-AID-DIvA cells, the Legube's lab did not observe RAD51, but instead XRCC4 accumulation at DSBs in both transcriptional active and inactive loci[43]. In addition, their follow-up work also unveils that persistent DSBs cluster at active genes in G1, lacking the HR machinery, and display delayed repair[44]. Nevertheless, how DSBs are repaired at active genes in G1 is still not well characterized.

Given the existence of both fast and slow NHEJ repair pathways during DSB repair, we can speculate that these persistent DSBs which exhibit delayed repair at active genes in G1, may preferentially undergo the resection-dependent NHEJ when the HR machinery is unavailable. Besides, recent work from the Shibata's lab raises another possibility in which the efficient DSB repair at transcribed regions in G1 may be dependent on BRCA1, Pol θ, and Lig I/III[50].

2.3 RNA-driven DSB repair

These findings regarding DSB repair at active genes could be in line with the hypothesis that RNA and transcription could be involved in DSB repair. Arising evidence highlights that RNA may facilitate DNA repair to precisely transfer genetic information[51–56]. In the central dogma of molecular biology, the special transfer of genetic information from RNA to DNA is conceived exclusively during reverse transcription only occurring in retroviruses, retrotransposons and telomeres (Fig. 2.6)[57–60].

However, many current findings uncover that reverse transcription is not limited to these three scenarios, but potentially is used more widely[61–64]. The Storici's group has demonstrated that transcript RNA can serve as a template for DSB repair in the absence of RNase H[61]. In addition, the Hazra's lab has reported that nascent RNA can be utilized as a template to restore the missing genetic information during DSB repair at transcribed genes[65]. Moreover, their results also suggest that the involvement of

nascent RNA improves the repair fidelity in c-NHEJ[65]. Several reports also indicate that RNA can contribute to the recruitment of DNA repair factors by forming DNA-RNA hybrids, stimulating a special HR repair pathway associated with transcription[43,56,66–69].

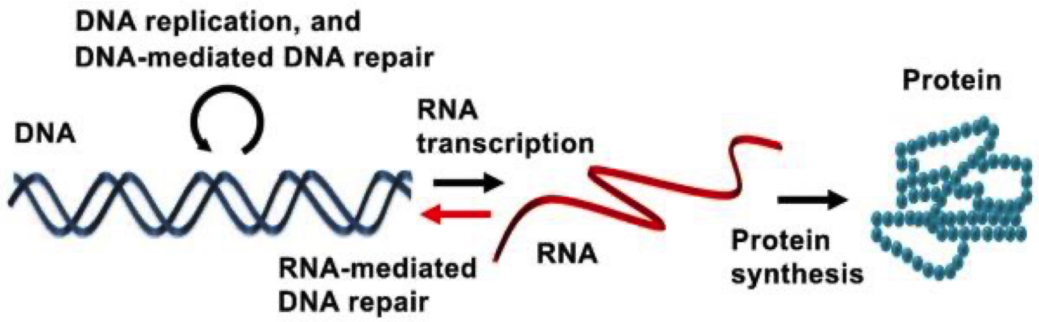

Figure 2.6 Re-interpretation of the central dogma of molecular biology

The central dogma of molecular biology explains the flow of genetic information transferring. DNA is labeled in dark blue, RNA in red and proteins in light blue. The usual transfer of sequential information is shown in black arrows, indicating DNA replication is followed by the transfer of information from DNA to RNA during transcription. Proteins can be synthesized using RNA as a template during translation. The red arrow indicates the special transfer of information from RNA to DNA which may mediate DNA repair (from Meers *et al*., 2016).

2.3.1 R-loop: a double-edge sword

In general, an R-loop is formed when a nascent RNA anneals with a template single-stranded DNA (ssDNA). As a consequence, an R-loop is characterized as a three-stranded nucleic acid structure consisting of an DNA-RNA hybrid and a displaced ssDNA during transcription (Fig. 2.7)[70]. Genome-wide mapping analyses show that R-loops mostly accumulate near transcriptionally active genes, especially in promoter regions[71,72]. Notably, accumulating evidence over decades suggests that R-loops play contradictory roles: threatening and also preserving genome stability (Fig. 2.8)[71–74]. The mechanisms to regulate R-loops and balance their detrimental and beneficial functions still need to be clarified.

Unscheduled R-loop formation can cause DNA damage and threaten genomic stability in multiple aspects[74–76]. The stretch of exposed ssDNA in the R-loop structure is more chemically vulnerable, since it can be cleaved by various endonucleases generating DNA breaks and/or mutations during transcription, unlike the transcribed DNA strand which is hybridized with RNA[77,78]. Moreover, exposed ssDNA can adopt G-quadruplexes and hairpin structures which are prone to cause breaks and impede DNA replication[79,80]. Besides, several findings indicate that persistent R-loop accumulation can stall both transcription and replication leading to head-on collisions between the replisome and RNA polymerases as a source of epigenetic instability[81–83].

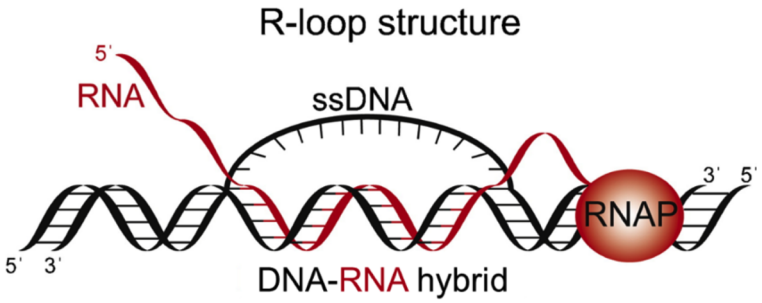

Figure 2.7 General structure of an R-loop.

The R-loop structure consists of a DNA-RNA hybrid and ssDNA. The DNA-RNA hybrids consist of nascent RNA (in red) which is synthesized by RNA polymerases as well as the complementary DNA template strand (in black). The non-templated DNA is ssDNA (modified from Hamperl and Cimprich, 2014).

Paradoxically, ever-growing evidence indicates that R-loops are recognized as beneficial structures which can actively contribute in physiological processes, including regulation of gene expression and transcription, alteration of epigenetic marks and DNA repair[74,80,84,85]. Several studies propose that the regulatory formation of R-loops in promoter regions enables gene expression through blocking DNA methylation, since the binding of DNA methyltransferases to DNA-RNA hybrids is much weaker than to dsDNA[71,86,87]. Additionally, some studies suggest that R-loops may promote efficient transcription termination due to the pausing of RNA polymerase and cleavage of RNA transcripts by DNA-RNA helicases such as senataxin and DHX9[88–90].

Remarkably, recent investigations suggest that DNA-RNA hybrids around DSBs can support controlled DNA repair. The di Fagagna's lab has reported that BRCA2 regulates the resolution of DNA-RNA hybrids at DSBs by interacting with RNase H2, thereby promoting HR-mediated repair[56]. Similarly, another study from the Bushell's group has also shown that DNA-RNA hybrids accumulate at DSBs in a Drosha-dependent manner contributing to DNA repair[69].

Moreover, several studies propose a relationship between DNA-RNA hybrids and resection during DSB repair, although they seem to be conflicting. The results in yeasts show that ssDNA overhangs generated by resection can promote the recruitment of RNA polymerase and the formation of DNA-RNA hybrids, but stabilization of such hybrids prevents excessive resection at DSBs[91]. Intriguingly, the Bushell's lab has discovered that absence of DNA-RNA hybrids by RNase H1 overexpression impairs end resection and thus DNA repair in human cells[69]. Altogether, these controversial findings indicate that R-loops may have dual roles in the regulation of resection during DSB repair.

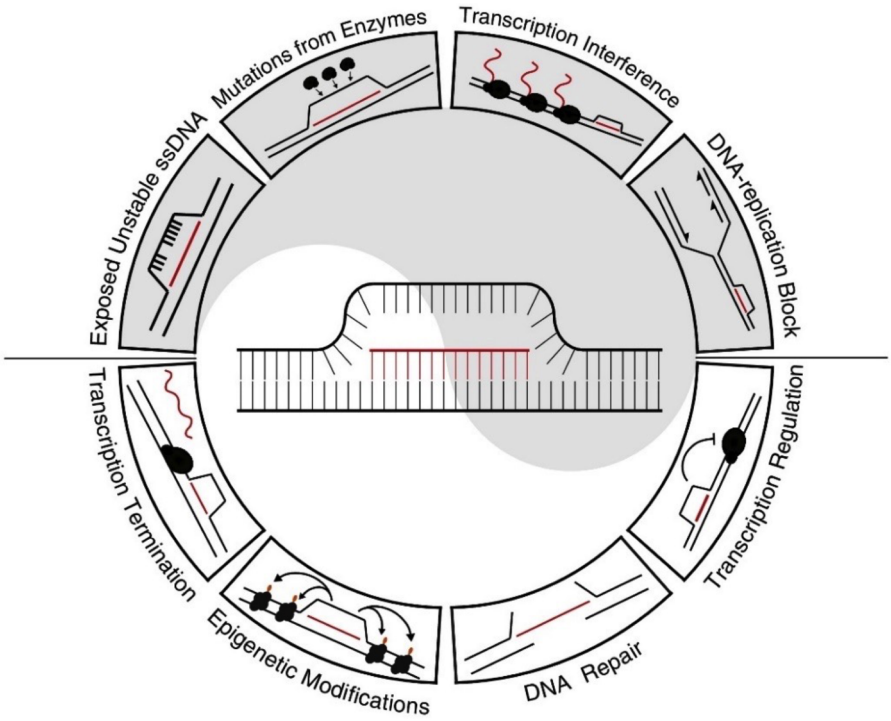

Figure 2.8 The Yin and Yang of R-loop functions.

R-loops can generate genomic threats: exposure of unstable ssDNA, mutations from enzymes to modify ssDNA and interference of transcription and replication. On a positive side, R-loops can facilitate transcription termination, modulation of gene expression and chromosome compaction, DNA repair and regulation of transcription at specific genes (from Costantino and Koshland, 2015).

Last, another role of R-loops has been highlighted in transcription-associated homologous recombination repair (TA-HRR) in a publication from Yasuhara and colleagues [67,92]. They unveil that both the formation and resolution of DNA-RNA hybrids are required for initiating TA-HRR which is crucial to protect the actively transcribed genome *via* real-time tracing techniques[67]. Meanwhile, their chromosome analyses have shown that the deficiency of TA-HRR can trigger an increase in interchromatin fusions which may be caused by irregular NHEJ repair in transcriptionally active sites, leading to genomic aberrations[67].

2.3.2 Transcription in response to DSB repair at active genes

Due to the tight correlation between R-loops and transcription, the transcription machinery and chromatin landscape are considered as some of the critical components for facilitating DSB repair at active genes. Furthermore, the Legube's lab has demonstrated that transcription-associated histone modifications may contribute to the HR pathway[43]. Their findings show that depleting SETD2 which

is the main H3K36 trimethyltransferease can reduce RAD51 recruitment and impairs HR in actively transcribed genes[43]. In addition, deficiency of LEDGF which recognizes H3K36 can reduce the recruitment of CtIP, impeding the initiation of resection at DSBs[43,93,94]. However, how this histone modification associated with active transcription fosters the regulation of DSB repair still needs to be investigated.

On the other hand, transcription repression following enzyme-induced DSB induction is also observed at active genes[95–101]. The occurrence of global transcription silencing in response to DSB induction is proposed to occur *via* the regulation of the RNAPII machinery, modification of chromatin and DNA methylation[100–103]. Recent studies show that transcription initiation and/or elongation by RNAPII after DSB damage is directly inhibited by TATA-box binding protein-like protein 1 (TLP), RECQL5 helicase or negative transcription elongation factor (NELF) complex (Fig. 2.9 A)[101,104–107]. Besides, transcription repression at DSBs is also tightly controlled by other DNA repair factors, including ATM, PARP1 and DNA-PK[99]. The ATM-involved transcription arrest around breaks is regulated by RNF168/RNF8/Ube2S/C which recruits other DNA repair factors (Fig. 2.9 B)[101,108–110]. Moreover, PARP1 promotes transcription repression and HR-directed repair by the recruitment of chromodomain Y-like protein (CDYL1) and other repressive chromatin modifiers (Fig. 2.9 C)[101,111–113]. Two further studies monitored the transcriptional arrest around DSBs with the aid of the I-PpoI system which induces site-specific breaks in the genome, and showed that it is dependent on DNA-PK which indirectly inhibits the activity of RNAPII (Fig. 2.9 D)[101,114,115].

In general, transcription repression around DSBs allows accurate coordination between DNA repair and transcription machineries. Chromatin compaction associated with transcription repression nearby DSBs may avoid detrimental translocation at active genes during DSB repair[103]. Notably, several laboratories showed that switching off transcription following DNA damage is closely correlated with the execution of DSB repair at actively transcribed loci, indicating transcription repression may promote the accessibility of DNA repair factors to damaged sites during early DSB repair[95,116,117]. Moreover, a number of evidence supports that paused RNAPII around DSBs is tightly linked to increased levels of R-loop formation and de novo transcription at 3' of resected DSB ends, which may facilitate DNA repair[55,56,68,102,118–121]. Of interest, following transcription repression upon DSB induction, emerging findings disclose that paused transcription can be restarted at DSBs within the gene body at actively transcribed regions, generating RNA transcripts which may participate DSB repair[97,122,123].

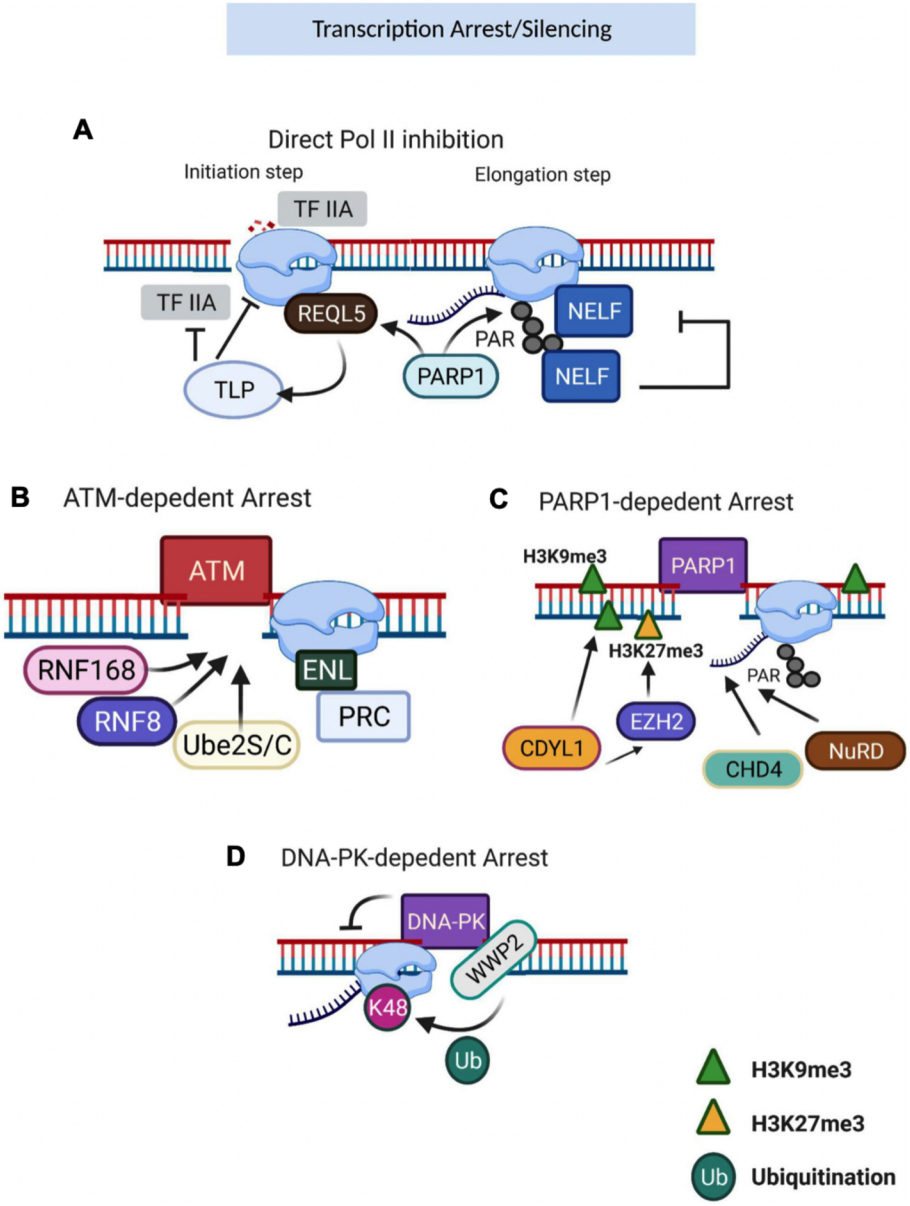

Figure 2.9 Mechanisms of transcription repression upon DSB induction.

A. RNAPII at DSBs is directly inhibited following DSB induction. In the transcription initiation step, REQL5 suppresses RNAPII activity and recruits TLP which can deactivate transcription factor IIA (TFIIA). PARP1 inhibits transcription elongation by recruitment of the NFLF complex, triggering RNAPII PARylation. **B.** ATM causes the pausing of actively transcribing RNAPII at DSBs by accumulation of RNF168/RNF8/Ube2S/C. **C.** The transcription activity at DSBs is silenced in a PARP1-dependent manner by recruiting CDYL1 which triggers the deposition of H3K9me3. CDYL1 also enhances transcription repression by promoting the presence of enhancer of zeste homolog 2 (EZH2). **D.** DNA-PK directly represses RNAPII activity at I-PpoI-induced DSBs (modified from Long *et al*., 2021).

2.3.3 Involvement of RAD52 in RNA-mediated DSB repair

In vitro studies show that RAD52 can bind DNA-RNA hybrids and single stranded RNA (ssRNA) in addition to dsDNA and ssDNA[61,124,125]; consequently, a role forRAD52 in DSB repair associated with transcription and RNAs has been proposed in recent investigations. Furthermore, two studies also shed light on the biochemical characterization of RAD52-promoted inverse strand exchange between dsDNA and ssRNA *in vitro*[124,125]. The Storici's group firstly proposed that Rad52 can promote RNA-templated DNA repair *via* the annealing of RNA to DNA at DSBs in yeast[61]. Then, the Lan's lab demonstrated that ROS-induced DNA damage during G0/G1 can trigger an RNA-templated HR pathway in a RAD52-dependent manner at actively transcribed sites in mammalian cells[126]. Later, they also observed a similar phenomenon in post-mitotic neurons[127,128]. In addition, the function of RAD52 in TA-HRR has been mentioned in Yasuhara *et al.*'s published work[67]. They suggest that RAD52 and XPG facilitate R-loop formation nearby DSBs in actively transcribed regions, resulting in accurate DSB repair and preservation of genomic integrity.

2.4 Aim of the study

Taken together, the above-mentioned studies provide insights into the regulation of DSB repair pathways, as well as the critical roles of R-loops and transcription during DSB repair, especially in actively transcribed gene regions. However, a great number of questions still need to be investigated regarding the exact mechanisms of DSB repair choice and the involvement of RNA in DNA repair. For example, in the absence of HR, it remains unclear whether resection-dependent c-NHEJ during the slow DSB repair component in G1 can potentially enhance deletions or translocations or improve repair fidelity. Recent work from Shibata's group implies that resection in the G1-slow DSB repair component may expose the vulnerable ssDNA regions in R-loops, leading to more deletions and chromosome translocations[50]. Conversely, given that transcription can be repressed upon early DSB induction and resumed at later times within actively transcribed sites, it can be speculated that the slow DSB repair component may utilize transcript-derived RNAs as templates to reduce the risk of deletions and mutations and enhance precise rejoining in G1. Moreover, the Legube's group also suggests that transcription probably facilitates the HR pathway by promoting DNA end resection[43]. Therefore, the aim of the presented work is to investigate the interactions between resection and transcription during the slow DSB repair in G1, and provide a better understanding on the involvement of RNA in resection-dependent NHEJ.

3 Materials and Methods

3.1 Materials

3.1.1 Cell line

mESCs: The J1 embryonic stem cells (ESCs), derived from a male agouti 129S4/SvJae embryo, were kindly provided by Prof. Dr. Leon Mullenders (Leiden university medical center, Netherlands).

3.1.2 Small molecule inhibitors

Table 3.1 Inhibitors.

Inhibitor	Concentration	Company
PLKi	1 μM	Tocris Bioscience
Triptolide	10 μM	Selleckchem
DRB	100 μM	Sigma-Aldrich

3.1.3 siRNA

Table 3.2 siRNA

siRNA	Sequence	Concentration (nM)	Company
Negative control	5'AATTCTCCGAACGTGTCACG3'	50	Qiagen
Artemis (mouse)	5'AAGGATCACATGAAAGGATTA3'	50	Qiagen
CtIP (mouse)	5'AAACAGATACTTACAAATAAA3'	50	Qiagen
BRCA1 SMARTpool (mouse)	5'GAGCAGCCCTTCACAAATA3' 5'GGAGGAAAGTGGATAGTTA3' 5'GTAGTAATCTCCAGAAAGA3' 5'GAATGCAGCTTACAAATGG3'	50	Dharmacon
RAD52 SMARTpool (mouse)	5'CCACATGACTCGAACATTA3' 5'TAAATAAGCTTCCACGACA3' 5'GGTCAGAAGGTGTGTGTTATA3' 5'AGTATACAGCGGATGAATA3'	50	Dharmacon

3.1.4 DNA vector

I-PpoI: pBABE-ddIPpoI is the vector for expression of the restriction enzyme under the control of shield-1, and purchased from AddGene.

AsiSI: pAID-AsiSI-ER is the vector for expression of the restriction enzyme with an auxin-inducible degron, and gifted from Gaelle Legube (Univsersité Paul Sabatier).

3.1.5 Transfection reagents

3.1.5.1 siRNA transfection reagents

Lipofectamine® RNAiMAX reagent	Invitrogen

3.1.5.2 DNA transfection reagent

Lipofectamine® 3000 with Plus reagent	Thermo Fisher

3.1.5.3 Serum free medium

Opti-MEM® medium	Thermo Fisher

3.1.6 Cell culture medium

Dulbecco's Modified Eagle's Medium (DMEM)	Sigma-Aldrich
Non-essential amino acids (NEAA)	Biochrom
LIF (mouse)	ProSpec
Cell culture guard	BD
Fetal calf serum (FCS)	Biochrom
Sodium pyruvate	Applichem
L-Glutamine	Sigma-Aldrich
β-mercaptoethanol	PanReac AppliChem

3.1.7 Kits

Click-iT™ EdU Imaging Kit	Baseklick
Genopure Plasmid Maxi Kit	Roche
ZR Plasmid Miniprep™-Classic	ZYMO RESEARCH
QIAquick® PCR Purification Kit	Qiagen
WesternBright™ Quantum	Advansta
Qubit™ dsDNA HS Assay Kit	Thermo Fisher
FastStart Universal SYBR Green Master (Rox)	Roche

3.1.8 Buffers and solutions

All pH analysis was measured by using HCl and NaOH.

3.1.8.1 Cell culture

PBS (pH 7.4)	137 mM NaCl
	2.7 mM KCl
	8 mM Na_2HPO_4
	1.5 mM KH_2PO_4
Trypsin/EDTA (pH 8.0 in PBS)	0.5 M EDTA
	2.5% (v/v) Trypsin

3.1.8.2 Western blot

Lysis buffer	20 mM Tris/HCl
	150 mM NaCl
	1% Triton X-100
	1x Complete
	1x PhosStop
RIPA buffer	50 mM Tris/HCl
	1% Triton X-100
	0.5% $C_{24}H_{39}NaO_4$
Electrophoresis buffer	25 mM Tris/HCl
	0.2 M Glycine
	0.5% (/w/v) SDS
5x Loading buffer (Laemmli)	60 nM Tris/HCl
	2% (w/v) SDS
	5% (v/v) ß-mercaptoethanol
	10% (v/v) Glycerin
	0.01% Bromophenol blue
Stacking gel buffer	0.5 M Tris/HCl
	1% SDS
Running gel buffer	1.5 M Tris/HCl
	1% SDS

3.1.8.3 Agarose gel electrophoresis

2% agarose gel

0.5×TBE buffer

3.1.8.4 Immunofluorescence

Cell fixation	2.5% Formaldehyde in PBS
Washing buffer	PBS
Permeabilization	0.2% TritonX-100 in PBS
Blocking buffer	10%Roti-Blocking
Primary/secondary antibody	10%Roti-Blocking
DAPI	0.4 µM/ml in PBS

3.1.8.5 Chromatin immunoprecipitation (ChIP)

1.25 M glycine (store at 4°C)

Stock Chemical Solutions (store at 4°C)**:**

0.5 M EDTA, pH 8 (14.612 g EDTA, to 100 mL with ddH2O)

1 M Tris, pH 7.5 (12.114 g Tris, to 100 mL with ddH2O)

4 M NaCl (23.376 g NaCl, to 100 mL with ddH2O)

1 M HEPES pH 7.9 (23.83 g HEPES, to 100 mL with ddH2O)

High Salt Lysis/Sonication Buffer (store at 4°C)

Reagent	Final Concentration	Amount in 50 ml
4 M NaCl	800 mM	10 ml
1 M Tris pH 7.5	25 mM	1.25 ml
0.5 M EDTA pH 8	5 mM	0.5 ml
Triton X-100	1% v/v	0.5 ml
SDS	0.1% w/v	0.05 g
Sodium deoxycholate	0.5% w/v	0.25 g
ddH_2O	n/a	To 100 ml
Protease inhibitor cocktail	1×	Add freshly
PhosSTOP™	1×	Add freshly

Chromatin Dilution Buffer (store at 4°C)

Reagent	Final Concentration	Amount in 50 ml
1 M Tris pH 7.5	25 mM	1.25 ml
0.5 M EDTA pH 8	5 mM	0.5 ml
Triton X-100	1% v/v	0.5 ml
SDS	0.1% w/v	0.05 g
ddH_2O	n/a	To 50 ml
Protease inhibitor cocktail	1×	Add freshly
PhosSTOP™	1×	Add freshly

Wash Buffer A (pH 7.9, store at 4°C)

Reagent	Final Concentration	Amount in 50 ml
4 M NaCl	140 mM	1.75 ml
1 M HEPES pH 7.9	50 mM	2.5 ml
0.5 M EDTA pH 8	1 mM	0.1 ml
Triton X-100	1% v/v	0.5 ml
SDS	0.1% w/v	0.05 g
Sodium deoxycholate	0.1% w/v	0.05 g
ddH_2O	n/a	To 50 ml

Wash Buffer B (pH 7.9, store at 4°C)

Reagent	Final Concentration	Amount in 50 ml
4 M NaCl	500 mM	6.25 ml
1 M HEPES pH 7.9	50 mM	2.5 ml
0.5 M EDTA pH 8	1 mM	0.1 ml
Triton X-100	1% v/v	0.5 ml
SDS	0.1% w/v	0.05 g
Sodium deoxycholate	0.1% w/v	0.05 g
ddH_2O	n/a	To 50 ml

Wash Buffer C (pH 8.0, store at 4°C)

Reagent	Final Concentration	Amount in 50 ml
1 M Tris pH 7.5	20 mM	1 ml
0.5 M EDTA pH 8	1 mM	0.1 ml
8 M LiCl	250 mM	1.625 ml
NP-40 Alternative	0.5% v/v	0.25 ml
SDS	0.5% w/v	0.25 g
ddH_2O	n/a	To 50 ml

TE Buffer (store at 4°C)

Reagent	Final Concentration	Amount in 50 ml
1 M Tris pH 7.5	10 mM	1 ml
0.5 M EDTA pH 8	1 mM	0.2 ml
ddH_2O	n/a	To 50 ml

Elution Buffer (store at room temperature)

Reagent	Final Concentration	Amount in 10 ml
1 M Tris pH 7.5	10 mM	0.1 ml
0.5 M EDTA pH 8	1 mM	0.02 ml
SDS	1% w/v	0.1 g
ddH_2O	n/a	To 100 ml

3.1.8.6 CytoSpin for mESCs

Cell fixation	2.5% Formaldehyde
Permeabilization	0.5% Triton X-100 in PBS

3.1.8.7 S9.6 staining

CSK buffer	10 mM PIPES
	100 mM NaCl
	300 mM sucrose
	3 mM $MgCl_2$
Pre-wash	0.5% Triton X-100 in CSK buffer

Cell fixation	Ice cold methanol
Blocking buffer	2% BSA, 0.5% FCS in PBS
RNaseA treatment	100 µg/ml RNase A
	5 mM EDTA, 300 mM NaCl and 10 Mm Tris-HCl, pH7.5
Hoechst	2 µg/µl

3.1.8.8 FACS

PI solution	0.1 mg/ml PI
	10 mg/ml RNaseA in PBS

3.1.8.9 Bacteria culture

Ampicillin	50 mg/ml in MiliQ water
LB Agar broth	10 g/l Tryptone
	2% Yeast extract
	5 g/l NaCl
LB Agar plates	1.5% agarose in LB broth

3.1.9 Antibodies

Table 3.3 Primary antibodies

Antibody	Species	Dilution	Company	Application
Anti-γH2AX (Ser139)	rabbit	1 µg/200 µg chromatin	Abcam	ChIP
Anti-γH2AX (Ser139)	mouse	1:1000	Millipore	IF
Anti-γH2AX (Ser139)	chicken	1:1000	Biozol	IF
Anti-53BP1	rabbit	1.1000	Bethyl	IF
Anti-pRPA32 (T21)	rabbit	1:10000	Abcam	IF
Anti-Artemis	mouse	1:1000	Bethyl	WB
Anti-CtIP	rabbit	1:1000	Santa Cruz	WB
Anti-pRPA32 (S4/S8)	rabbit	1 µg/7.5 µg chromatin	Bethyl	ChIP
Anti-RAD52	rabbit	1:1000	Sigma-Aldrich	WB
Anti-S9.6	mouse	1:500	Kerafast	IF
Anti-GAPDH	mouse	1:1000	Santa Cruz	WB
Anti-Vinculin	rabbit	1:1000	Santa Cruz	WB

Table 3.4 Secondary antibodies

Antibody	Dilution	Company	Application
Goat anti-rabbit Alexa Fluor 488	1:1000	Molecular Probes	IF
Goat anti-mouse Alexa Fluor 488	1:1000	Molecular Probes	IF
Goat anti-rabbit Alexa Fluor 594	1:1000	Molecular Probes	IF
Goat anti-mouse Alexa Fluor 594	1:1000	Molecular Probes	IF
Donkey anti-rabbit Dylight 550	1:1000	Invitrogen	IF
Goat anti-mouse IgG-HRP	1:10000	Santa Cruz	WB
Goat anti-rabbit IgG-HRP	1:10000	Santa Cruz	WB

3.1.10 PCR primers for ChIP-qPCR in mESC-I-PpoI cells

Target	Sequence	Vendor
Chr1_fwd for γH2AX	5'-CCTACAAAGCAGAGTGGCGA-3'	Eurofins
Chr1_rev for γH2AX	5'-AATCTGCCACCTGACACCTG-3'	Eurofins
Chr3_fwd for γH2AX	5'-ATGTGGCTAGTGGGGAACATC-3'	Eurofins
Chr3_rev for γH2AX	5'-AAAAGCCAAATGGGCAACTCC-3'	Eurofins
Chr4_fwd for γH2AX	5'-AATCTGCCACCTGACACCTG-3'	Eurofins
Chr4_rev for γH2AX	5'-AATCTGCCACCTGACACCTG-3'	Eurofins
Chr9_fwd for γH2AX	5'-CCTACAAAGCAGAGTGGCGA-3'	Eurofins
Chr9_rev for γH2AX	5'-AATCTGCCACCTGACACCTG-3'	Eurofins
Chr13_fwd for γH2AX	5'-ATGTGGCTAGTGGGGAACATC-3'	Eurofins
Chr13_rev for γH2AX	5'-AAAAGCCAAATGGGCAACTCC-3	Eurofins
Chr6_Hoxa9_fwd	5'-AAATCTGGCAAAGGGACCCAAAGC-3'	Eurofins
Chr6_Hoxa9_rev	5'-TTCACAAACTGTGGCAGCAACGTC-3'	Eurofins
Chr7_H19-ICR_fwd	5'-CGGACTCCCAAATCAACAAG-3'	Eurofins
Chr7_ H19-ICR_rev	5'-GCAATCCGTTTTAGGACTGC-3'	Eurofins
Chr1_fwd for pRPA	5'-GAGGTGCCCAGTACCACAAT-3'	Eurofins
Chr1_rev for pRPA	5'-GTGTTCTCTGGCCTGACGTT-3'	Eurofins
Chr3_fwd for pRPA	5'-CTTCAGGGTAATGGCAAATCACA-3'	Eurofins
Chr3_rev for pRPA	5'-GGGCACAAGTTAAATCGGAACT-3'	Eurofins
Chr4_fwd for pRPA	5'-GCATGTGATGGACTGACCAC-3'	Eurofins

Chr4_rev for pRPA	5'-TGGGCTGGTAACAGACATAACA-3'	Eurofins
Chr9_fwd for pRPA	5'-GAAACAGTCTATGGCAGGCGA-3'	Eurofins
Chr9_rev for pRPA	5'-TGCCAGACAGCCTCATAAAGT-3'	Eurofins
Chr13_fwd for pRPA	5'-TATCAGGGGTATGTCGCCCA-3'	Eurofins
Chr13_rev for pRPA	5'-GGCAGAATGGTCTATGAGGCA-3'	Eurofins

3.1.1 Protein standard

Page Ruler™ Plus Prestained Protein Ladder, 10-250 kDa	Thermo Scientific
ProSieve QuadColor Protein Marker, 4.6-300 kDa	Biozym

3.1.2 Laboratory consumables

Blotting paper, 703	VWR
Cell culture dishes (35x10 mm, 60x15mm)	NUNC™ VWR
Cell culture flask (20 cm², 75cm²)	TPP
Cover slips, 15x15mm	Carl Roth
Centrifuge tubes (15 ml, 50ml)	Greiner
FACS tubes	Beckman Coulter
Filter Cards, one-hole	Tharmac Cellspin
Filterpaper, Whatman	Schleicher & Schüll
Immersion oil	Zeiss
Kim Wipes	NeoLab
Kuvets, plastic	Carl Roth
Microtubes (Eppis)	Carl Roth
Microscope slides, superfront	Carl Roth
MicroAmp™ 96-well optical response plate	Applied Biosystems
MicroAmp™ optical adhesive film	Applied Biosystems
Parafilm	Bermis
Pasteur pipets, glass	Carl Roth
Pasteur pipets, plastic	Carl Roth
Pipettips	Sarstedt
Pipettips, filtered	Carl Roth
Polysine® Slides	Thermo Scientific
PVDF membrane	Carl Roth
Qubit™ assay tubes	Invitrogen

3.1.3 Chemicals

Agar	Carl Roth
APS	Carl Roth
Bromphenol blue	USB
BSA	AppliChem
BrdU (1mM)	BD Bioscience
Calcium chloride ($CaCl_2$)	Carl Roth
DAPI	Sigma-Aldrich
Disodium phosphate (Na_2HPO_4)	Carl Roth
DMSO	Sigma-Aldrich
Dynabeads™ Protein G	Invitrogen
Ethylenediaminetetraacetic acid (EDTA)	Carl Roth
5-Ethynyl-2′-deoxyuridine (EdU)	Carl Roth
5-Ethynyl-uridine (EU)	Carl Roth
Ethanol, denatured	Carl Roth
Formaldehyde (4%)	AppliChem
Formaldehyde (Pierce 16%, methanol-free)	Thermo Fisher
Glycerin	Carl Roth
Glycine	Carl Roth
HEPES	Sigma-Aldrich
Hydrochloric Acid (HCl)	Carl Roth
Isopropanol	Carl Roth
Lithium chloride (LiCl)	Carl Roth
Magnesium chloride ($MgCl_2$)	Carl Roth
Methanol	Carl Roth
Monopotassium phosphate (KH_2PO_4)	Carl Roth
Mounting medium	Vectashield® Axxora Alexis
Non-fat-dried-milk	Carl Roth
NP-40 Alternative	Millipore
PhosStop10X	Roche
PIPES	Carl Roth
Potassium chloride (KCl)	Carl Roth
Protease inhibitor 25xCompelete	Roche
Proteinase K	Carl Roth
RNase A powder	Sigma-Aldrich
RNase A (DNase and protease-free, 10 mg/ml)	Thermo Scientific

Roti®-Block	Carl Roth
Sodium dodecyl sulfate (SDS)	Carl Roth
Sodium chloride (NaCl)	Carl Roth
Sodium hydroxide (NaOH)	Carl Roth
Sodium deoxycholate	Sigma-Aldrich
Sucrose	Carl Roth
TEMED	Carl Roth
Tris base	Carl Roth
Triton X-100	Carl Roth
Trypsin	Carl Roth
Tween® 20	Carl Roth
β-mercaptoethanol	Sigma-Aldrich

3.1.4 Instruments

Equipment	Model	Company
Camera system (microscope)	Axio Cam MRm	Zeiss
Centrifuge	5451 R/5804 R	Eppendorf
Centrifuge	Biofugepico	Heraeus
Centrifuge	Cellspin I	THARMAC
Cell counting chamber	Neubauer improved	Marienfeld Superior
Cell sorter	S3	BIO-RAD
Chemiluminescence detection	Fusion FX	Viber Lourmat
DynaMag-2™ Magnet		Thermo Scientific
Electrophorese system	SE260	Hoefer
Flow box	Herasafe	Thermo Scientific
Flow cytometer	Cytomics FC 500	Beckman Coulter
Incubator	Hera cell 240	Thermo Scientific
Microscope	Imager Z2	Zeiss
Microscope (cell culture)	Eclipse TS100	Nikon
Microscope (Live cell)	AXIOVERT200M	Zeiss
Microscope (confocal)	TCS SP5 II	Leica
Nanophotometer	P-Class	Implen
pH meter	pMX2000	WTW

Power supply	PowerPac™ HC	BIO-RAD
Qubit™ 4 Fluorometer	-	Thermo Scientific
Scale	TE 1502S/TE 153S-DS	Sartorius
Shaker	3011	GFL
Real-Time PCR System	StepOnePlus™	Applied Biosystems
Thermomix	Comfort	Eppendorf
Ultrasonic cleaning device	Sonorex Super RK 31(H)	Bandelin
Ultrasonic processor	Sonopuls UM70/GM70HD	Bandelin
Vortex	Vortex genie2	Scientific Industries
Water bath	1083	GFL
Western blot system	Mini Trans-Blot® Cell	BIO-RAD
X-ray machine	X-RAD 320	PXi

3.1.5 Software

Flow cytometry	CXP	Beckmann Coulter
Gele reader	ChemiCapt	Viber Lourmat
Fluorescent microscopy	Metafer4	Metasystems
Fluorescent microscopy	LAS AF Lite	Leica
Image analysis	ImageJ	Open Source

3.2 Methods

3.2.1 Cell culture

mESCs were grown in DMEM supplemented with 15% fetal calf serum (FCS), 0.5% leukemia inhibitory factor (LIF), 1% cell culture guard, 1% glutamine, 1% non-essential amino acids, 1% sodium pyruvate and 0.5% ß-mercaptoethanol. In order to obtain fresh cells, the stock of cells with low passage number in the liquid nitrogen were thawed in a water bath at 37°C for 2-3 min, and resuspended in 10 ml of fresh medium. Then, cells were centrifuged down at 200 g for 3 min and seeded in a 25 or 75 cm^2-culture flask with 5 or 15 ml of medium. After 18-20 h-incubation at 37°C in a 5% CO_2 incubator, cells were changed with fresh medium. mESCs were passaged every two days.

For cell passaging, cells were washed once with sterile PBS and incubated with pre-warmed trypsin/EDTA for 2-3 min at 37°C for detachment. Then, cells were resuspended in 10 ml of medium and centrifuged down at 200 g for 3 min. After removal of supernatant, cell pellets were resuspended in 10 ml of medium and seeded in a new flask with a dilution of 1:7-1:10.

3.2.2 Cell cycle-specific DSB repair analysis

For analyzing DSB repair in a cell cycle-dependent manner, 10 µM of thymidine analog 5-ethynyl-2'-deoxyuridine (EdU) and 100 ng/ml of nocodazole were added to cells 30 min prior to DSB induction and maintained throughout the experiment. EdU incorporates into the newly synthesized DNA, thus labeling all S phase cells before and after DSB induction. Nocodazole can prevent G2 phase cells from progressing into G1 phase after induction of DSBs. After cell fixation and permeabilization, cells were stained with the click-it reaction cocktail for EdU labeling and DAPI for DNA staining. The intensities of EdU and DAPI were measured and plotted by a Zeiss microscope with MetaCyte software. EdU-positive cells represent as S phase cells, whereas EdU-negative cells include both G1 and G2 phase cells (Fig. 3.1). Among those EdU-negative cells, G1 and G2 phase cells were distinguished from each other depending on the DNA content stained by DAPI (Fig. 3.1).

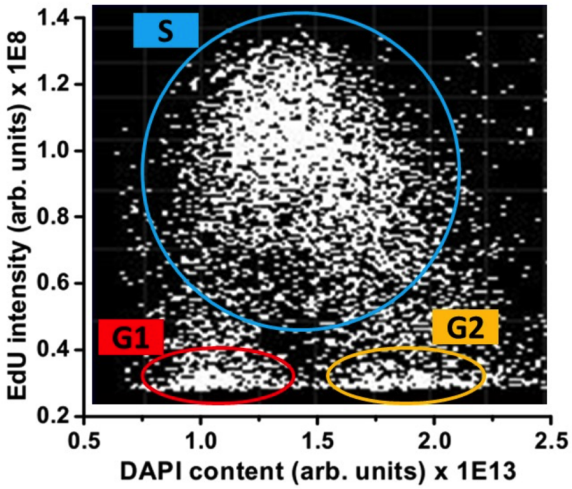

Figure 3.1 Cell cycle-specific DSB repair analysis

Cell cycle phase-specific analysis was performed by using a semi-automated microscopy system. Cells were scanned for EdU and DAPI. According to the intensity of DAPI and EdU, the distribution of cell cycle stages was shown as a horseshoe pattern. EdU-positive cells were identified as S phase cells, while EdU-negative cells were sub-classified as two groups: G1 and G2 phase cells based on their DNA content.

3.2.3 DNA damage induction

3.2.3.1 X-ray irradiation (X-IR)-induced DSB

mESCs were plated on sterile 4-cm dishes 24 h prior to X-IR. 2 Gy X-IR was performed by the X-ray machine with a 1 mm-aluminum plate holder at 90 kV and 19 mA for 64 seconds. The machine used a Philips X-ray tube and equipped with a tungsten anode and a thin beryllium window.

3.2.3.2 Restriction enzyme-induced DSB

After incubated with EdU and nocodazole for 30 min, mESC-AsiSI cells were induced DSBs by 300 nM of 4-hydroxytamoxifen (4-OHT) for 2 h. And then cells were treated with 500 µg/ml of auxin for the rapid degradation of nuclear localized AsiSI restriction enzyme to allow repair (Fig. 3.2 A). Cells were fixed at 1 or 6 h after the addition of auxin for cell cycle-specific DSB repair analysis.

Before the treatment of 1 µM of 4-OHT for 15 min, mESC-I-PpoI cells were treated with 1 µM of shield-1 for 3 h to stabilize the I-PpoI restriction enzyme into the nuclear (Fig. 3.2 B). Moreover, cells were also treated with EdU and nocodazole for 30 min before 4-OHT treatment for cell cycle-specific DSB repair analysis. In order to stop DSB induction and allow DSB repair, cells were washed with fresh medium for 3 times to remove shield-1 and 4-OHT, and then fixed at 1, 4 or 6 h post DSB induction.

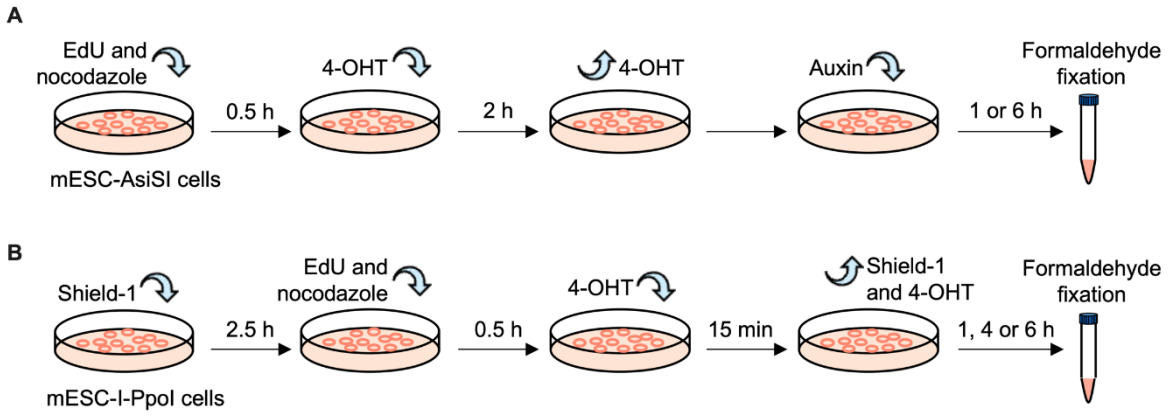

Figure 3.2 Experimental flowcharts of induced DSBs by restriction enzymes in mESCs

A. The experiment process of AsiSI-induced DSBs was used in mESC-AsiSI cells. **B.** The schematic flow chart showed I-PpoI-induced DSBs in mESC-I-PpoI cells.

3.2.4 Plasmid transfection

3.2.4.1 Amplification of plasmids

The DNA vector of pBABe-ddIPpoI was purchased in an agar stab. Bacteria was streaked on a plate containing ampicillin and incubated at 37°C overnight. After isolation, single colonies were selected and inoculated into liquid LB medium with ampicillin. After amplification of bacteria, the plasmid DNA was purified by the Maxiprep Kit and verified by diagnostic digestion with restriction enzymes, including EcoRI and SalI.

The DNA vector of pAID-AsiSI-ER was gifted in the form of DNA suspension. The plasmid was transformed into chemically competent DH5α *E. coli*. After thawing on ice, cells were gently mixed with 10 ng plasmid DNA and incubated on ice for 30 min. Then, cells were heated shock at 42°C for 90 sec, followed by 5 min-on ice. For recovery, cells were added into 900 µl LB medium and rotated at 220 rpm at 37°C for 1 h. Next, cells were centrifuged at 10,000 g for 1 min. After the removal of 800 µl of the supernatant, cells with remaining medium were transferred on agar plates with 50 mg/ml ampicillin and incubated at 37°C overnight, in order to select single colonies. The picked single colony was added in 200 ml of LB medium containing 50 mg/ml ampicillin and rotated at 220 rpm at 37°C overnight. After overnight-amplification, a glycerol stock containing 770 µl of 65% glycerol and 230 µl of bacterial culture was kept at -80°C for long-time storage. Plasmid DNA was purified by the Miniprep Kit and verified by diagnostic digestion with the restriction enzyme (EcoRI). Following verification, the Maxiprep Kit was used to purified more plasmids for transfection. The DNA concentration was measured by Nanophotometer at the absorption of 260 nm.

3.2.4.2 Transient plasmid transfection

Reverse transfection was applied for plasmid transfection in mESCs. Following the manufacture's instruction, 2.5 µg of plasmids were mixed with 5 µl of P3000 reagent and Opti-MEM® medium. The master mix of DNA was added to diluted Lipofectamine 3000 reagent with the ratio of 1:1, and incubated at room temperature (RT) for 30 min. The DNA-lipid complex was added dropwise into the diluted cell suspension and incubated at 37°C with 5% CO_2. Irradiation or 4-OHT treatment was performed after 24 h-plasmid transfection.

3.2.4.3 Generation of mixed stable cell lines with the expression of restriction enzyme

mESCs were reversely transfected with two different plasimds respectively: pBABe-ddIPpoI and pAID-AsiSI-ER. After 24 h transfection, cells were treated with different antibiotics for selection of transfected cells. mESC-I-PpoI cells were selected by 1 µg/ml of puromycin for two weeks. mESC-AsiSI cells were treated with 800 µg/ml of G418 for at least two weeks. After selection, mixed stable cell lines were maintained with puromycin or G418 during cell culture.

3.2.5 Inhibitor treatment

Small molecule inhibitors, including DRB, triptolide and Polo-like kinase inhibitor (PLKi) were added into fresh medium at 1 h before irradiation or 4-OHT treatment. The concentrations of these inhibitors were listed in the Table 3.1.

3.2.6 siRNA transfection

Reverse transfection was applied for siRNA transfection in mESCs. According to the manufacture's instruction, siRNA was mixed with Lipofectamine RNAiMAX transfection reagent and Opti-MEM® medium, and incubate for 30 mins at room temperature. The concentrations of siRNA were listed in the Table 3.2. siRNA mixture was added dropwise into the diluted cell suspension and incubated at 37°C with 5% CO2. X-IR or 4-OHT treatment was performed after 48 h siRNA transfection.

3.2.7 Protein analysis

Western blot analysis was applied to measure the efficiency of siRNA transfection in mESCs.

3.2.7.1 Sample preparation and protein extraction

After 48 h-siRNA transfections, cells were collected for western blot analysis and stored at -80°C.

Cell pellets were lysed in a lysis buffer containing the cOmplete™ proteinase inhibitor cocktail and phosSTOP™. Following the incubation on ice for 5-10 min, lysed samples were sonicated in the ultrasound bath with ice-cold water for 1 min and centrifuged down at 15,000 rpm at 4°C for 10 min.

After the transferring of supernatants into new tubes, the protein concentration of each sample was measured by Bradford assay. The Bradford reagent was diluted at the ratio of 1:5 in MilliQ water. Then, 1 µl of extracted sample was mixed well with 1 ml diluted Bradford reagent, followed by the measurement of light absorption at 590 nm by Nanophotometer. Samples were diluted into 20-25 µg/µl of protein concentration with Milli Q water and laemli buffer. Following boiled at 95°C for 5 min, all samples were store at -80°C.

3.2.7.2 SDS-Polyacrylamide-Gel (SDS-PAGE) electrophoresis

According to the size of each targeted protein, samples were loaded into the 5% or 10% polyacrylamide gel immersed in 1×electrophoresis buffer and run at 80 V for 10-20 min. When all proteins entered the running gel, the voltage was increased to 120 V until the required resolution reached.

3.2.7.3 Western blot

Following SDS-PAGE electrophoresis, proteins were transferred to a PVDF membrane which was activated by methanol for at least 1 min at RT. The gel was placed on the PVDF membrane and sandwiched between multiple layers of Whatmann filter paper and two layers of sponge. After the removal of air bubbles among the gel, membrane and filter paper, the assembled cassette was placed into the transfer chamber containing pre-chilled transfer buffer with the orientation of the membrane towards the anode. The blotting was conducted in the cold room at 4°C with a current of 300 mA for 2-3 h, depending on targeted sizes of proteins. After the blotting, the membrane was washed once with TBS-T buffer for 5 min and blocked with 5% low-fat milk in TBS-T buffer on the shaker at RT for 1 h. Then, the membrane was cut and incubated with desired primary antibodies diluted with 5% BSA (Table 3.3) on a shaker at 4°C overnight. On the following day, the membrane was washed with TBS-T buffer for 3×10 min and then incubated with corresponding HRP-conjugated secondary antibody diluted with 5% low-fat milk (Table 3.4) on a shaker at RT for 1 h. Next, the membrane was washed with TBS-T for 3×10 min and developed by the WesternBright™ Quantum chemiluminescent detection. All images of western blot were captured by the Fusion FX image acquisition system.

3.2.8 Immunofluorescence

At the time point of fixation for immunostaining, cells were washed once with PBS and incubated with trypsin/EDTA for 3 min at 37°C. After trypsinization, cells were resuspended in 1xPBS and spun down on polysine slides by the Cytospin centrifuge at the speed of 1000 rpm for 2 min. Then, different immunostaining approaches were used for different antibodies.

3.2.8.1 Co-immunostaining of γH2AX and pRPA

Cells were fixed by 2.5% formaldehyde (FA) in PBS at RT for 10 min and washed with 1xPBS for three times. And then cells were permeabilized by 0.25% Triton X-100 in PBS at 4°C for 10 min, and blocked with the 1×Roti-block at RT for 1 h. After blocking, cells were incubated with primary antibodies diluted with 1x Roti-block overnight at 4°C. Two primary antibodies were used: γH2AX mouse-monoclonal antibody (1:1000) and pRPA rabbit-polyclonal antibody (1:10,000). On the following day, the cells were washed with PBS and stained with the Click-iT™ cocktail at RT for 30 min, for cell cycle-specific analysis by EdU labeling. Then, cells were washed again with PBS and incubated with secondary antibodies, goat anti-mouse Alexa Fluor 488 and goat anti-rabbit Alex Fluor 594 conjugate with a dilution of 1:1000. After 1 h-incubation at RT, cells were washed with PBS and stained with DAPI (0.4 μg/ml) at RT for 5 min. Finally, cells were embedded with mounting media and stored at 4°C.

3.2.8.2 Immunostaining of S9.6 and EU

Before ice-cold methanol fixation at -20°C for 7 min, cells were pe-extracted with 0.5% Triton X-100 in CSK buffer for 3 min and washed three times with PBS. In order to remove unspecific binding of S9.6 or EU to single or double-stranded RNA, cells were treated with RNase A for 15 min at the final concentration of 100 μg/ml in high salt buffer which includes 0.5 mM EDTA, 300 mM NaCl and 10 mM Tris-HCl. The representative images and quantification analysis showed that pretreatment of RNase A under high salt buffer reduce around 50% of S9.6 foci and background signal in G1-mESCs at 1 h after 2 Gy X-IR (Fig. 3.3 A and B). After blocked with 2% BSA and 0.5% FBS in PBS at RT for 1 h, cells were incubated with S9.6 antibody (1:500) at 4°C overnight. On the next day, the staining of EdU, secondary antibody and DAPI was same as mentioned above. The EU staining was followed by the instruction of Click-iT™ EdU kit. Cells were embedded with mounting media and stored at 4°C.

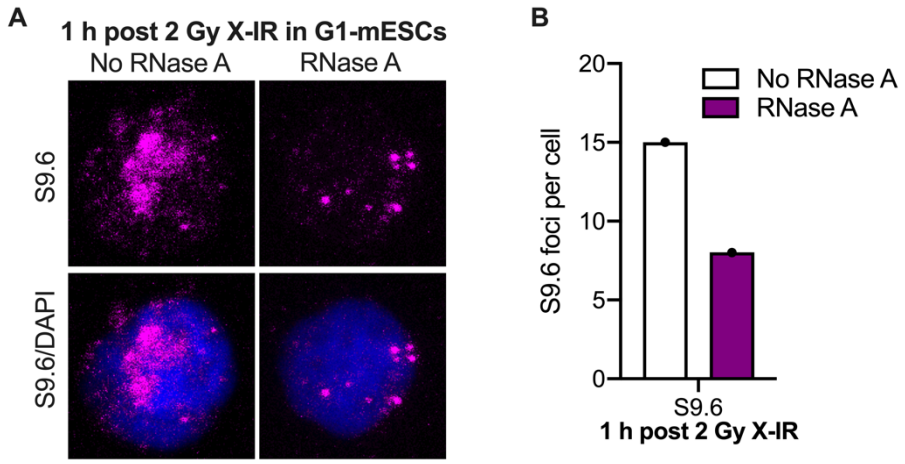

Figure 3.3 Effects of RNase A pretreatment on the immunostaining of S9.6 in mESCs

A. Representative images of S9.6 immunostaining with and without with and without the pretreatment of RNase A in G1-mESCs at 1 h after 2 Gy X-IR. **B.** Quantification of S9.6 foci numbers with and without the pretreatment of RNase A in G1-mESCs at 1 h after 2 Gy X-IR.

3.2.8.3 Triple immunostaining of γH2AX, pRPA and S9.6 for confocal imaging

The fixation method and RNase treatment for the triple immunostaining of γH2AX, pRPA and S9.6 was same as the immunostaining of S9.6. The chicken-polyclonal antibody of γH2AX was used as at dilution of 1:1000. Three different secondary antibodies were goat anti-chicken Alex Fluor 488, goat anti-rabbit Dylight 550 and donkey anti-mouse Alexa Fluor 647. In order to distinguish the G1 cells, EdU was labeled by Alexa Fluor 594 azide. After the staining of DAPI, Cells were embedded with mounting media and stored at 4°C.

3.2.9 Confocal microscopy

The imaging for triple immunofluorescence staining was performed by a confocal laser scanning microscope with the LAS AF Lite software. Z-stack confocal images were taken under the fixed interval of 0.3 µm. Fixed cells were stained with three antibodies (γH2AX, pPRA and S9.6) in three different secondary fluorescent antibodies (Alexa 488, Dylight 550 and Alexa 647 respectively), EdU in Alexa 594 and DAPI. To avoid the crosstalk among these five fluorophores, images were taken under three of sequential scans using different excitation and emission settings. The first scan was applied for imaging γH2AX (Alexa 488) and S9.6 antibody (Alexa 647) together, while the second scan was performed for imaging pRPA (Dylight 550) alone (Fig. 3.4 A and B). Then, the last scan was taken for imaging EdU (Alexa 594) and DAPI (Fig. 3.4 C). Owing to the spectral overlaps between two fluorophores of Alexa 594 and Dylight 550, different emissions were used for separating these two fluorophores during scanning showed in the Fig. 3.4 B and C.

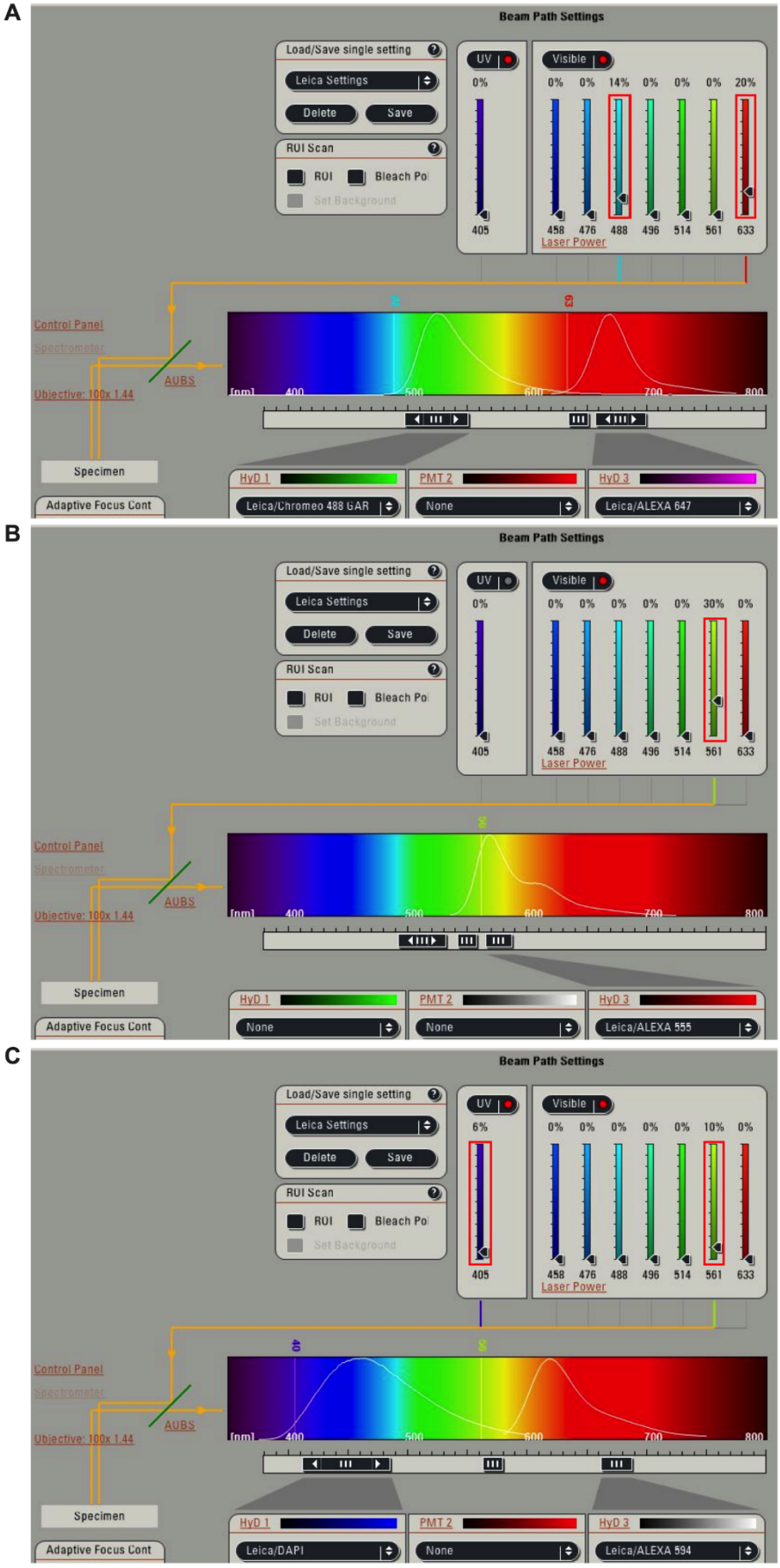
A
Beam Path Settings
Load/Save single setting
Leica Settings
Delete
Save
ROI Scan
ROI
Bleach Po
Set Background
UV
0%
405
Visible
0% 0% 14% 0% 0% 0% 20%
458 476 488 496 514 561 633
Laser Power
Control Panel
Spectrometer
AOBS
Objective: 100x 1.44
Specimen
Adaptive Focus Cont
[nm] 400 500 600 700 800
HyD 1
Leica/Chromeo 488 GAR
PMT 2
None
HyD 3
Leica/ALEXA 647
B
Beam Path Settings
Load/Save single setting
Leica Settings
Delete
Save
ROI Scan
ROI
Bleach Po
Set Background
UV
0%
405
Visible
0% 0% 0% 0% 0% 30% 0%
458 476 488 496 514 561 633
Laser Power
Control Panel
Spectrometer
AOBS
Objective: 100x 1.44
Specimen
Adaptive Focus Cont
[nm] 400 500 600 700 800
HyD 1
None
PMT 2
None
HyD 3
Leica/ALEXA 555
C
Beam Path Settings
Load/Save single setting
Leica Settings
Delete
Save
ROI Scan
ROI
Bleach Po
Set Background
UV
6%
405
Visible
0% 0% 0% 0% 0% 10% 0%
458 476 488 496 514 561 633
Laser Power
Control Panel
Spectrometer
AOBS
Objective: 100x 1.44
Specimen
Adaptive Focus Cont
[nm] 400 500 600 700 800
HyD 1
Leica/DAPI
PMT 2
None
HyD 3
Leica/ALEXA 594

Figure 3.4 Parameters of sequential scans for triple immunofluorescence confocal microscopy

A. The excitation and emission setting in the first scan was used for imaging γH2AX in Alexa 488 and S9.6 antibody in Alexa 647. **B.** The excitation and emission parameters in the second scan were applied for imaging pRPA in Dylight 550. **C.** The excitation and emission parameters in the third scan were performed for EdU in Alexa 594 and DAPI.

3.2.10 Cell sorting of mESC-I-PpoI cells in G1 phase

The sorting of G1 cells was based on the Click-iT™ EdU Alexa Fluor™ 488 and the DNA content which was labeled by SYTOX® AAdavanced™ Dye. Cells were sorted by the Bio-Rad S3™ sorter equipped with a 488/561 nm laser and a 525/30 nm bandpass filter, a 615/25 nm bandpass filter and a 655LP long pass filter. The schematic summary of G1-cell soring was shown in the Fig. 3.5.

After 4-OHT-indcued DSBs and formaldehyde fixation, mESC-I-PpoI cells were washed twice with DPBS, resuspended in the freezing medium to protect the intactness of cells under freeze-thaw cycles, and stored at -80°C to avoid the degradation of targeting proteins.

Before sorting, cells were thawed on ice for 30 min, and then centrifuged at 760 g for 5 min at 4°C to remove the freezing medium. Cells were permeabilized in the 1× Perm/Wash™ Buffer for 15 min on ice, and then incubated with the Click-iT™ Alexa Fluor® 488 azide which was prepared following with the instruction of Click-iT™ EdU kit. After 30 min of incubation at room temperature, cells were washed once with the 1× Perm/Wash™ Buffer and then resuspended into 1× Perm/Wash™ Buffer to reach the cell concentration of 1×10^6 cells/ml. In order to stain the DNA content for flow cytometry, RNase A and SYTOX® AAdavanced™ were added into the cell suspension at the final concentration of 10 μg/ml and 1 μM respectively. After 30 min-incubation on ice, single cells were selected by the plot of forward scatter (FSC) and side scatter (SSC). Among these single cells, G1-cells were gated under the plot of EdU-DNA content. 5×10^5-3×10^6 of sorted G1-cells were collected for ChIP-qPCR.

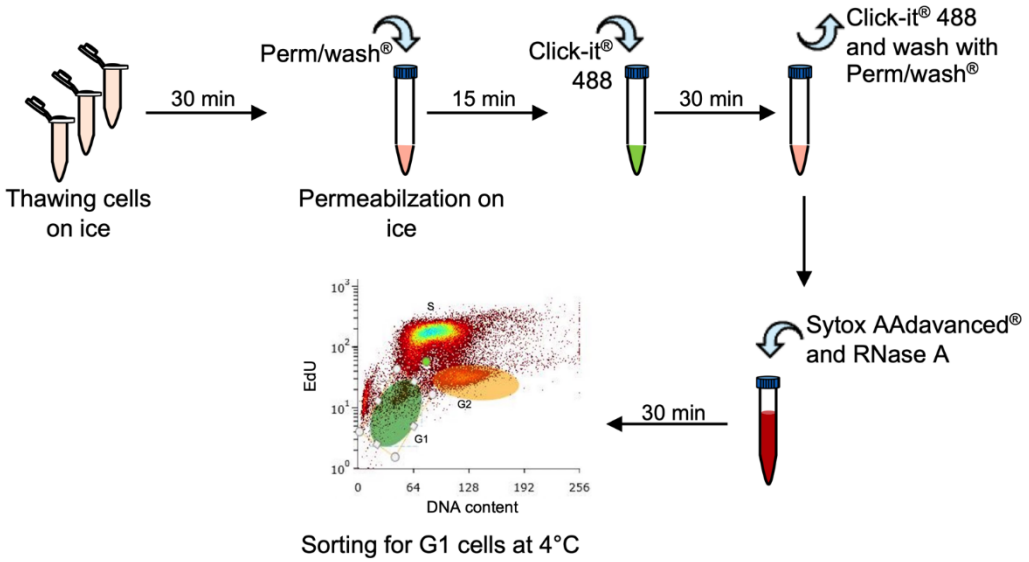

Figure 3.5 Schematic summary of cell sorting in G1

3.2.11 Chromatin immunoprecipitation-quantitative PCR (ChIP-qPCR)

The schematic summary of ChIP-qPCR assay was shown in the Fig. 3.6. mESC-I-PpoI cells were induced DBSs by 4-OHT and dissociated at 1 or 4 h post damage, before being fixed in culture medium with 1% methanol-free formaldehyde (Pierce) at RT for 10 min and quenched by 125 mM glycine at RT for 5 min. After washed with cold PBS for 3 times, cells were frozen in FCS with 10% DMSO and stored at -80°C for cell sorting. The 5×10^5-1×10^6 G1-sorted cells were resuspended in 300 µl of cold High Salt Sonication Buffer containing 800 mM NaCl, 25 mM Tris, 5 mM EDTA, 1% Triton X-100, 0.1% SDS, 0.5% sodium deoxycholate, protease inhibitor cocktail and PhosSTOP™. Chromatin was sheared by the ultrasonic processor (Bandelin Sonopuls UM70/GM70HD) for 30 sec on and 30 sec off on 50% of power. 15-25 cycles were optimized for a fragment size range of 100 bp to 500 bp which were confirmed by 2% agarose gel electrophoresis (Fig. 3.7).

Following to the sonication, 300 µl of sheared chromatin was added 1 ml of cold Chromatin Dilution Buffer with fresh protease inhibitor cocktail and PhosSTOP™ and spun down at 13,600 g at 4°C for 30 min. Next, the supernatant containing soluble chromatin was transferred into a 1.5 ml-protein low-bind tube and incubated with Protein G Dynabeads™ for 1 h in a rotator at 4°C. Then, primary antibody was incubated with the pre-cleared chromatin with rotation at 4°C overnight. 10 ng of γH2AX antibody was used for 200 ng of chromatin, while 1 µg of pRPA antibody was applied for 7.5 µg of chromatin. On the following day, 30 µl of Protein G Dynabeads™ was added to each sample and incubated with rotation at 4°C for 3 h. Beads were then washed with 1 ml of Wash Buffer A, Wash Buffer B, Wash Buffer C and TE Buffer (twice) at 4°C for 10 min respectively. Chromatin-

bound beads were eluted twice by 100 µl of Elution Buffer and incubated with rotation at 65°C for 15 min, followed by incubation and rotation at 25°C for 15 min.

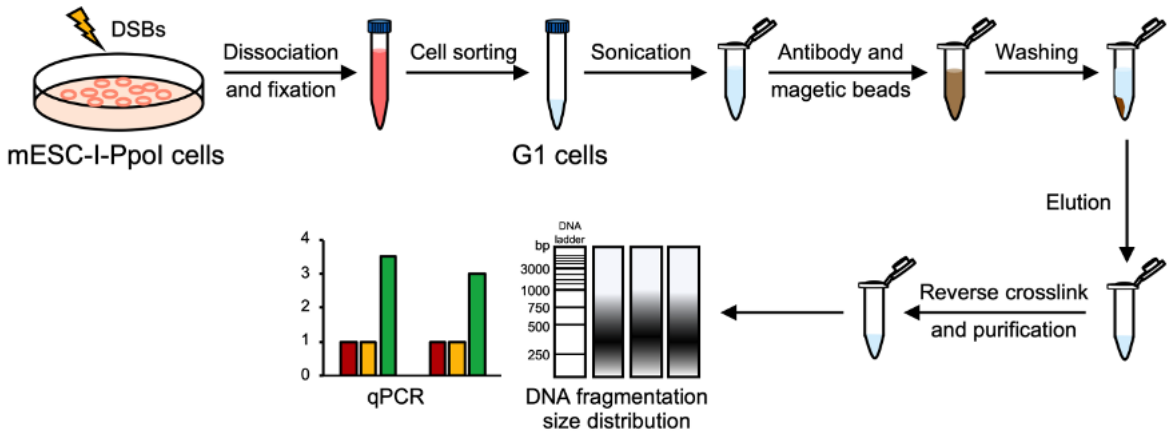

Figure 3.6 Schematic summary of ChIP-qPCR in G1-mESC-I-PpoI cells

Pooled eluates were added with NaCl and RNase A to reach the concentration of 160 mM and 20 µg/ml respectively and incubated with rotation at 65°C overnight to reverse crosslinks. On the next day, all samples were added with 2 µl of 5 M EDTA and 2 µl of 10 mg/ml Proteinase K and incubated with rotation at 65°C for 3 h to digest proteins. Finally, DNA was purified by using the QIAquick® PCR Purification Kit and stored at -20°C. All qPCRs were performed with FastStart Universal SYBR Green Master (Rox).

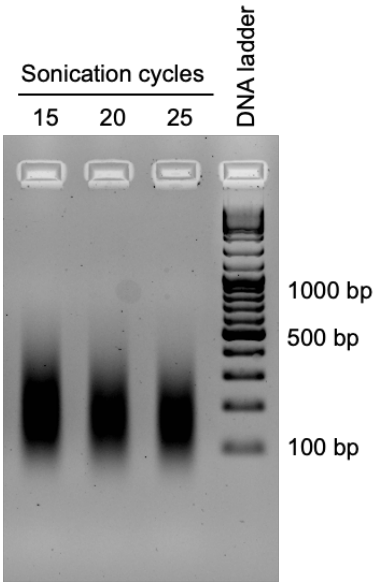

Figure 3.7 Optimization of sonication for ChIP-qPCR in mESC-I-PpoI cells

Purified DNA after shearing was separated on a 2% agarose gel. The minimal cycles to fragment the majority of chromatin into the range of 100 to 500 bp was 15.

3.2.12 Qubit fluorometric quantification

The concentration of DNA was quantified by the Invitrogen Qubit™ 4 Fluorometer based on a fluorescent dye which emits a signal only when bound to dsDNA. For accurate quantification, 10 µl of dsDNA standards, combing with 190 µl of Qubit™ 1x dsDNA high sensitivity (HS) working buffer for 2 min at RT, was applied to calibrate the Qubit™ 4 Fluorometer. For each assay, 2 µl of each sample was incubated with 198 µl of Qubit™ 1× dsDNA HS working buffer at RT for 2 min and measured by the Qubit™ 4 Fluorometer.

4 Results

4.1 Impacts of resection in NHEJ during G1 phase

4.1.1 Resection occurs in G1-mESCs at IR-induced DSBs

Previous data from this laboratory showed that resection occurs in G1 after X-IR or α-IR in HeLa cells and human fibroblasts[40]. In brief, PLK3 phosphorylates CtIP in G1 to mediate the interaction between CtIP and BRCA1 and promote limited resection[40]. Following these studies, it was of interest to validate whether resection also took place at DSB sites in G1-mESCs after 2 Gy X-IR. For this purpose, pRPA and γH2AX immunofluorescence analyses were performed. Phosphorylation of histone H2AX on Ser139, producing γH2AX, is one of the initial steps of DSB repair[129]. Thus, quantification of γH2AX foci by immunofluorescence is an appropriate and sensitive approach to detect DSBs, since each DSB corresponds to one γH2AX focus[130,131]. Additionally, immunostaining of pRPA is a direct way to monitor DNA resection in cells[132]. Moreover, to monitor DSB repair in a cell cycle-specific manner, cells were treated with nocodazole and EdU before X-IR, in order to stop G2/M cells from going into the next G1 phase after DSB induction and to label all S phase cells, respectively.

The representative immunofluorescence images showed that pRPA foci were found in G1 at 1 h after X-IR. In addition, most of pRPA foci were visible at areas positive for γH2AX signal (Fig. 4.1 A). To quantify the resection in G1-mESCs at DSBs, the colocalization of pRPA and γH2AX foci in single stacks of confocal images was measured using the RGB Profile Plot macro in the ImageJ software (Fig. 4.1 B). The quantification result showed that few of pRPA foci were observed before X-IR (Fig. 4.1 C). After subtracted the background level, 80-90% of pRPA foci, induced by 2 Gy X-IR, overlapped with γH2AX foci (Fig. 4.1 C), indicating that the resection-dependent NHEJ also occurs in mESCs during G1. Furthermore, the resection in mESCs could be easily observed under low doses of IR, while pRPA foci can only be found in HeLa cells and human fibroblasts after high doses of IR which produce complex DSBs. Thus, it potentially indicates that a resection-dependent repair process is crucial or more prominent in embryonic stem cells.

The regulation of resection in G1 highly depends on the phosphorylation of CtIP by PLK3, while phosphorylation of CtIP in G2 is regulated by cyclin-dependent kinases[24,30,40]. In order to further distinguish the resection process in G1-mESCs from that in HR in G2, resection was inhibited by PLKi or depletion of CtIP before IR. The accumulation of pRPA foci at DSBs in G1-mESCs was significantly reduced after resection inhibition at 1 h post 2 Gy X-IR (Fig. 4.1 D). This confirms that the occurring of resection in G1-mESC after DSB induction is dependent on PLK3 and CtIP. The depletion efficiency of siCtIP in mESCs was verified by western blot (Fig. 4.1 E).

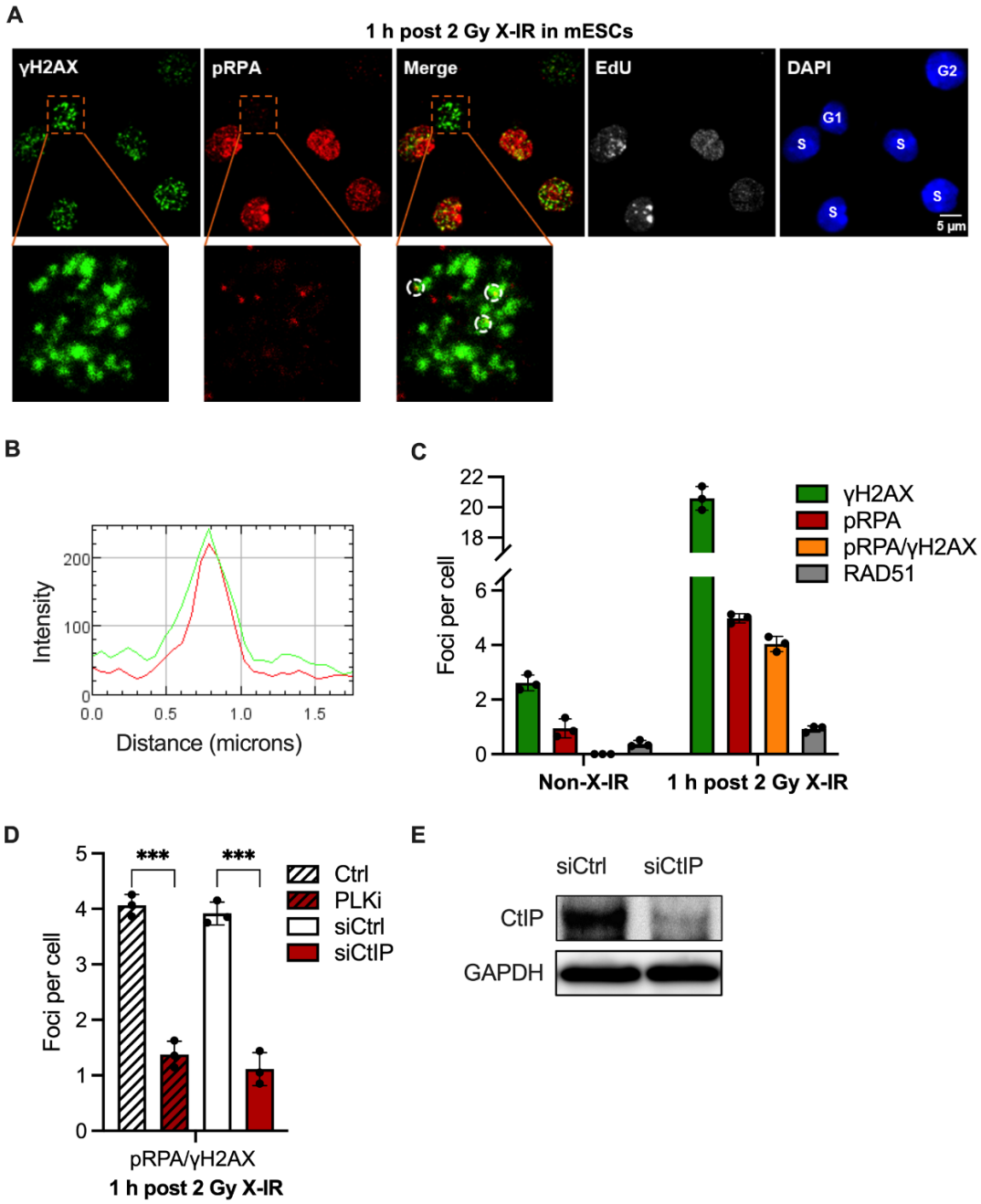

Figure 4.1 Resection occurs in G1 at IR-induced DSBs in mESCs

A. Immunofluorescence images of γH2AX and pRPA in mESCs at 1 h after 2 Gy X-IR. mESCs were treated with EdU and nocodazole 30 min before X-IR and kept on during repair time. Z-stack images were taken by a Leica TCS SP5 II confocal microscope. The interval between two stacks was 0.3 µm. **B.** Example of the colocalization analysis by the RGB Profile Plot in the ImageJ software. **C.** Quantification of γH2AX and pRPA foci in G1-mESCs without X-IR or after 2 Gy X-IR. Colocalization of γH2AX and pRPA was evaluated based on the analysis of RGB profiles. **D.** Number of pRPA foci at DSBs after resection inhibition by PLKi or depletion of CtIP (siCtIP). All data show the mean ± S.D. and statistical significance tested by t-test (***$p < 0.001$). Three individual experiments are shown as dots. **E.** The depletion efficiency of CtIP by siRNA transfection in mESCs was confirmed by western blot.

ESCs have relatively high expression level of HR-related proteins during the whole cell cycle, due to the short duration of G1 compared with somatic cells[133]. In accordance with this, other studies suggested that the HR repair process in ESCs may be preferentially utilized throughout the whole cell cycle, in order to maintain the genome integrity[133–136]. To evaluate the frequency of HR in G1 after DSB induction, RAD51 foci in mESCs were enumerated, since RAD51 is a crucial player of HR. However, only few RAD51 foci were observed in G1-mESC after 2 Gy X-IR (Fig. 4.1 C). Thus, these results indicate that the main DSB repair process in G1-mESCs is potentially the resection-dependent NHEJ, but not RAD51-dependent HR.

4.1.2 Resection is essential for DSB repair in G1-mESCs

Next, since previous studies showed that inhibition of resection leads to repair defects in G1-HeLa cells and human fibroblasts after treatment with 2 Gy X-IR[40], the effect of resection inhibition in mESCs was also examined. Thus, cells were treated with PLKi or depleted for CtIP or Artemis with siRNAs and then damaged with 2 Gy X-IR. The detection of elevated γH2AX foci levels in G1 phase in cells treated with PLKi or siCtIP/Artemis, compared to the controls, indicated that the inhibition of resection in mESCs caused a repair defect at 6 h after 2 Gy X-IR (Fig. 4.2 A).

In HeLa cells and human fibroblasts, depletion of CtIP did not lead to a repair defect but instead rescued it in Artemis-deficient cells, suggesting that an early interruption of the resection pathway by CtIP-depletion may cause a pathway switch from the resection-dependent to the resection-independent repair process in G1[40]. In contrast, depletion of CtIP or Artemis led to the accumulation of unrepaired breaks in mESCs after 2 Gy X-IR. Compared with single use of PLKi, siCtIP and siArtemis, different combinations of these treatments caused epistatic repair defects (Fig. 4.2 B). Moreover, there was no rescue of the repair defects seen in Artemis-depleted cells when co-depleting both CtIP and Artemis in G1-mESCs (Fig. 4.2 B). This indicates that mESCs may not be able to switch from the resection-dependent repair process to resection-independent one upon depletion of CtIP. Furthermore, the resection-dependent repair pathway seems to be essential in G1-mESCs during X-IR-induced DSB repair. The knockdown efficiency of CtIP and Artemis by siRNA transfection in mESCs was confirmed *via* western blot analysis (Fig. 4.2 C).

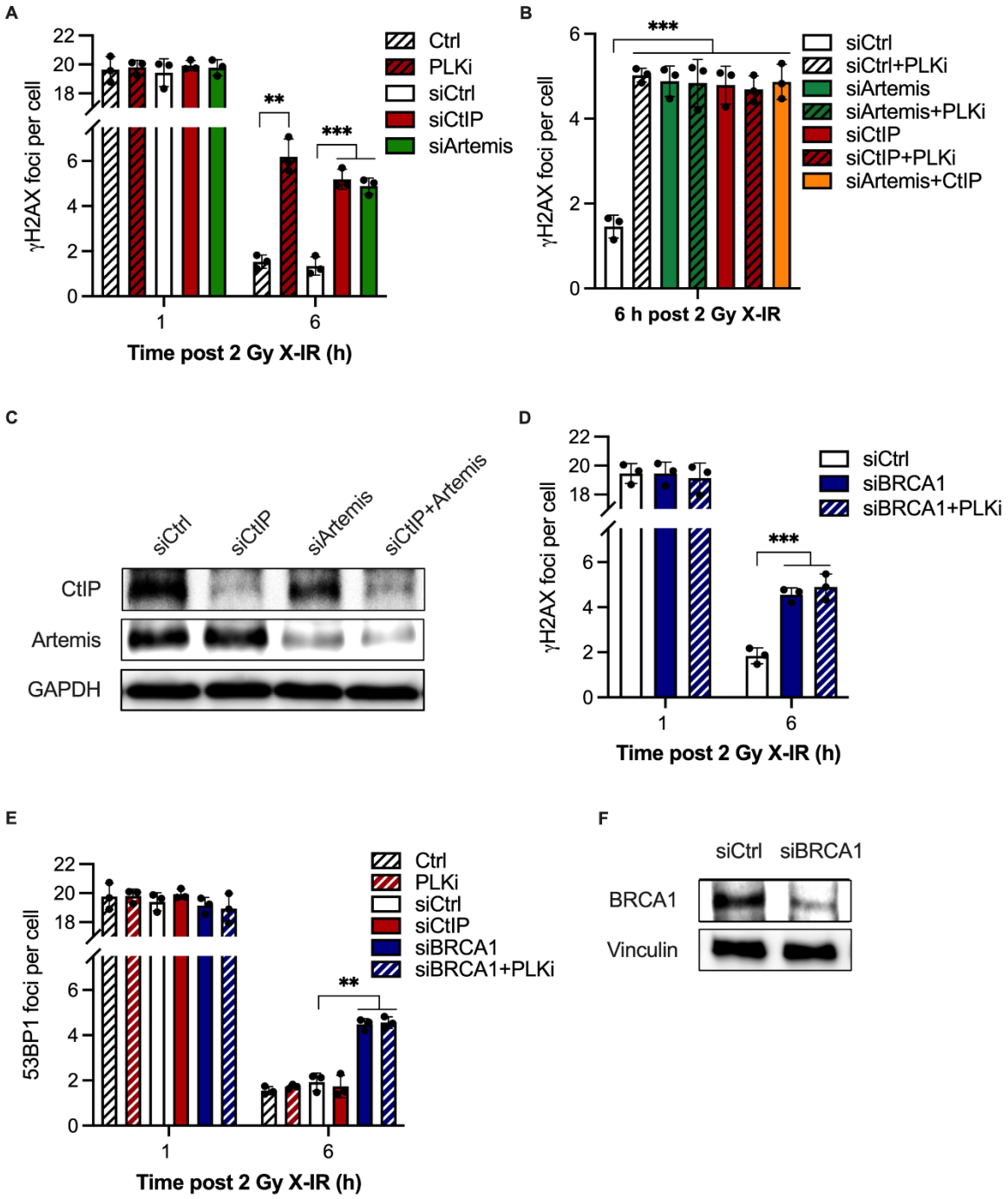

Figure 4.2 Inhibition of resection causes repair defects at IR-induced DSBs in G1-mESCs

A. γH2AX foci after resection inhibition using PLKi or siRNAs against CtIP and Artemis. **B.** γH2AX foci after combining different treatments for resection inhibition. **C.** Knockdown efficiencies of siCtIP and/or siArtemis in mESCs were confirmed by western blot analysis. **D.** γH2AX foci after depletion of BRCA1 with or without PLKi treatment. **E.** 53BP1 foci after resection inhibition, depletion of BRCA1 or combination of both. All cells were fixed at 1 and/or 6 h after 2 Gy X-IR. All data show the mean ± S.D. and statistical significance tested by t-test (**p < 0.01, ***p < 0.001). Three individual experiments are shown as dots. **F.** The depletion efficiency of BRCA1 by siRNA transfection in mESCs was verified by western blot.

Several studies show that BRCA1 plays a critical role in removing the 53BP1-mediated resection block during HR[137–140]. Moreover, the interaction of CtIP-BRCA1 was previously shown to mediate the initial process of resection in G1 phase. Loss of BRCA1 in G1-HeLa cells and human fibroblasts caused a reduction of pRPA foci after 2 Gy α-IR[40]. Depletion of BRCA1 did not lead to a repair defect but, as siCtIP, it rescued the repair defect in Artemis-deficient somatic cells[40]. Conversely, siBRCA1 caused an increase in the γH2AX foci level in G1-mESCs at 6 h after 2 Gy X-IR (Fig. 4.2 D), further confirming that resection is probably required for the DSB repair in G1-mESCs.

Additionally, the combined treatment of siBRCA1 and PLKi did not show an additive repair defect, but instead led to an epistatic effect in G1-mESCs after 2 Gy X-IR (Fig. 4.2 D). This suggests that BRCA1 and phosphorylated CtIP participate in the same pathway promoting the resection-dependent NHEJ repair. As it is well established that BRCA1 counteracts the anti-resection roles of 53BP1[141], 53BP1 foci were numerated in G1-mESCs after treatment with siBRCA1, siCtIP or PLKi and X-IR. Inhibition of resection by PLKi or siCtIP increased the level of γH2AX foci (Fig. 4.2 A), but did not affect the 53BP1 recruitment in G1 at 6 h post 2 Gy X-IR (Fig. 4.2 E). However, the depletion of BRCA1 or co-treatment of siBRCA1 and PLKi both caused the persistence of 53BP1 foci at DSBs in G1 at later time points post damage (Fig. 4.2 E). It raises a possibility that BRCA1 may indirectly promote the resection process in G1-mESCs by removing 53BP1. The knockdown efficiency of siBRCA1 in mESCs was verified by western blot (Fig. 4.2 F).

4.2 Involvement of RNA in resection-dependent NHEJ repair

Current findings have highlighted that RNA plays important roles in efficient DSB repair. Many different species of RNA have been identified to interact with different DNA repair factors during DSB repair[142]. In particular, several studies have reported that DNA-RNA hybrids, which are generated during active transcription, can promote or impair resection in DSB repair depending on local chromatin context[91,143,144]. However, it is still under debate how transcription impacts on DSB repair and interacts with DNA end resection.

4.2.1 Transcription inhibition affects resection-dependent NHEJ repair in G1

With the aim of investigating whether transcription is involved in DSB repair in G1-mESCs, transcription was inhibited before DSB induction by two different inhibitors, namely 5,6-Dichloro-1-β-D-ribofuranosylbenzimidazole (DRB) and triptolide. Quantification of γH2AX foci at 6 h post 2 Gy X-IR showed that transcription inhibition caused a repair defect in G1-mESCs (Fig. 4.3 A). In order to clarify whether the effects caused by transcription- and resection-deficiencies are linked, cells were

treated with DRB or triptolide to inhibit transcription, in combination with PLKi, siCtIP or siArtemis for resection inhibition. Inhibition of both processes before X-IR, led to no additive repair defects in comparison to the single transcription or resection inhibition (Fig. 4.3 A and B). These results suggest that transcription and resection are epistatic and both play important roles under the same DSB repair pathway in G1-mESCs.

Next, to better understanding how transcription inhibition affects repair efficiency and resection, mESCs were inhibited by DRB and triptolide before or after DSB induction, and fixed at 1h post 2 Gy X-IR followed co-immunostaining of γH2AX and pRPA antibody. DRB can rapidly prevent RNAPII transcription, but as a reversible transcription inhibitor, its effects can be reverted upon removal and replacement of medium, hence efficiently switching transcription on again[145–147]. Using DRB's reversibility feature, in an attempt to further investigate the potential role of transcription during DSB repair, cells were treated with this inhibitor in three different ways: 1) 1 h-treatment with DRB before IR and no removal afterwards; 2) 1 h-treatment with DRB before IR and immediate removal after IR; and 3) 5 min-treatment with DRB before IR and no removal afterwards (Fig. 4.3 C). Since transcription inhibition caused by triptolide is irreversible, cells were only treated with triptolide in two different ways, both without triptolide's removal after IR: 1) 5 min-treatment with triptolide before IR; and 2) 1 h-treatment with triptolide before IR (Fig. 4.3 C).

The analysis of γH2AX foci levels at 6 h after IR showed how transcription affects repair in G1. In any of the cases, inhibition of transcription after IR by either of the inhibitors led to similar repair defects. In contrast, the repair defect was rescued if the transcription was only inhibited before IR and was resumed after IR upon removal of DRB (Fig. 4.3 D). This indicates that transcription after DSB induction is required for the efficient repair process in G1, whereas transcription before DSB induction may be relatively less essential for repair. On the contrary to our hypothesis, pre-existing RNA may not be used as a template in the studied system. However, it does not exclude the possibility that transcription inhibition before DSB induction affects the repair fidelity on the genomic context, although it does cause repair defects in G1.

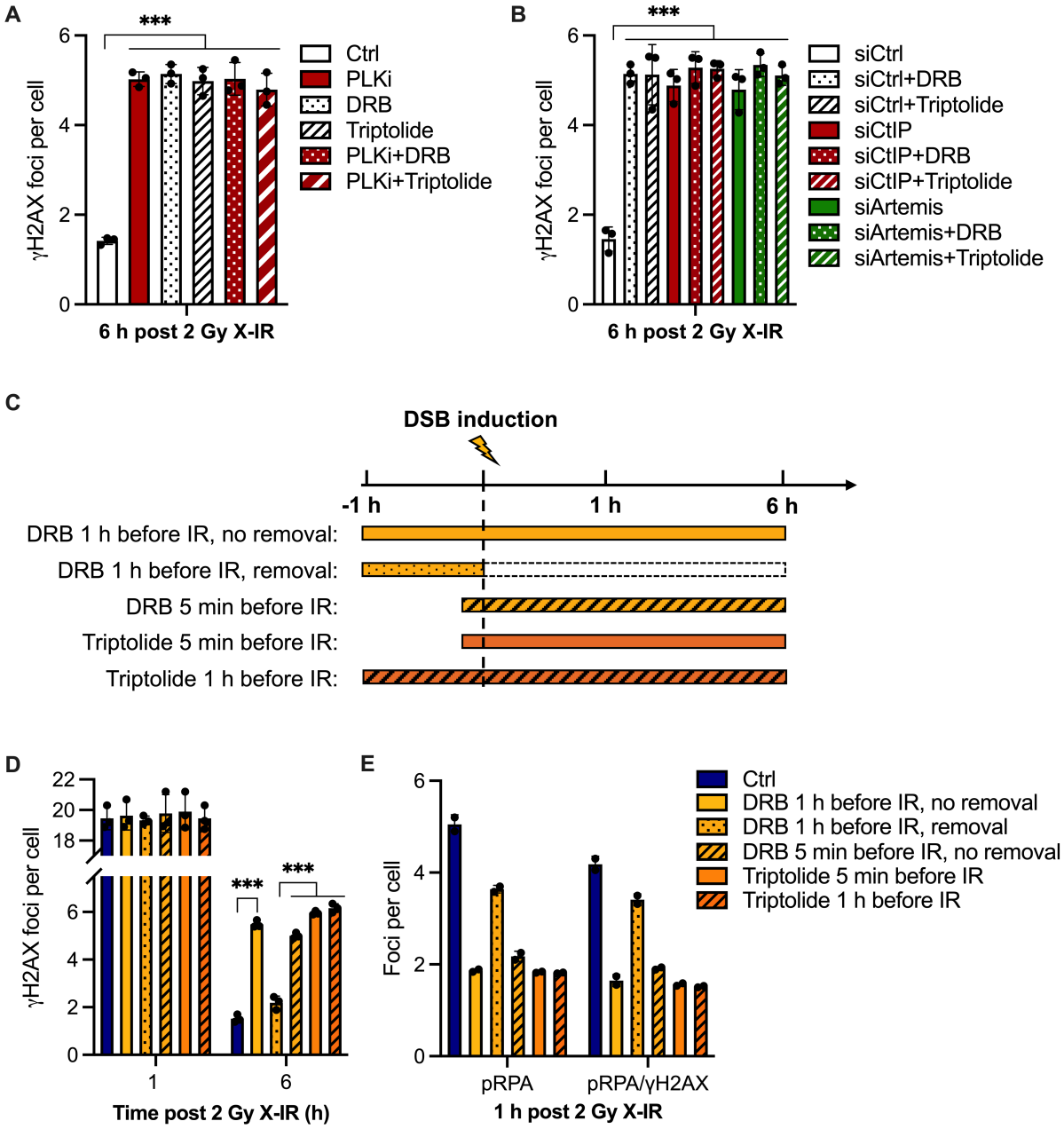

Figure 4.3 Impact of transcription inhibition at IR-induced DSBs in G1-mESCs

A. Number of γH2AX foci after resection inhibition in combination with transcription inhibition at 6 h post 2 Gy X-IR. PLKi were used for resection inhibition, while DRB and triptolide were used for transcription inhibition. **B.** As in (A) but using siCtIP or siArtemis to inhibit resection. **C.** Scheme of different approaches for inhibiting transcription before or after 2 Gy X-IR. **D.** Quantification of γH2AX foci in G1-mESCs after 2 Gy X-IR under different treatments of transcription inhibition. **E.** Effects of transcription inhibition on resection after 2 Gy X-IR. Cells were fixed at 1 h after 2 Gy X-IR and the total number of pPRA foci and the foci number which colocalized with γH2AX were counted. Colocalization of γH2AX and pRPA was evaluated based on the analysis of RGB profiles. All data show the mean ± S.D. and statistical significance tested by t-test (***p < 0.001, ns: not significant). Individual experiments are shown as dots.

Moreover, transcription inhibition also led to a notable impact on pRPA accumulation at DSBs after X-IR. The colocalization analysis showed that the number of pRPA foci at DSBs was significantly reduced at 1 h post damage when transcription was inhibited by DRB or triptolide at 5 min or 1 h before X-IR (Fig. 4.3 E). However, when transcription was only inhibited by DRB for 1 h before IR but it was resumed after damage, higher pRPA foci numbers were observed than when it was inhibited also during repair times (Fig. 4.3 E). These results reveal that transcription after DSB induction promotes the occurrence of resection at DSBs in G1. Moreover, since the number of pRPA foci was slightly lower than in the control group (Fig. 4.3 E), transcription inhibition before DSB induction might not directly affect the resection-dependent NHEJ repair, but it may cause a delay in the recruitment of resection factors after DSB induction in G1.

4.2.2 Resection and transcription inhibition affect nascent RNA synthesis at IR-induced DSBs in G1

Since abovementioned results clearly showed that transcription influences resection-dependent NHEJ repair in G1, it can be speculated that RNA produced by transcription is also potentially involved in DSB repair. To further examine impacts of transcription and resection on RNA during DSB repair, pre-existing or DSB-induced nascent RNA was separately monitored by EU labeling. mESCs were treated with EU in three different ways: 1) EU was added at 1 h before X-IR without removal to label all nascent RNA; 2) EU was added at 1 h before X-IR, but was immediately removed and replaced by BrU after X-IR to specifically label pre-existing RNA before DSB induction; and 3) EU was added immediately after X-IR to only label DSB-induced RNA (Fig. 4.4 A). Then, cells were fixed at 1 h after 2 Gy X-IR and treated with RNase A which specifically degrades dsRNA at the high NaCl concentration of 300 mM[128]. Using these methods of EU labeling, the accumulation of nascent RNA at different stages during DSB repair can be visualized by fluorescence imaging. Representative images reveal that EU foci labeled only before X-IR is relatively smaller than those labeled only after X-IR, while the EU foci labeled before damage without removal seems to include both small and big ones (Fig. 4.4 B). Moreover, the quantification of EU and γH2AX foci showed that around most of EU foci occurred at DSBs at 1 h post 2 Gy X-IR in G1-mESCs (Fig. 4.4 C).

To confirm the specificity of this approach to detect nascent RNA in G1-mESCs, transcription was hindered by DRB and triptolide before the addition of EU, and EU and γH2AX foci were evaluated. The quantification of foci showed that transcription inhibition caused a marked reduction of EU foci at DSBs under all different labeling conditions after 2 Gy X-IR (Fig. 4.4 D).

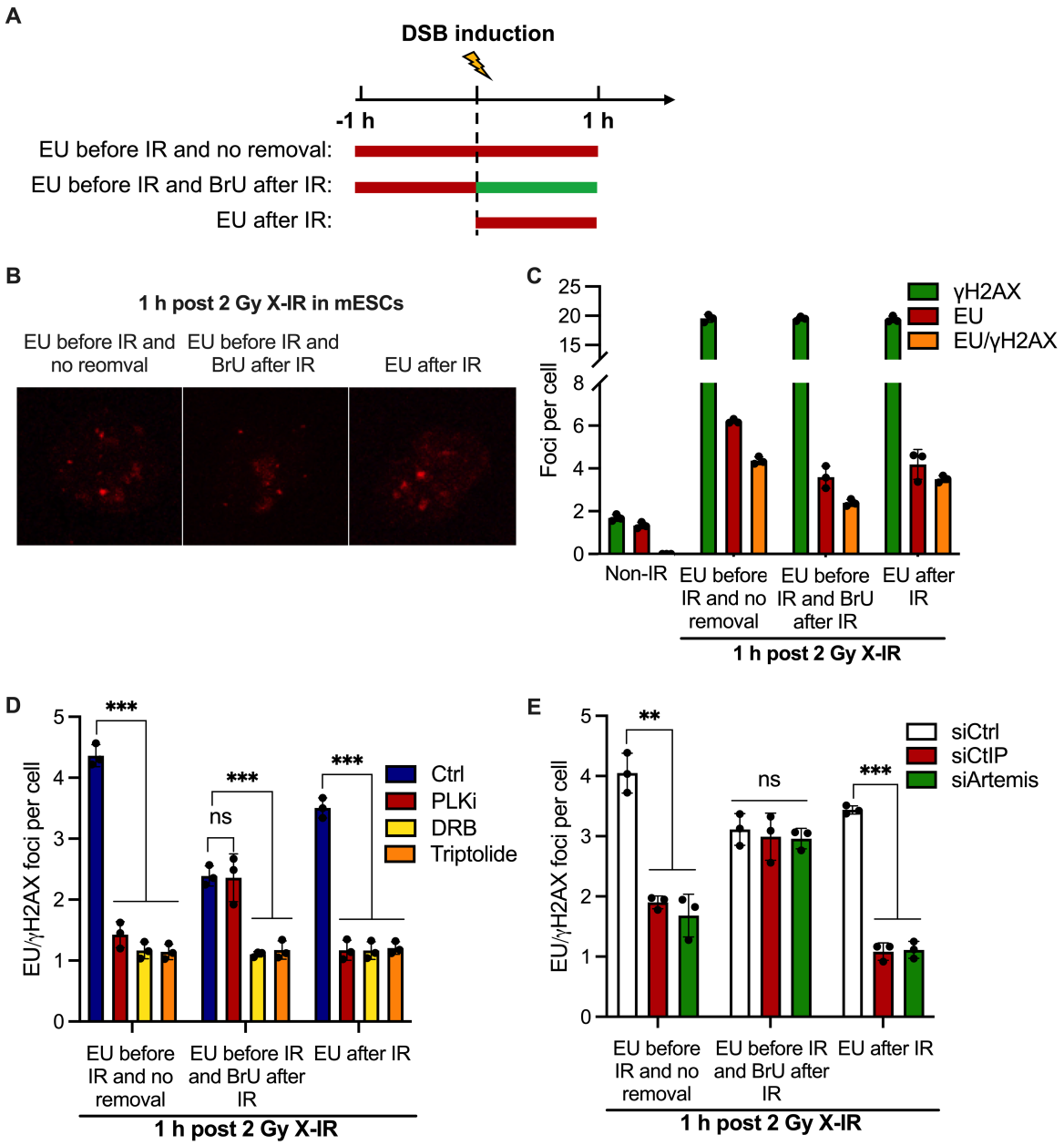

Figure 4.4 Effect of transcription and resection inhibition on nascent RNA after 2 Gy X-IR in G1-mESCs

A. Scheme of EU labeling approaches for the detection of nascent RNA transcripts at different stages during DSB repair. **B.** Representative confocal z-stack images of EU foci before and after 2 Gy X-IR in G1-mESCs. Cells were treated with EU using the three different labeling methods and EU and γH2AX foci analyses were carried out. Z-stack images were taken by a Leica TCS SP5 II confocal microscope using four different lasers (405, 488 and 594 nm). The interval between two stacks was 0.3 µm. **C.** Quantification of γH2AX and EU foci in G1-mESCs without X-IR or after 2 Gy X-IR. The number of EU foci at DSBs was evaluated based on the analysis of RGB profiles. **D** and **E.** Quantification of EU foci colocalizing with γH2AX in G1-mESCs after 2 Gy X-IR. The colocalization was analyzed using the RGB Profile Plot in the ImageJ software. All data show the mean ± S.D. and statistical significance tested by t-test (**p < 0.01, ***p < 0.001, ns: not significant). Three individual experiments are shown as dots.

The contribution of resection to RNA synthesis during repair was also analyzed. To do this, resection was inhibited by PLKi, siCtIP or siArtemis in mESCs before EU labeling and the number of EU foci which colocalized with γH2AX was quantified under the three different labeling conditions. Upon treatment with 2 Gy X-IR, resection inhibition caused a pronounced reduction of EU foci numbers at breaks during the initial DSB repair process in G1-mESCs (Fig. 4.4 D and E). In addition, resection inhibition also impaired the accumulation of newly synthesized RNA after DSB induction, but not the pre-existing RNA in G1-mESCs (Fig. 4.4 D and E). These results demonstrate that resection may only affect the formation of nascent RNA transcripts after DSB induction. Thus, it also raises a possibility that resection might also have impacts on the formation of DNA-RNA hybrids which are usually formed during transcription.

4.2.3 Kinetics of DNA-RNA hybrids and pRPA foci formation at IR-induced DSBs

In yeast, DNA-RNA hybrids have been demonstrated to regulate DNA end resection and promote the accumulation of the ssDNA-binding RPA complex during the HR-mediated repair process[91]. A direct approach to monitor the formation of DNA-RNA hybrids in DSB repair is the immunostaining by using the S9.6 antibody. However, it has been shown that the S9.6 antibody does not only specifically bind to DNA-RNA hybrids, but also to double-stranded RNA (dsRNA)[148,149]. Therefore, in order to diminish the non-specific binding of the S9.6 antibody and since RNase A can specifically degrade dsRNA at the high NaCl concentration of 300 mM[128], fixed cells were pretreated with RNase A under high salt conditions before incubating with the S9.6 antibody.

To confirm the effect of RNase A pre-treatment, mESCs were fixed by cold methanol at 1 h after 2 Gy X-IR and then incubated in 300 mM NaCl solution with or without RNase A before immunostaining. Representative immunofluorescence images showed a much clearer S9.6 foci signal and a lower background signal after the pretreatment with RNase A (Fig. 3.3 A). Additionally, the quantification analysis also shows that this pretreatment significantly reduced the S9.6 foci number (Fig. 3.3 B). These results indicate that pre-incubation with RNase A improves the specificity of the S9.6 antibody for the detection of DNA-RNA hybrids.

In order to investigate whether DNA-RNA hybrids accumulate at DSB sites and interact with resection in mammalian cells during G1 phase, a triple-immunostaining and confocal imaging approach was applied. Fixed cells were stained with γH2AX, pPRA and S9.6 antibodies simultaneously and Z-stack confocal images were taken under optimized excitation and emission settings (see in the Fig. 3.4) to avoid the interference among the different fluorescence stains. In the representative images, it can be seen that some DNA-RNA hybrids colocalized with γH2AX and a few occurred at resected DBS sites (shown as white arrows in the Fig. 4.5 A) in G1-mESCs at 1 h post 2 Gy X-IR. To better understand

how DNA-RNA hybrids participate in resection-dependent DSB repair, mESCs were fixed at different time points from 15 min to 2 h after 2 Gy X-IR. Using confocal microscopy analyses, the kinetics of pRPA and S9.6 foci formation and the colocalization of these two factors, as well as γH2AX, were numerated and subtracted the unspecific background before X-IR. Additionally, these background levels of pRPA and S9.6 were shown in the Fig. 4.5 B. The results show that DNA-RNA hybrid formation at DSBs takes place earlier than pRPA recruitment Additionally, the accumulation of DNA-RNA hybrids peaked at between 0.75 and 1 h after DSB induction. This suggests that some DNA-RNA hybrids may form before resection occurs at DSBs, supporting the hypothesis that pre-existing RNA may exist in close proximity to DSBs and serves as a template for DNA repair.

In addition, only partial colocalization between S9.6 and pRPA foci at DSBs occurred after 2 Gy in G1-mESCs (Fig. 4.5 C), indicating that the interaction of DNA-RNA hybrids and resection is either a dynamic process, or does not occur at every break. Thus, to validate their interaction, resection was inhibited in mESCs by PLKi or siCtIP and cells were fixed at 1 h post 2 Gy X-IR. The number of S9.6 foci which colocalized with γH2AX was counted. In comparison to the control group, resection inhibition caused a pronounced reduction in DNA-RNA hybrid formation at DSBs (Fig. 4.5 D). This suggests that DNA-RNA hybrids may have an indirect or direct but dynamic interaction with the resection process. Furthermore, this also implies that resection in G1 probably affects transcription, as DNA-RNA hybrids dynamically arise during transcription and mostly accumulate at actively transcribed loci[71,72].

To confirm the effect of transcription inhibition on the DNA-RNA hybrid formation after DSB induction, mESCs were treated with DRB and triptolide in different methods shown in the Fig. 4.3 C. The colocalization analysis of S9.6 and γH2AX foci showed that transcription inhibition after DSB induction caused more than a 50% reduction in DNA-RNA hybrids in G1-mESCs after 2 Gy X-IR. However, the accumulation of S9.6 foci was rescued when transcription was only inhibited at 1 h before DSB induction but resumed after damage, although it was slightly lower than in the control group (Fig. 4.5 E). This result indicates that transcription inhibition before DSB induction may only cause a delay repair in G1, similar as its impacts on resection shown in the Fig. 4.3 E. Collectively, although both transcription and resection inhibition reduced the formation of DNA-RNA hybrids and pRPA after 2 Gy X-IR, the relationship between these two processes is still unclear.

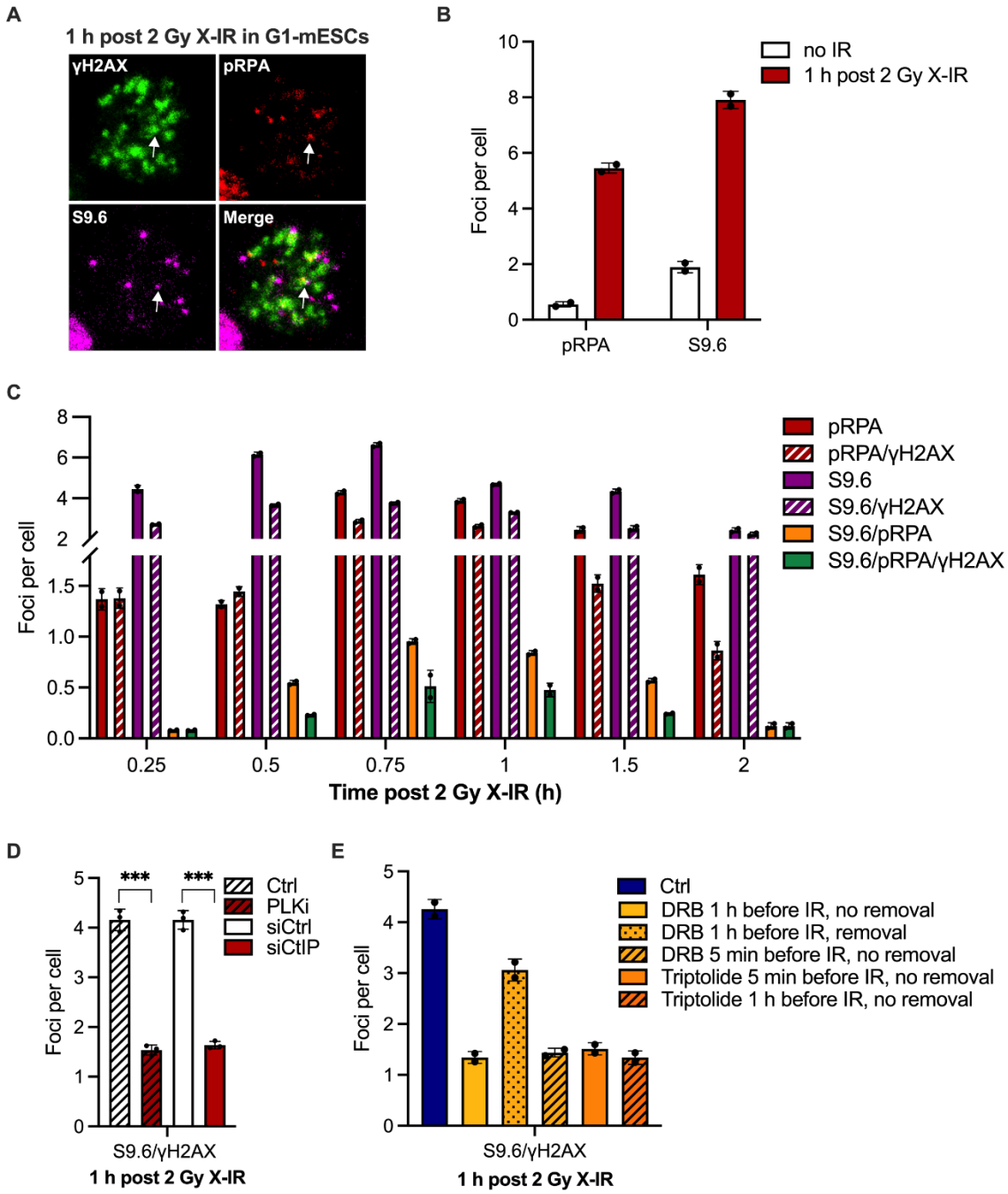

Figure 4.5 Formation of DNA-RNA hybrids at IR-induced DSBs in G1-mESCs

A. Representative images of the triple immunostaining using γH2AX, pRPA and S9.6 at 1 h post 2 Gy X-IR. **B.** Quantification of pRPA and S9.6 foci without X-IR or after 2 Gy X-IR. **C.** Kinetics of the pRPA and S9.6 foci formation at DSBs after 2 Gy X-IR. The total number of pRPA and S9.6 foci, as well as those which colocalized with γH2AX, were numerated. Cells were fixed at different time points after 2 Gy X-IR. **D.** Impacts of resection inhibition on the DNA-RNA hybrid formation at DSBs after 2 Gy X-IR. PLK inhibition (PLKi and depletion of CtIP were applied to inhibit resection in mESCs. The S9.6 foci which colocalized with γH2AX were counted. **E.** S9.6 foci at DSBs after the indicated transcription inhibition treatments. All data show the mean ± S.D. and statistical significance tested by t-test (***p < 0.001). Individual experiments are shown as dots.

4.3 Involvement of RAD52 in RNA-mediated NHEJ

4.3.1 RAD52 depletion impacts repair of IR-induced DSBs in G1

Current findings demonstrate the Rad52 is involved in RNA-mediated DNA repair by utilizing RNA as a bridge to promote annealing, or by inverse strand exchange between dsDNA and RNA or ssDNA in yeast[61,125,150]. It also has been shown that RAD52 plays a role in transcription-coupled HR in G0/G1 mammalian cells at oxidative-induced DSBs[126–128]. To evaluate whether RAD52 is required for the proper execution of DSB repair in G1-mESCs, γH2AX foci analyses were performed at 6 h post 2 Gy X-IR. The results showed that deficiency in RAD52 impaired the normal DSB repair in G1-mESCs (Fig. 4.6 A). In addition, depletion of RAD52 also caused a reduction of S9.6 foci at DSBs, indicating that RAD52 may be necessary for DNA-RNA hybrid formation after DSB induction (Fig.4.6 B). However, the lack of RAD52 did not affect the accumulation of pRPA foci in G1 after 2 Gy. This suggests that RAD52 does not regulate the initiation of resection after DSB induction, but is a downstream factor of resection in G1.

4.3.2 Additive effects of RAD52 depletion and resection or transcription inhibition at IR-induced DSBs in G1

Next, to investigate whether RAD52 also plays a role in the resection-dependent NHEJ pathway in G1 after IR, mESCs were depleted for RAD52 in combination with resection inhibition by PLKi, siCtIP or siArtemis. Surprisingly, measurement of γH2AX foci showed that the combined treatment caused an additive repair defect at 6 h after 2 Gy X-IR (Fig. 4.6 C). Moreover, partially additive repair defects were also observed under the combined treatment with siRAD52 and transcription inhibition by DRB or triptolide before DSB induction (Fig.4.6 D). These results suggest that potential roles of RAD52 may exist in the resection-independent NHEJ repair pathway, since transcription inhibition prevents resection upon DSB induction.

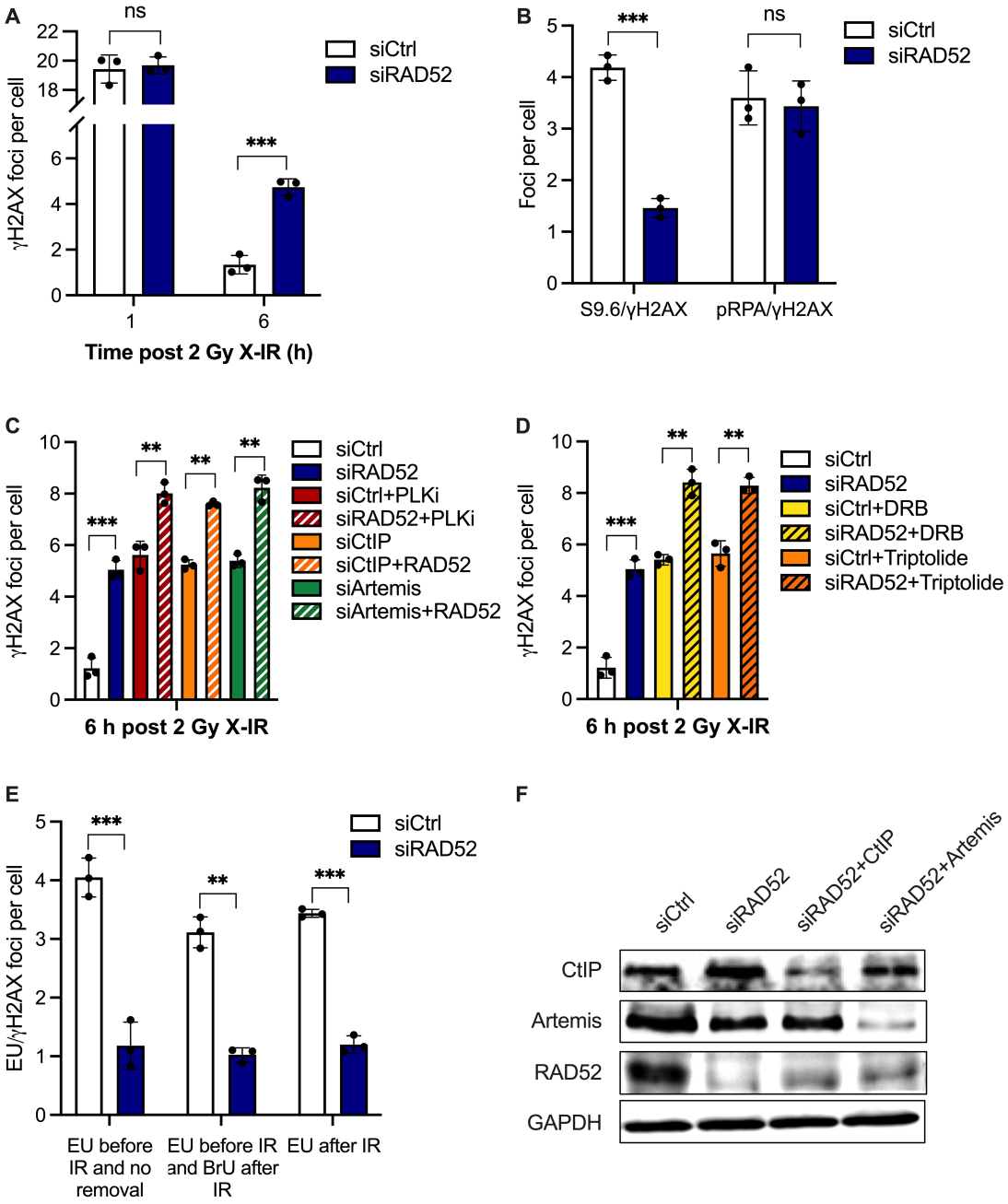

Figure 4.6 Impact of RAD52 depletion at IR-induced DSBs in mESCs

A. Numeration of γH2AX foci upon RAD52 knockdown at 1 and 6 h post 2 Gy X-IR. **B.** Quantification of S9.6 or pRPA foci colocalizing with γH2AX foci in G1-mESCs at 1 h post 2 Gy X-IR. **C.** γH2AX foci in cells treated with siRAD52 in combination with resection inhibition by PLKi, siCtIP or siArtemis at 6 h post 2 Gy X-IR. **D.** γH2AX foci in cells treated with siRAD52 and transcription inhibition by DRB or triptolide at 6 h post 2 Gy X-IR. **E.** EU foci colocalizing with γH2AX in G1-mESCs after 2 Gy X-IR. Cells were treated with siRAD52, labeled with the three EU labeling methods (shown in the Fig. 4.4 A) and damaged with 2 Gy X-IR. The colocalization was analyzed using the RGB Profile Plot in the ImageJ software. **F.** Western blot of RAD52 levels in siCtrl- and siRAD52-mESCs. All data show the mean ± S.D. and statistical significance tested by t-test (**p < 0.01, ***p < 0.001, ns: not significant). Three individual experiments are shown as dots.

4.3.3 RAD52 deficiency impairs de novo RNA synthesis at IR-induced DSBs in G1

As RAD52 affected the formation of DNA-RNA hybrids (Fig. 4.6 B), it was of interest to investigate whether RAD52 also affects the nascent RNA synthesis in G1 through the EU labeling analysis. The three different EU labeling methods explained above were used (see the section 4.2.4). The quantification analysis showed that depletion of RAD52 impairs the accumulation of nascent RNA at DSBs in all cases, independently of whether EdU was added before or after IR or whether it was removed or kept on after damage (Fig. 4.6 E). These data indicate that RAD52 depletion negatively impacts both pre-existing and DSB-induced RNA synthesis. The depletion efficiencies of siRAD52, siRAD52/CtIP and siRAD52/Artemis were verified by western blot analysis (Fig. 4.6 F).

4.4 AsiSI endonuclease-induced DSBs in G1

In order to investigate the impact of transcription and resection on DSB repair in the chromatin context during G1, the AsiSI DSB-inducible system that enables to generate DSBs at specific loci was employed in mESCs, since IR-induced DSBs occur at random locations across the genome. For this purpose, the AID-AsiSI-ER construct consisting of fused AsiSI restriction enzyme to an estrogen receptor (ER) ligand-binding domain and an auxin-inducible degron (AID)[43,48,151], was transiently transfected into mESCs. While break-induction is achieved by treatment with 4-hydroxytamoxifen (4-OHT), which binds to the ER mediating the enzyme translocation to the nucleus, auxin enables to efficiently degrade the AID-AsiSI-ER fusion enzyme, allowing to study repair (shown in the Fig. 4.7 A).

4.4.1 Repair kinetics of AsiSI-induced DSBs in G1

To confirm whether resection and DNA-RNA hybrid formation in G1 also occur at AsiSI-induced DSBs, using the AID-AsiSI-ER system, breaks were induced by a 2 h-treatment with 4OHT, and fixed at different time points after the addition of auxin. Immunofluorescence analyses for γH2AX, pRPA and S9.6 were then performed and images were taken by the confocal microscopy. The representative images showed that pRPA and S9.6 foci at AsiSI-induced DSBs were both observed in G1-mESCs (Fig. 4.7 B), which was consistent with the findings obtained upon 2 Gy X-IR (Fig. 4.5 A).

This time-course experiment also suggested that resection occurred at early time after DSB induction (from 0.25 to 1 h post DSB induction) shown in the Fig. 4.7 C. In addition, colocalization analyses of pRPA and γH2AX showed that almost 50% of AsiSI-induced DSBs were resected (Fig. 4.7 C), while only around 25% of IR-induced DSBs were dependent on resection (Fig. 4.1 C). This reveals that, in comparison to the IR-induced DSBs, the DNA repair triggered by AsiSI-induced DSBs is likely more

dependent on the resection pathway. Moreover, the repair kinetics also showed that around 50% of the DNA-RNA hybrids detected were present at AsiSI-induced DSBs (Fig. 4.7 C). Similar to the IR-induced DSBs, there were very few DNA-RNA hybrids colocalizing with pRPA foci at AsiSI-induced DSBs. This also confirms the possibility of a dynamic interaction between resection and DNA-RNA hybrid formation during DSB repair in G1.

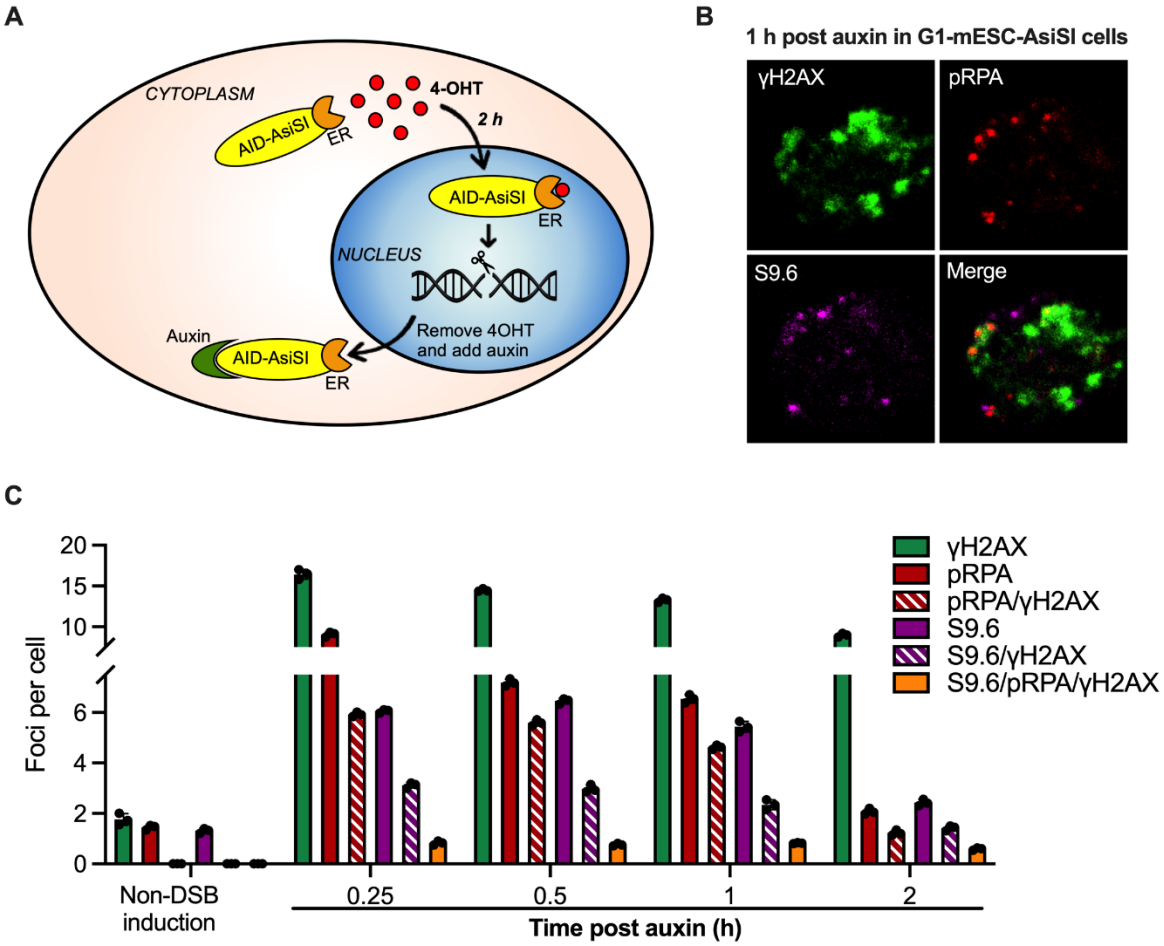

Figure 4.7 Repair kinetics of AsiSI-induced DSBs in G1-mESC-AsiSI cells

A. Scheme of DSB induction and repair in the AID-AsiSI-ER system. **B.** Representative immunofluorescence images of γH2AX, pRPA and S9.6 foci in G1 at 1 h post the addition of auxin. mESCs were treated with EdU and nocodazole for 30 min before DSB induction with 4-OHT. Z-stack images were taken by a Leica TCS SP5 II confocal microscope using four different lasers (405, 488, 594 and 633 nm). The interval between two stacks was 0.3 µm. **C.** Repair kinetics of pRPA and DNA-RNA hybrids at AsiSI-induced DSBs. The number of γH2AX, pRPA and S9.6 foci was quantified at different time points after adding auxin and subtracted the corresponding background. The number of γH2AX and pRPA foci colocalizing was counted based on the RGB Profile Plot in the ImageJ software. All data shows the mean ± S.D., and three individual experiments are shown as dots.

4.4.2 Resection and transcription inhibition affect repair in G1-AsiSI-mESCs

Next, the effect of resection on repair at AsiSI-induced DSBs in G1 was evaluated. Thereby, resection was inhibited by PLKi, siCtIP or siArtemis before break induction with 4-OHT and cells were fixed at 6 h post the addition of auxin. The quantification of γH2AX foci numbers showed that the lack of these resection factors caused a repair defect in G1 (Fig. 4.8 A). As expected, inhibition of resection by combining any two of these factors showed an epistatic effect (Fig. 4.8 A). This confirms that upon CtIP depletion, cells are not able to switch from resection-dependent to resection-independent NHEJ pathway after DSBs induction by AsiSI.

Additionally, the effects of transcription inhibition were also analyzed. The use of the transcription inhibitors DRB and triptolide also caused a repair defect in G1 at 6 h post the addition of auxin (Fig. 4.8 B). Moreover, combining resection and transcription inhibition did not trigger additive repair defects (Fig. 4.8 B), corroborating that both resection and transcription are potentially involved in the same DSB repair pathway in G1.

4.4.3 Resection and transcription inhibition impact pRPA and S9.6 foci formation at AsiSI-induced DSBs

Since repair defects were observed by resection and transcription inhibition at AsiSI-induced DSBs in G1, it was of interest to further investigate how resection and transcription impact DSB repair. For this purpose, pRPA and S9.6 foci formation was examined at 1 h post adding auxin addition in mESC-AsiSI cells which resection was inhibited by PLKi, siCtIP or siArtemis. Colocalization analyses of pRPA and S9.6 foci at DSBs showed that resection inhibition impedes not only the accumulation of pRPA at breaks, but also DNA-RNA hybrid formation in G1 (Fig. 4.8 C). This indicates that resection inhibition may impair transcription after DSB induction *via* AsiSI. However, a decrease in pRPA recruitment at breaks was observed when transcription was inhibited before DSB induction (Fig. 4.8 D), clarifying that instead transcription may promote resection after DSB induction. Taken together, this confirms that an interaction between resection and transcription during DSB repair also exists in the AsiSI-inducible system.

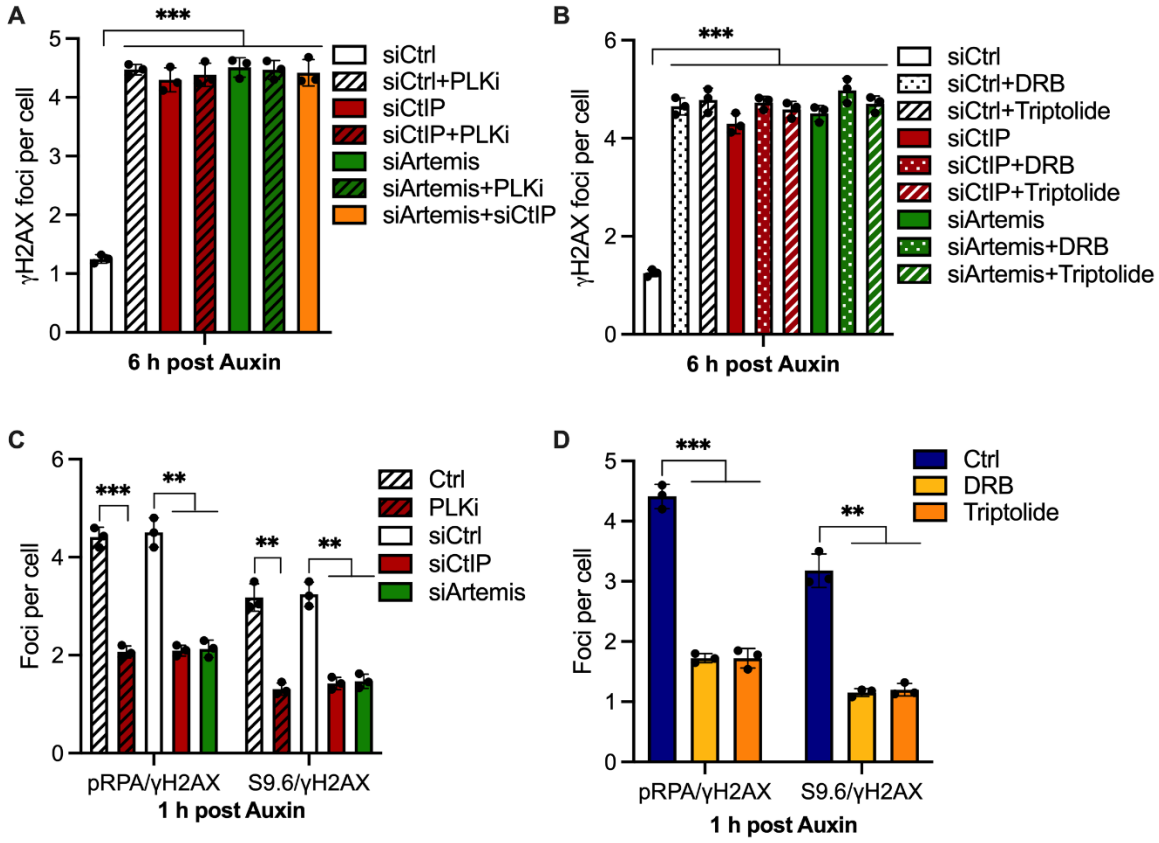

Figure 4.8 Effects of resection and transcription inhibition on DSB repair in G1-mESC-AsiSI cells

A. γH2AX foci after resection inhibition by PLKi, siCtIP and siArtemis or upon combination of these treatments at 6 h post the addition of auxin. **B.** γH2AX foci after transcription inhibition by DRB or triptolide and upon the combination of resection and transcription inhibition at 6 h post the addition of auxin. **C** and **D**. pRPA foci and DNA-RNA hybrids (S9.6 foci) after resection (C) and transcription (D) inhibition at AsiSI-induced DSBs in G1. The pRPA and S9.6 foci at DSBs were numerated at 1 h after the addition of auxin. PLKi and depletion of CtIP or Artemis were used for resection inhibition, while DRB and triptolide were used for transcription inhibition. All data show the mean ± S.D. and statistical significance tested by t-test (**p < 0.01, ***p < 0.001). Three individual experiments are shown as dots.

4.4.4 RAD52 deficiency affects repair of AsiSI-induced DSBs in G1

Considering the role of RAD52 at IR- induced DSBs, it was also examined whether RAD52 played a similar role at enzyme induced breaks. For this, the repair capacity of mESC-AsiSI cells upon RAD52 depletion was first evaluated through the quantification of γH2AX foci in G1 both at 1 and 6 h post auxin addition. These analyses showed that there was no difference between mock and siRAD52 treatment at 1 h after DSB induction. However, deficiency of RAD52 led to an increased number of γH2AX foci at 6 h post the addition of auxin in G1 (Fig. 4.9 A). To further investigate the function of RAD52 in DSB repair in G1-mESC-AsiSI cells, the colocalization of γH2AX, pRPA and S9.6 in cells

depleted for RAD52 was evaluated at 1 h after adding auxin. Quantification analyses showed that deficiency of RAD52 did not affect the recruitment of pRPA, but impaired the formation of DNA-RNA hybrids at DSBs in G1 after AsiSI-induced DSBs (Fig. 4.9 B). Hence, this suggests that RAD52 acts downstream of pRPA and thus that the occurrence of resection at AsiSI-induced DSBs is independent of RAD52, while DNA-RNA hybrid formation is promoted by RAD52.

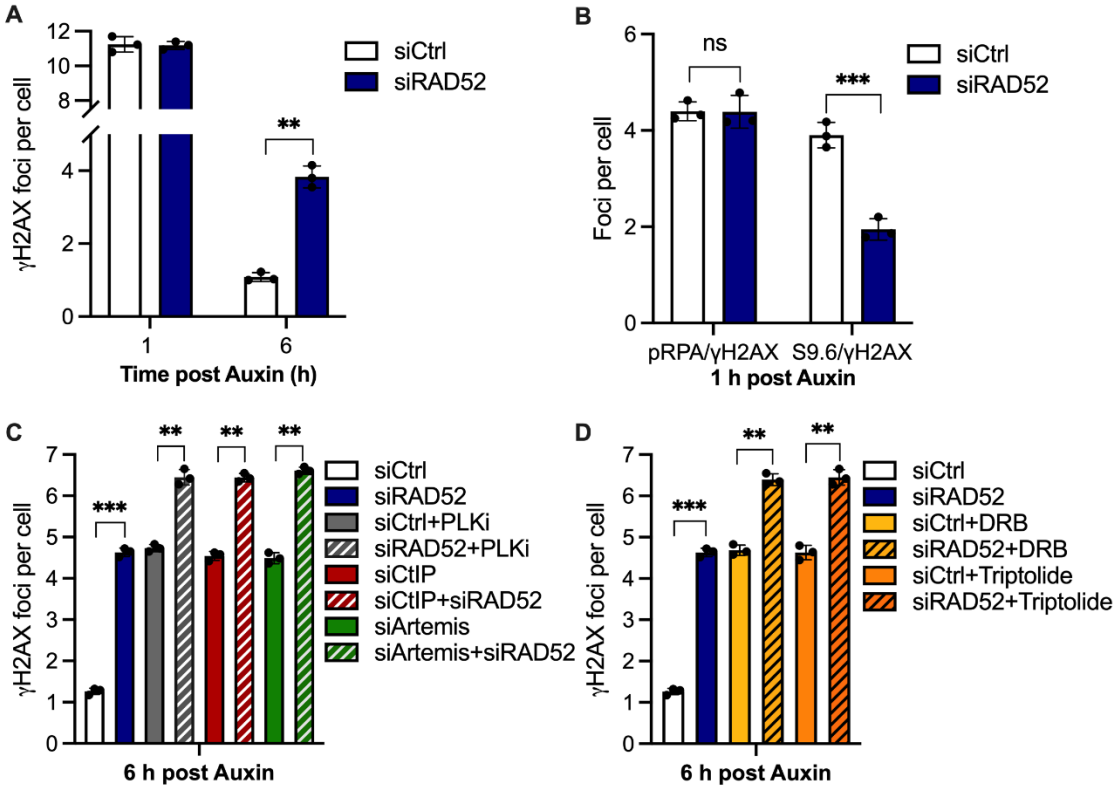

Figure 4.9 Impact of RAD52 depletion on AsiSI-induced DSBs in G1-mESC-AsiSI cells

A. γH2AX foci upon RAD52 knockdown at 1 and 6 h post the addition of auxin in G1. **B.** Quantification of S9.6 and pRPA foci colocalizing with γH2AX foci at 1 h post the addition of auxin. **C.** γH2AX foci in cells treated with siRAD52 in combination with resection inhibition by PLKi, siCtIP or siArtemis at 6 h post auxin addition. **D.** γH2AX foci in cells treated with siRAD52 and transcription inhibition by DRB or triptolide at 6 h post auxin addition. All data show the mean ± S.D. and statistical significance tested by t-test (**p < 0.01, ***p < 0.001, ns: not significant). Three individual experiments are shown as dots.

4.4.5 Additive effects of RAD52 depletion and resection or transcription inhibition at AsiSI-induced DSBs in G1

With the aim of exploring whether RAD52 has other roles during AsiSI-induced DSB repair which are independent of resection and transcription, mESCs were co-treated with siRAD52 and resection

or transcription inhibition before DSB induction. In comparison to the individual treatments, these combinations caused higher repair defects at 6 h post the addition of auxin (Fig. 4.9 C and D). These data confirm that deficiency of RAD52 may also impair the resection- and transcription-independent DSB repair components in G1-AsiSI-mESCs.

4.5 I-PpoI endonuclease-induced DSBs in G1

Although all above data support that the AsiSI-inducible system is a potentially suitable approach to study locus specific DSB repair in the genome, a limitation of this system is the long time required for DSB induction (2 h incubation with 4-OHT). Since G1 phase lasts only 2-3 h in mESCs, using the AsiSI system, it would not be technically possible to collect sufficient G1-mESCs to do a deep genomic analysis using ChIP-qPCR. Hence, the I-PpoI homing endonuclease-inducible system, DD-ER-I-PpoI, was considered for this purpose. This system allows break induction based on the same estrogen receptor (ER) as in the AsiSI system, which upon the addition of 4-OHT mediates the re-localization of the I-PpoI enzyme to the nucleus (shown in the Fig. 4.10 A). Additionally, to monitor DSB repair this approach relies on a destabilization domain (DD) to tightly control the expression of the ER-I-PpoI fusion protein. With the aid of shield-1 which binds and blocks the DD, the ER-I-PpoI fusion protein will be stabilized before DSB induction. This allows the reduction of the induction time with 4-OHT to 15 min, making it an ideal system to monitor DSB repair at specific cut sites in mESCs during G1 phase.

4.5.1 Repair kinetics of I-PpoI-induced DSBs in G1

To validate the DD-ER-I-PpoI system and investigate whether resection and DNA-RNA hybrid formation occur at I-PpoI-induced DSBs, DNA repair kinetics were monitored in G1. Immunofluorescence analyses using a confocal microscope were used to study the formation of γH2AX, pRPA and S9.6 foci in mESC-I-PpoI cells at 1 h post the DSB induction by 4-OHT in G1 (Fig. 4.10 B). Both resection and DNA-RNA hybrid formation were observed at DSBs induced by I-PpoI-ER. Colocalization analyses of γH2AX and pRPA showed that resection appeared at early times after DSB induction, and predominantly occurred at DSBs (Fig. 4.10 C). Furthermore, the quantification of γH2AX and S9.6 foci indicated that most of DNA-RNA hybrids were found at DSBs induced by I-PpoI in G1-mESCs. However, consistently with the results for IR- and AsiSI-induced DSBs (Fig. 4.5 C and Fig. 4.7 C), the colocalization of pRPA and DNA-RNA hybrids was also limited after I-PpoI-induced DSBs (Fig. 4.10 C). This result is in an agreement with the hypothesis that the interaction between resection and DNA-RNA hybrids at DSBs is likely to be indirect.

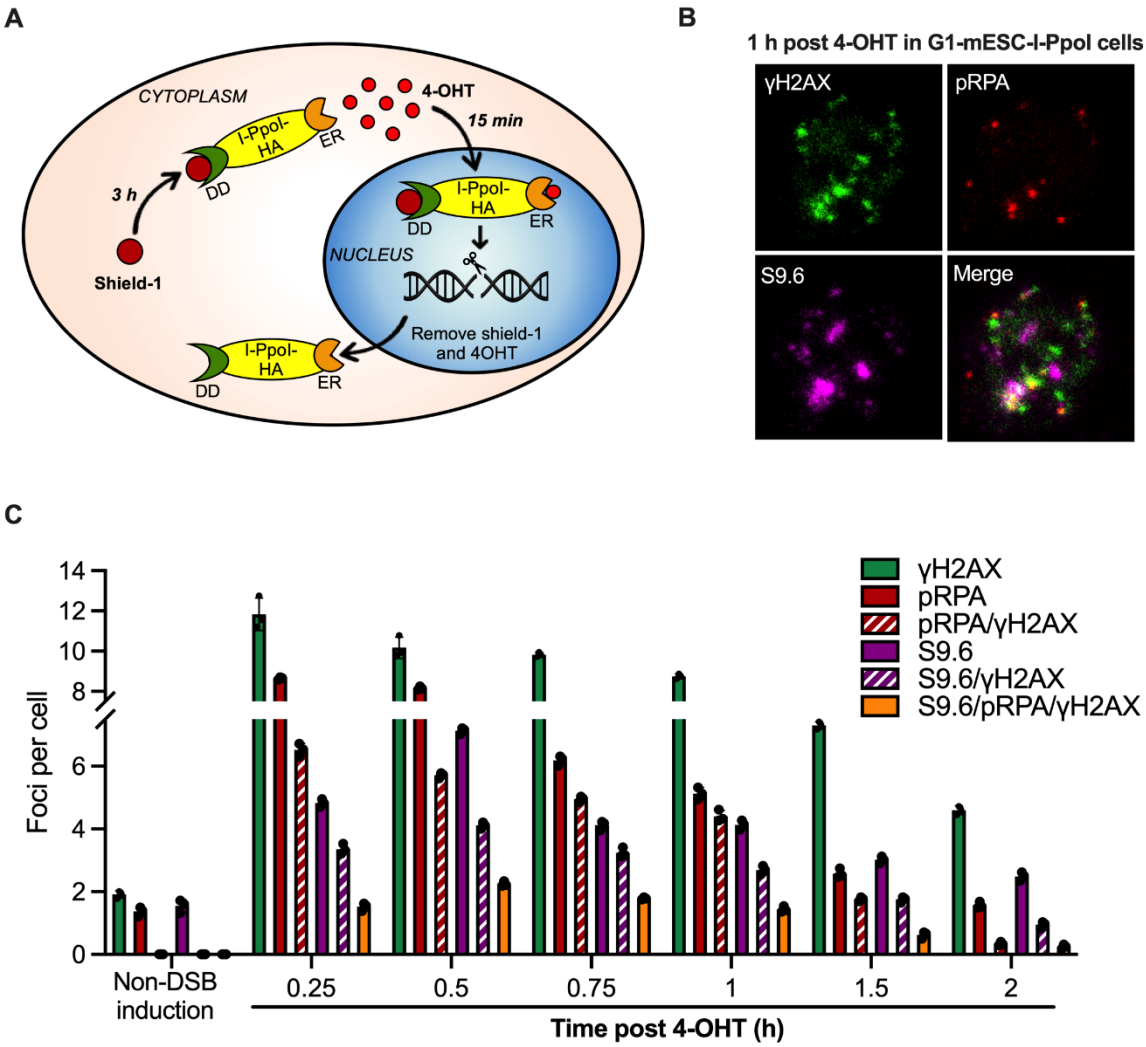

Figure 4.10 Repair kinetics of I-PpoI-induced DSBs in G1-mESC-I-PpoI cells

A. Scheme of DSB induction and repair in the DD-I-PpoI-ER system. **B.** Representative immunofluorescence images of γH2AX, pRPA and S9.6 foci in G1 at 1 h post the removal of 4-OHT. mESCs were treated with EdU and nocodazole for 30 min before DSB induction with 4-OHT. Z-stack images were taken by a Leica TCS SP5 II confocal microscope using four different lasers (405, 488, 594 and 633 nm). The interval between two stacks was 0.3 µm. **C.** Repair kinetics of pRPA and DNA-RNA hybrid at I-PpoI-induced DSBs. The number of γH2AX, pRPA and S9.6 foci was quantified at different time points after the removal of 4-OHT. The number of γH2AX and pRPA foci colocalizing was counted based on the RGB Profile Plot in the ImageJ software. All data shows the mean ± S.D., and three individual experiments are shown as dots.

4.5.2 Resection and transcription inhibition affect repair in G1-mESC-I-PpoI cells

Subsequently, the roles of resection and transcription during DNA repair at I-PpoI-induced DSBs were evaluated. mESC-I-PpoI cells were treated with inhibitors or siRNAs to block resection and

transcription before the 4-OHT-treatment. Increased levels of γH2AX foci were found at 6 h post DSB induction upon resection or transcription inhibition. On the contrary, combined inhibition of resection and transcription did not cause additive repair defects in G1-mESC-I-PpoI cells (Fig. 4.11 A and B). This is consistent with the previous data, suggesting that resection and transcription are involved in the same DSB repair sub-pathway in G1.

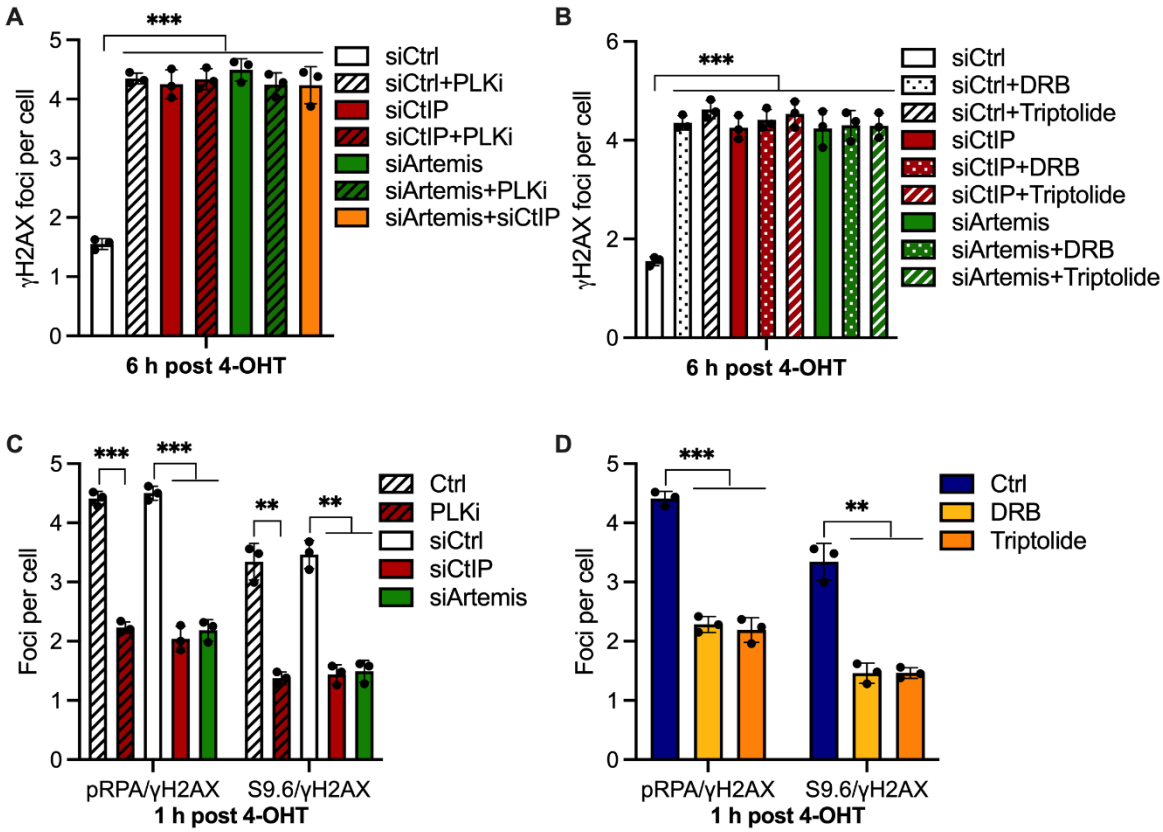

Figure 4.11 Effects of resection and transcription inhibition on DSB repair in G1-mESC-I-PpoI cells

A. γH2AX foci after resection inhibition by PLKi, siCtIP and siArtemis or upon combination of these treatments at 6 h post the removal of 4-OHT. **B.** γH2AX foci after transcription inhibition by DRB or triptolide, and upon the combination of resection and transcription inhibition at 6 h after removing 4-OHT. **C** and **D.** pRPA foci and DNA-RNA hybrids (S9.6 foci) after resection (C) and transcription (D) inhibition at I-PpoI-induced DSBs in G1. The pRPA and S9.6 foci at DSBs were numerated at 1 h after removal of 4-OHT. PLKi and depletion of CtIP or Artemis were used for resection inhibition, while DRB and triptolide were used for transcription inhibition. All data shows the mean ± S.D. and statistical significance tested by t-test (**p < 0.01, ***p < 0.001). Three individual experiments are shown as dots.

4.5.3 Resection and transcription inhibition impact pRPA and S9.6 foci formation at I-PpoI-induced DSBs

Using the DD-ER-I-PpoI system, the effect of resection and/or transcription inhibition on the formation of pRPA foci and DNA-RNA hybrids at I-PpoI-induced DSBs was also evaluated. As expected, inhibiting resection caused a reduction in the accumulation of pRPA, as well as in the DNA-RNA hybrid formation at I-PpoI-induced DSBs (Fig. 4.11 C). Strikingly, when transcription was hindered before DSB induction, a decrease of pRPA foci formation was also observed at 1 h post 4-OHT treatment (Fig. 4.11 D). These observations support the notion that resection could positively impact transcription after DSB induction, while the initiation of resection also requires transcription.

4.5.4 RAD52 deficiency affects repair of I-PpoI-induced DSBs

Since RAD52 was shown to be required for the repair of IR- and AsiSI-induced breaks, it was also of interest to study whether RAD52 is required for DNA repair at I-PpoI-induced DSBs. For this purpose, the number of γH2AX foci was numerated in G1 cells at 1 and 6 h after 4-OHT-treatment. Whereas RAD52-deficiency did not affect the initial γH2AXlevels (1h-time point), it led to increased levels of unrepaired breaks at the 6 h-repair time point (Fig. 4.12 A). This suggests that deficiency of RAD52 also causes a repair defect at I-PpoI-induced DSBs. Additionally, measurement of pRPA foci and DNA-RNA hybrids using the S9.6 antibody showed that knockdown of RAD52 did not affect resection, but reduced the formation of DNA-RNA hybrids at DSBs during the early stages of DSB repair (Fig. 4.12 B). These results are consistent with the previous observations in the repair of X-IR- and AsiSI-induced DSBs.

4.5.5 Additive effects of RAD52 depletion and resection or transcription inhibition at I-PpoI-induced DSBs in G1

Subsequently, as it was previously shown for the other DSB induction systems that RAD52 has also resection-independent roles, mESC-I-PpoI cells were treated with siRAD52 in combination with resection inhibition before DSB induction and fixed at 6 h post 4-OHT treatment. The combination of these caused an accumulation of additional γH2AX foci when compared to the individual treatment, indicating that RAD52 may also have other functions which are independent of resection during I-PpoI-induced DSB repair (Fig. 4.12 C).

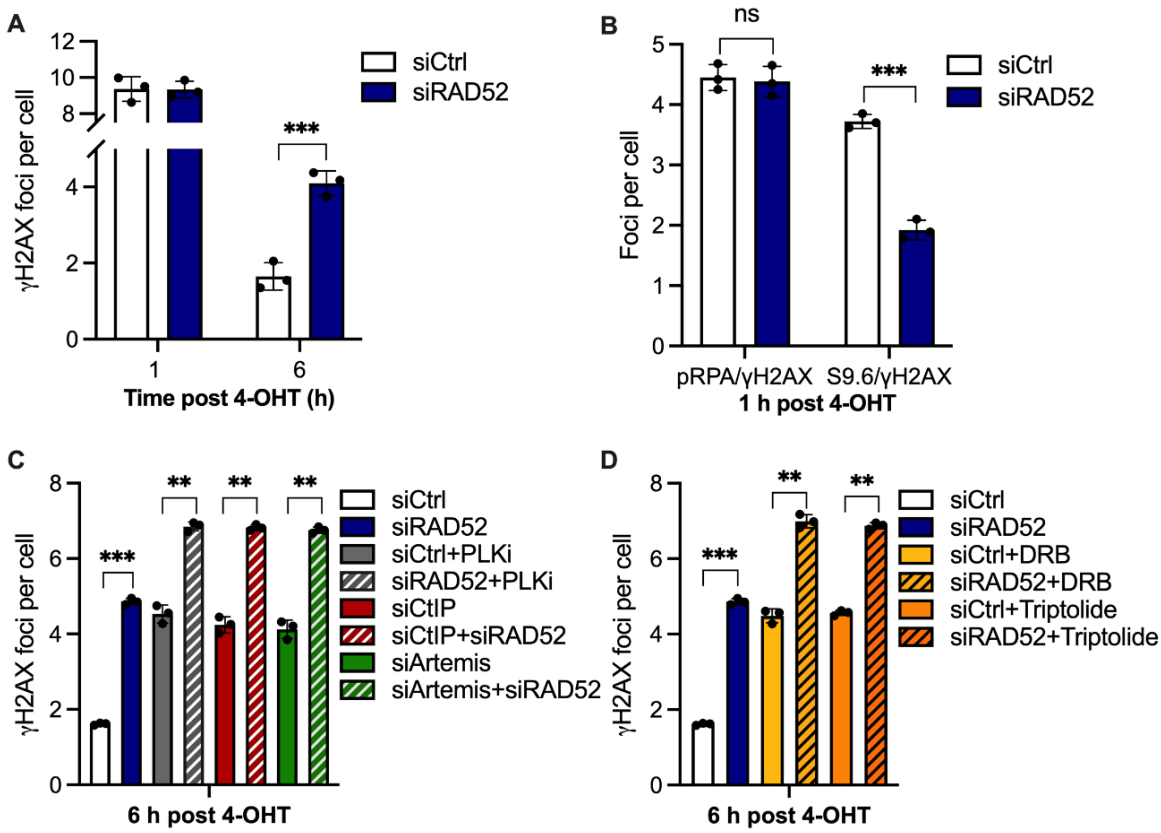

Figure 4.12 Impact of RAD52 depletion on DSB repair in G1-mESC-I-PpoI cells

A. γH2AX foci upon RAD52 knockdown at 1 and 6 h post the addition of auxin in G1. **B.** Quantification of S9.6 and pRPA foci colocalizing with γH2AX foci at 1 h post the addition of auxin. **C.** γH2AX foci in cells treated with siRAD52 in combination with resection inhibition by PLKi, siCtIP or siArtemis at 6 h post auxin addition. **D.** γH2AX foci in cells treated with siRAD52 and transcription inhibition by DRB or triptolide at 6 h post post auxin addition. All data show the mean ± S.D. and statistical significance tested by t-test (**p < 0.01, ***p < 0.001, ns: not significant). Three individual experiments are shown as dots.

Furthermore, it was also of interest to validate the impact of combining RAD52 depletion with DRB or triptolide on the repair of I-PpoI-induced DSBs. Again, an increased number of γH2AX foci remaining at 6 h post damage was also observed for the combined treatment in G1-mESC-I-PpoI cells (Fig. 4.12 D). This is consistent with the above result for the combination treatment with siRAD52 and resection inhibition. Taken together, these results indicate that an additional role of RAD52 may exist in a resection- and transcription-independent manner.

4.6 Impact of resection on the repair of I-PpoI-induced DSBs in G1 in a genome-wide context

4.6.1 Optimization of cell sorting for genome-wide functional analysis in G1

According the above results, the I-PpoI-inducible system appears to be a suitable model to further investigate how resection affects the DSB repair at specific loci in the genome through ChIP-qPCR analyses. Using this strategy, since resection-dependent repair also involves transcription, it was set to investigate whether this process occurred at specific genomic locations, such as genes. In order to do this in a cell cycle-specific manner, cell synchronization was necessary. To do this, cell sorting was chosen as it allowed synchronization without physiological perturbation. To enrich for G1 cells, asynchronous cells were fixed with 1% FA, labeled by EdU for S phase discrimination and stained with SYTOX™ AADvanced™ for nucleic acid detection. Taking advantage of the differences in the DNA content and EdU incorporation, the cell cycle of mESCs was monitored by fluorescence-activated cell sorting (FACS), thus allowing the sorting of G1 cells. Briefly, the single cells were first identified in the forward versus side scatter (FSC and SSC) plot (Fig. 4.13 A), allowing the exclusion of debris and doublets. Three cell cycle stages (G0/G1, S and G2) were distinguished from this single cell population depending on the DNA content and EdU labeling. The normal cell cycle profile of mESCs is shown in the Fig.4.13 B, which consists of around 13.5% of G0/G1phase, 64% of S phase and 22.5% of G2 phase cells (Fig. 4.13 C).

For genomic analyses of DSB repair in G1 phase, mESC-I-PpoI cells were treated with nocodazole before DSB induction to avoid cell cycle progression from G2 to G1. Cells were then fixed at an early time after DNA damage (1 h) and at a later time during DSB repair (4 h). FACs results showed that 8% of cells remained in G1 phase at 1 h after 4-OHT treatment, while only 2% of cells were in G1 phase at 4 h after DSB induction (Fig. 4.13 D and E). Due to the short G1 phase in mESCs and the millions of cells required for ChIP-seq analysis, it was challenging to obtain sufficient G1 cells at 4 h after DSB induction by cell sorting. Hence, in order to increase the number of G1 cells obtained at this time point without affecting DSB repair, aphidicolin (APH), which prevents DNA replication by hindering DNA polymerases, was used to arrest cells in G1[152]. The FACS results showed that the percentage of cells remaining in G1 when they were treated with APH at 4 h after DSB induction was around 4 % (Fig. 4.13 F). Other synchronization methods such as treatment with lovastatin were also tested, however, the proportion of G1 cells could not be improved further (data not shown). Last, resection inhibition by PLKi or siCtIP, and depleting RAD52 did not affect the cell cycle progression of after DSB induction (Fig. 4.13 G and H).

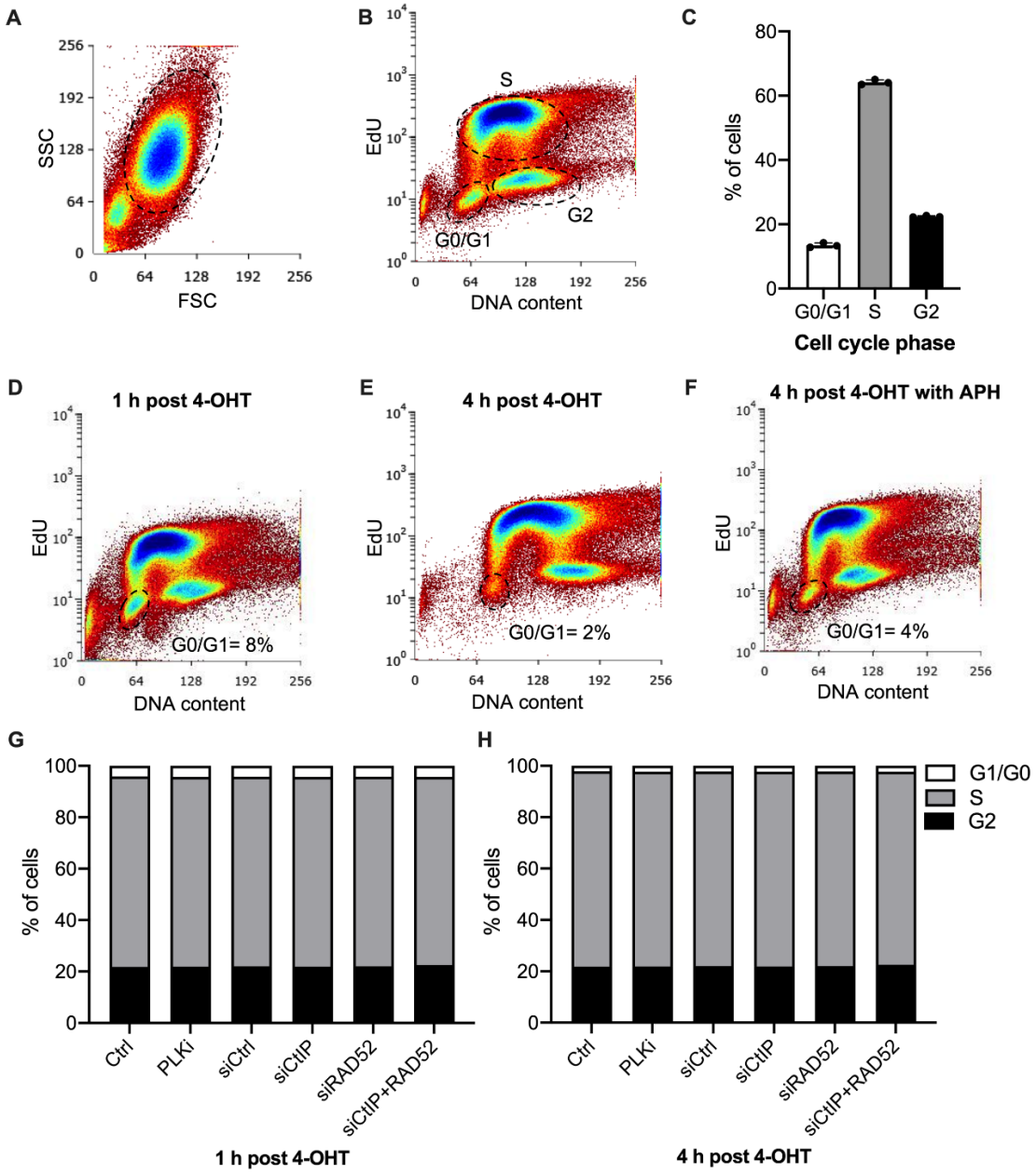

Figure 4.13 FACS analyses of mESC-I-PpoI cells

A. Representative example of the single cell population gating strategy. For this, asynchronous cells were visualized in the FSC/SSC scatterplot, allowing the discrimination of single cells (encircled) from debris and doublets. **B.** FACS profile of the normal cell cycle in mESC-I-PpoI cells, according to 30 min-EdU incorporation and DNA content. **C.** Histograms showing the percentage of cells in each cell cycle phase in panel B, which was calculated by the ProSort™ software. All data show the mean ± S.D. Three individual experiments are shown as dots. **D-E.** Representative cell cycle profile of mESC-I-PpoI cells at 1 h (D) and 4 h (E) post 4-OHT treatment. **F.** Representative cell cycle profile of mESC-I-PpoI cells upon treatment with 2 μM APH at 1 h after 4OHT for 3 h. **G** and **H.** Histograms showing the cell cycle distribution at 1 h (G) or 4 h (F) post 4-OHT under different treatments, including PLKi, siCtIP, siRAD52 and co-depletion of CtIP and RAD52. The data shows a single experiment.

4.6.2 Resection-dependent DSB repair in G1 occurs in genes

The I-PpoI homing endonuclease has a 15 bp-recognition sequence (CTCTCTTAA▼GGTAGC) to induce sequence-specific DSBs in the genome[153]. To identify the I-PpoI restriction sites in the mouse genome, an *in silico*-digestion of I-PpoI in the Genome Reference Consortium Mouse Build 38 (GRCm38), also known as mm10, was performed using the software of Integrative Genomics Viewer. 19 canonical cutting sites were detected, including 9 intragenic and 10 intergenic sites (Table 4.1). For ChIP-qPCR analyses, primers at three intragenic sites and two intergenic sites were designed for studying DSB repair, while primers for two non-cut sites were used as negative controls. In particular, the three intragenic sites were monitored at Chr1: 93152778-93152793 (Chr1), Chr9: 113566729-113566744 (Chr9) and Chr13: 45898836-45898851 (Chr13), whereas the two intergenic sites were located in Chr3: 5860448-5860463 (Chr3) and Chr4: 72028079-72028094 (Chr4).

Table 4.1 Canonical cutting sites of I-PpoI in the mouse genome

	Chr	Start	End	Closest_gene	Distance (bp)
1	Chr1	46076092	46076107	NM_001160386	0
2	Chr1	93152778	93152793	NM_172411	0
3	Chr1	113904181	113904196	NM_001077425	1,780,941
4	Chr1	191121000	191121015	NM_030060	12,059
5	Chr3	5860448	5860463	NM_001163302	284,202
6	Chr3	121249933	121249948	NM_178936	0
7	Chr3	138077304	138077319	NR_037975	9,918
8	Chr4	72028079	72028094	NM_011599	89,048
9	Chr5	114852057	114852072	NM_026263	1,642
10	Chr7	120754158	120754173	NM_177697	0
11	Chr9	113566729	113566744	NR_040760	0
12	Chr10	55572700	55572715	NM_001033385	441,579
13	Chr12	80441526	80441541	NM_177267	4,927
14	Chr13	45898836	45898851	NM_001199305	0
15	Chr14	56694145	56694160	NM_023773	0
16	Chr17	6941932	6941947	NM_001083945	0
17	Chr17	7952357	7952372	NM_025789	0
18	Chr17	24666011	24666026	NM_183149	3,726
19	ChrX	116287261	116287276	NM_001033471	161,668

To confirm the DSB generation by I-PpoI in G1, a γH2AX ChIP-qPCR analysis was performed in mESC-I-PpoI sorted G1 cells which were fixed at 1 h post 4-OHT treatment. In comparison with the uninduced controls, a 2 to 2.5-fold increase in the γH2AX signal was observed in both intragenic and intergenic sites, whereas as expected no increase was found at the two uncut sites. Moreover, resection inhibition by PLKi led to no difference in the γH2AX signal in comparison to the control group at 1 h post DSB induction in all cutting sites (Fig. 4.14 A). This suggests that resection inhibition before DSB induction does not affect the initial stages of DSB repair in G1.

To validate whether resection arises in G1 after DSB induction by I-PpoI (1 h post 4-OHT treatment), the pRPA ChIP-qPCR analysis in mESC-I-PpoI sorted G1 cells was employed. Interestingly, in comparison with the uninduced controls, a 2 to 3-fold increase in the pRPA level was observed when DSBs occurred in the three intragenic cutting sites. However, no increased signals were detected when DSBs arose in intergenic and uncut regions. In addition, a remarkable reduction in pRPA recruitment in the intragenic regions was observed when resection was abolished by PLKi (Fig. 4.14 B). Altogether, these results indicate that resection likely occurs in genes during DSB repair in G1-mESCs, but not in non-genic regions.

To elucidate how resection impacts DSB repair at the different genomic locations studied, cells were fixed at 4 h post DSB induction by I-PpoI. Then γH2AX ChIP-qPCR analysis in sorted G1 cells was performed. In comparison with the non-inhibited controls, a 1.5-fold increase in the γH2AX signal upon PLKi treatment was observed in the three intragenic sites, whilst no increase was found in intergenic and uncut regions (Fig. 4.14 C). This indicates that in G1-mESCs resection seems to be required only for DSB repair in genes.

As previously discussed, one of the limitations of doing genome-wide analysis by ChIP-seq is the requirement of millions of cells, which is a bottleneck for G1-mESCs as they have a very short G1 phase. To circumvent this problem, addition of APH at 1 h post 4-OHT for 3 h until cell fixation took place was shown to efficiently increase the G1 population. To validate whether treatment with APH to arrest cells in G1 may also affect DSB repair in G1, APH-treated sorted G1 cells were analyzed by γH2AX ChIP-qPCR at 4 h post damage induction. In contrast to the induced γH2AX levels at 1 h post 4-OHT, a decrease in the γH2AX signal was also found in APH-treated G1 cells at 4 h post DSB induction (Fig. 4.14 D). This decrease was similar to the one observed for cells without APH (Fig. 4.14 C), suggesting that APH does not impede normal DSB repair in G1. Furthermore, upon arrest by APH, the elevated γH2AX signal in the PLKi group at 4 h post 4-OHT in G1 was still specific for intragenic regions, but neither intergenic nor uncut sites (Fig. 4.14 D). Overall, these data support that APH treatment does not hinder DSB repair, therefore allowing monitoring of the impact that resection has on this process through ChIP-seq analysis.

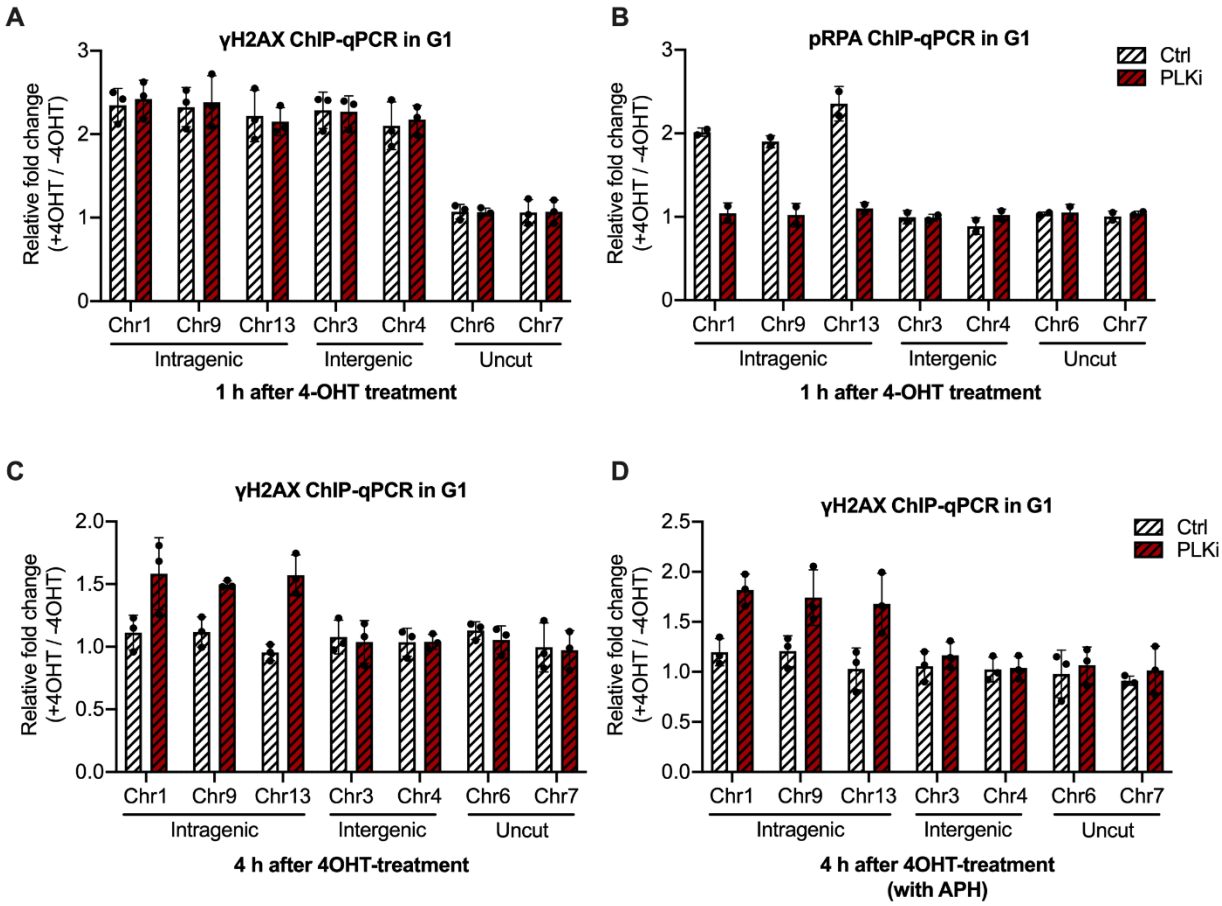

Figure 4.14 ChIP-qPCR analysis of I-PpoI-induced DSBs after PLKi treatment

A. γH2AX ChIP-qPCR analysis in G1-mESC-I-PpoI cells at 1 h post 4-OHT treatment, with or without PLKi. All data show the mean ± S.D. Three individual experiments are shown as dots. **B.** pRPA ChIP-qPCR analysis in G1-mESC-I-PpoI cells at 1 h post 4-OHT treatment, with or without PLKi. All data show the mean ± S.D., and two individual experiments are shown as dots. **C.** γH2AX ChIP-qPCR analysis in G1-mESC-I-PpoI cells at 4 h post 4-OHT treatment, with or without PLKi. **D.** γH2AX ChIP-qPCR analysis in G1-mESC-I-PpoI cells at 4 h post 4-OHT and APH treatment, with or without PLKi at 1 h post break induction by 4-OHT. Cells were treated with 2 μM APH at 1 h after DSB induction kept until fixation. All data show the mean ± S.D., and three individual experiments are shown as dots. The relative fold change was calculated by the ratio between +4OHT and -4OHT. Three different genomic locations were analyzed (intragenic cut sites, intergenic cut sites and uncut sites).

4.6.3 Deficiency of RAD52 in G1 does not affect DSB repair in genes

Next, the effect of RAD52 depletion on DSB repair was also studied at different genomic locations. Previous γH2AX studies showed that single RAD52 depletion caused a repair defect in G1-mESCs and that additional defects were observed by co-depleting CtIP and RAD52. Following this, it still remained to be clarified whether those repair defects caused by siRAD52 arose in a resection-

dependent or -independent manner. For this, γH2AX ChIP-qPCR analysis were performed in G1-mESC-I-PpoI sorted cells at 1 h post DSB induction by I-PpoI and after different treatments, including siCtrl, siCtIP, siRAD52 and co-depletion of CtIP and RAD52. No substantial difference in the γH2AX level after DSB induction was observed for all cutting sites under both individual and combined depletion of siCtIP and siRAD52 (Fig. 4.15 A). This confirms that resection inhibition, deficiency of RAD52 and combination of both treatments do not affect the DSB induction in G1.

Additionally, cells were fixed at 4 h post 4-OHT to study DSB repair and G1 cells were also sorted for γH2AX ChIP-qPCR analysis. In accordance to the results of resection inhibition by PLKi, CtIP depletion caused an increase in the γH2AX signal in the intragenic but not intergenic cutting sites (Fig. 4.15 B). Strikingly, upon RAD52 depletion, there was no increase in the level of γH2AX detected in these three intragenic regions, while elevated γH2AX levels occurred in the two intergenic regions analyzed (Fig. 4.15 B). This indicates that RAD52 is dispensable for resection-dependent DSB repair in G1, but may be required for the repair of DSBs that fall in resection-independent regions.

Moreover, pRPA ChIP-qPCR analysis in G1-mESC-I-PpoI sorted cells at 1 h post 4-OHT was conducted to directly study the impact of of resection inhibition and depletion of RAD52 on pRPA formation at these genomic locations. Similar to PLKi, resection inhibition by siCtIP also caused a decline of pRPA levels in intragenic cutting sites. However, deficiency of RAD52 did not reduce the pRPA signal in these intragenic regions (Fig. 4.15 C). Similar as previously shown, pRPA signals were also not increased upon DSB induction at intergenic or uncut regions (Fig. 4.15 C). This suggests that deficiency of RAD52 does not affect the recruitment of pRPA and therefore resection during DSB repair in G1. Taken together, these results demonstrate that G1-resection in genes is likely not dependent on the protein RAD52.

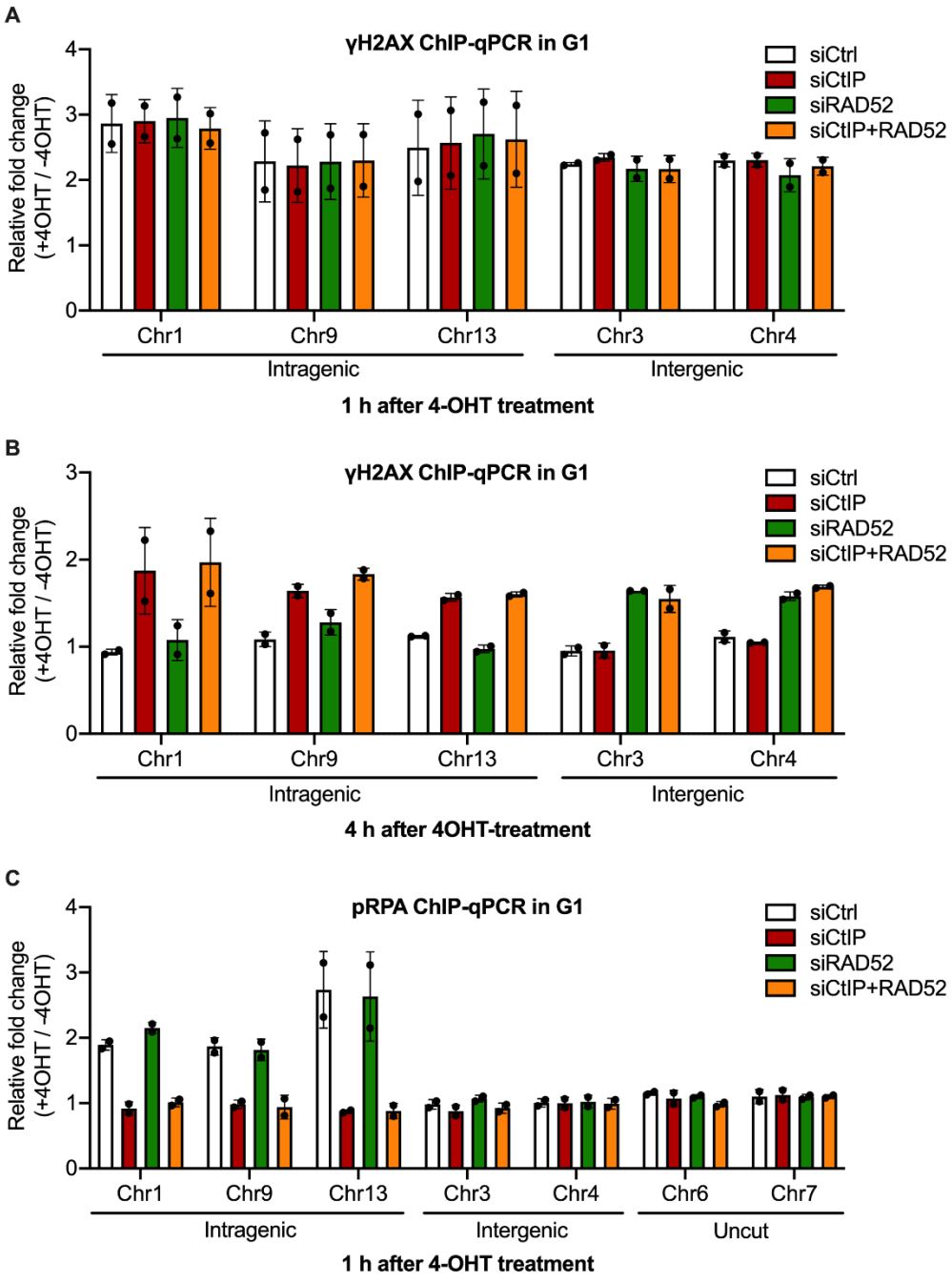

Figure 4.15 ChIP-qPCR analysis of I-PpoI-induced DSBs after CtIP and/or RAD52 depletion

A. γH2AX ChIP-qPCR analysis in G1-mESC-I-PpoI cells at 1 h post 4-OHT treatment, upon single or combined CtIP and RAD52 depletion. **B.** γH2AX ChIP-qPCR analysis in G1-mESC-I-PpoI cells at 4 h post 4-OHT treatment, upon single or combined CtIP and RAD52 depletion. All data show the mean ± S.D. Three individual experiments are shown as dots. **C.** pRPA ChIP-qPCR analysis in G1-mESC-I-PpoI cells at 1 h post 4-OHT treatment, upon single or combined CtIP and RAD52 depletion. All data show the mean ± S.D. Two individual experiments are shown as dots. The relative fold change was calculated by the ratio between +4OHT and -4OHT. Two different genomic locations were analyzed in A and B (intragenic and intergenic cut sites), while panel C also includes uncut sites.

5 Discussion

5.1 RNA involvement in resection-dependent NHEJ repair

NHEJ is the predominant repair process existing in G1 and is thought to be potentially prone to generate insertions/deletions (indels) and chromosomal translocations, therefore causing genome instability[154,155]. Recent studies have highlighted emerging roles of RNA and DNA-RNA hybrids during NHEJ, which have been proposed to improve the repair fidelity of this repair pathway[61,65,126,127,150]. Hence, transcription seems to be an essential component of DSB repair in G1. Previous studies from this laboratory have also revealed that a sub-pathway of NHEJ in G1 involves resection, which is initiated by the phosphorylation of CtIP by PLK3 and involves various nucleases including Artemis[40]. Following this knowledge and since resection and transcription have been also linked in other repair contexts[91], in this work the role of RNA during resection-dependent NHEJ in G1-mESCs was investigated.

Supporting the notion that RNA and therefore transcription are essential for repair by NHEJ, DNA-RNA hybrids were observed at both IR- and endonuclease-induced DSBs in G1-mESCs (Fig. 4.5 A; Fig. 4.7 B; Fig. 4.10 B). Additionally, direct inhibition of transcription by the use of DRB or triptolide inhibitors halts repair of these DSBs in G1-mESCs (Fig.4.3; Fig.4.8 B; Fig.4.11 B). Meanwhile, inhibition of RNA Pol II not only reduces DNA-RNA hybrid formation, but also impairs the initiation of resection at DSBs in G1, indicating that RNA is probably required for resection-dependent NHEJ (Fig. 4.3 D and E; Fig. 4.5 D and E; Fig. 4.8 D; Fig. 4.11 D). On the other hand, DNA-RNA hybrid formation was also reduced at IR- and endonucleases-induced DSBs when resection was inhibited in G1-mESCs, demonstrating that resection is necessary for hybrid formation and possibly promotes transcription during RNA-dependent DSB repair (Fig. 4.5 D; Fig. 4.8 C; Fig. 4.11 C). Altogether, these observations suggest that there is a co-dependency of the transcription and resection processes in resection-dependent NHEJ in G1.

In addition, the RAD52 protein has also been recently described as an important component of the RNA-dependent repair pathways. Thanks to its annealing activity, RAD52 has been reported to facilitate the formation of DNA-RNA hybrids[124,156]. Consistent with this finding, depletion of RAD52 was found to negatively impact on the accumulation of DNA-RNA hybrids at DSBs (Fig. 4.6 B). Surprisingly, both pRPA immunostaining analysis and pRPA ChIP data show that the deficiency of RAD52 does not affect the resection occurring in G1. This indicates that RAD52 and DNA-RNA hybrids are likely to be downstream factors of resection during NHEJ repair (Fig. 4.6 B; Fig. 4.15 C). Nevertheless, the exact mechanism of how resection and RAD52 regulate transcription and the formation of DNA-RNA hybrids remains still unclear. To further investigate this, with the aid of EU

foci analysis, nascent RNA was observed at DSBs upon 2Gy X-IR in G1-mESCs (Fig. 4.4 B and C). Additionally, using different EU pulse labeling methods it was possible to distinguish whether the RNA was pre-existing before DSB induction or whether it was damaged-induced RNA (Fig. 4.4 A). The results show that resection inhibition does not affect the accumulation of pre-existing RNA, but impedes the recruitment of DSB-induced RNA (Fig. 4.4 D). This supports the hypothesis that resection in G1 may affect RNA synthesis and thus regulate DNA-RNA hybrid formation after DSB induction. Moreover, RAD52 deficiency affects both pre-existing and DSB-induced RNA synthesis, revealing that the RNA transcripts accumulate in a RAD52-dependent manner (Fig. 4.6 E).

5.2 Requirements for resection-dependent NHEJ during DSB repair in G1

In G1 phase, the two NHEJ sub-pathways, resection-dependent and -independent, likely co-exist during DNA repair. However, mESCs strictly rely on resection-dependent NHEJ for repair of a sub-set of breaks in G1 (Fig. 4.2). This highlights the unknown requirements that determine the usage of resection during DNA repair in G1. Previous studies by Biehs *et al.* has shown that HeLa cells and human fibroblasts also use resection-dependent NHEJ in G1[40]. Yet, these systems show several differences to mESCs. Resection is observed in HeLa and fibroblast cells during G1 upon 20 Gy X-IR or 2 Gy α-IR[40]. This could raise the concern that resection in G1 may only take place due to the complex lesions caused by high doses of X-IR and 2 Gy α-IR. Strikingly, resection in G1-mESCs is also visible post 2 Gy X-IR and endonuclease-induced DSBs (Fig. 4.1 A and C). Moreover, the pRPA immunostaining analysis showed resection can be efficiently inhibited by PLK3i and siCtIP, confirming that the usage of resection in G1-mESCs is consistent with the previous findings in G1-HeLa and fibroblasts upon complex DSB induction, but differs from the resection occurring in G2 (Fig. 4.1 D). This suggests that the type or complexity of breaks does not seem to determine the use of resection-dependent NHEJ.

A different hypothesis to answer this could be that the use of resection-dependent NHEJ might be cell type specific. Previous evidence has shown that CtIP deficiency does not impair repair by NHEJ during G1 in HeLa and fibroblast cells after 2 Gy X-IR, but instead it enables cells to rescue the siArtemis-induced repair defect by switching from the resection-dependent to resection-independent NHEJ pathway[40]. Remarkably, resection inhibition by PLK3i or siCtIP/Artemis in mESCs causes repair defects in G1 upon 2 Gy X-IR and endonuclease-induced DSB damage (Fig. 4.2 A). Additionally, depleting CtIP does not rescue the repair defects caused by siArtemis (Fig. 4.2 B), indicating that mESCs cannot switch from the resection-dependent to the resection-independent NHEJ component. These data indicate that resection-dependent NHEJ repair probably plays irreplaceable roles in G1-mESCs after DSB damage. However, the dependence on resection-dependent NHEJ for

repair is not restricted to mESCs, as another PhD candidate in this laboratory, Emina Merdan, also found a similar phenomenon in MCF 10A, which are non-malignant breast epithelial cells. Resection was also observed in G1-MCF 10A post 2 Gy X-IR and resection inhibition by PLKi and siArtemis/CtIP also compromised repair under those conditions (data not shown). Hence, this suggests that the reliance on resection during NHEJ repair in G1 is not unique to stem cells, but also seems to occur in certain somatic systems, such as MCF 10A.

Since the type of breaks and cells systems analyzed did not bring light into the features required for using resection-dependent NHEJ, a genome-wide analysis of resected DSBs in G1 cells was carried out to closely examine the genomic locations where this pathway is used. γH2AX and pRPA ChIP-qPCR in mESCs I-PpoI G1-sorted cells was selected as the optimal approach for this purpose. The γH2AX ChIP-qPCR data shows that, while DSBs are induced by I-PpoI in both intragenic and intergenic regions independently of resection (Fig. 4.14 A; Fig. 4.15 A), only the repair of intragenic breaks depends on this process (Fig. 4.14 C; Fig.4.15 B). This is shown by the repair defects detected at the investigated intragenic loci upon resection inhibition by PLKi and siCtIP, whereas repair at intergenic loci remained unaffected. Consistently, the pRPA ChIP-qPCR result also confirmed that increased levels of pRPA can be found at intragenic loci, but not at intergenic loci (Fig. 4.14 B; Fig. 4.15 C). Meanwhile, resection inhibition by PLK3i and siCtIP completely abrogated the pRPA signal, confirming its specificity (Fig. 4.15 C). All these data provide an indication that resection possibly occurs at DSBs which are located in genes. This is consistent with previous publications where repair in G2 by HR and therefore involving resection is also found in genes[44]. Nevertheless, why resection preferentially takes place in intragenic regions in G1 after DSB induction still needs to be clarified. One hypothesis is that active transcription is more frequently associated with intragenic regions than intergenic regions. Additionally, single-stranded overhangs provided by resection perhaps enable DNA ends to be more accessible for the binding of RNA molecules, therefore potentially promoting RNA-involved NHEJ repair. Previous reports have also described a mechanism called transcription-associated homologous recombination repair (TA-HRR), in which the presence of R-loops, along with the proteins RAD52 and XPG promote accurate DSB repair[67]. How these observations are related to our findings in G1, regarding the use of RNA as well as the role of RAD52, still remains to be investigated.

5.3 Potential mechanisms of RNA involvement during NHEJ repair in G1

Although R-loops are considered as threats for genomic stability that interfere with DNA replication machinery, recent studies have proposed that R-loop formation could have beneficial roles during DSB repair[84,157]. In accordance with the findings of this work, DNA-RNA hybrids have been observed

at some DSBs induced by X-IR, AsiSI and I-PpoI, while the loss of DNA-RNA hybrids impairs DSB repair in G1. However, it is still unclear how nascent RNA present at breaks and leading to the formation of DNA-RNA hybrids contributes to DSB repair.

5.3.1 Current hypotheses of DNA-RNA hybrids accumulation at DSBs

Three potential hypotheses have been reported to explain why R-loops accumulate at DSBs: i) DSB-promoted RNA Pol II stalling[68], ii) hybridization of pre-existing RNA with the resected DSB[158], and iii) DSB damage-induced de novo transcription at the resected strand (Fig. 5.1)[67,91,159].

In the first model, it has been proposed that transcriptional repression can be triggered by DSBs at actively transcribed loci. This is a process that would lead to the formation of DNA-RNA hybrids independently of resection occurrence. DRIP-seq analyses, consisting of DNA-RNA hybrid immunoprecipitation followed by sequencing, also validate that DNA-RNA hybrids preferentially accumulate in active genes, but not at intergenic or silent loci[68,160]. Thus, a prerequisite for this model is that DSBs arise in regions which are transcriptionally active before DNA damage.

The second hypothesis suggests that pre-existing RNA, located also at areas transcribed before DSB induction, is able to span the break and thus directly hybridize to the resected ssDNA at resected DSBs. Moreover, our findings show that deficiency of RAD52 triggers the reduction of pre-existing RNA at DSBs in G1 (Fig. 4.6 E). Thus, it is possible that RAD52 is required for stabilizing nascent RNA so as to promote DNA-RNA hybrid formation. This model provides the chance to improve the repair fidelity since pre-existing RNA can be utilized as a template to restore the loss of genetic information.

In comparison to DSB-induced transcription repression, the last model proposes that DSB ends act as promoters so as to generate de novo bidirectional transcription[56,91,159,161]. The published *in vitro* data confirm that DNA ends are able to directly recruit RNA Pol II depending on the MRN complex[159,162]. Furthermore, the recruitment of RNA Pol II is also detectable *in vivo* at I-PpoI-induced DSBs[91,163,164]. Accordingly, in this work it has been shown that newly synthesized RNA at DSBs after DNA damage is also observed and depends on resection in G1 (Fig. 4.4 D and E). Meanwhile, DNA-RNA hybrid formation after DSBs also requires resection and RAD52 (Fig. 4.5 D; Fig. 4.6 B; Fig. 4.8 C; Fig. 4.9 B; Fig. 4.11 C; Fig. 4.12 B). Thus, this raises the possibility that DNA damage induced-transcription may promote the initiation of resection in G1, since single strand overhangs at resected DSBs could be accessible for de novo RNA to anneal with the support of RAD52.

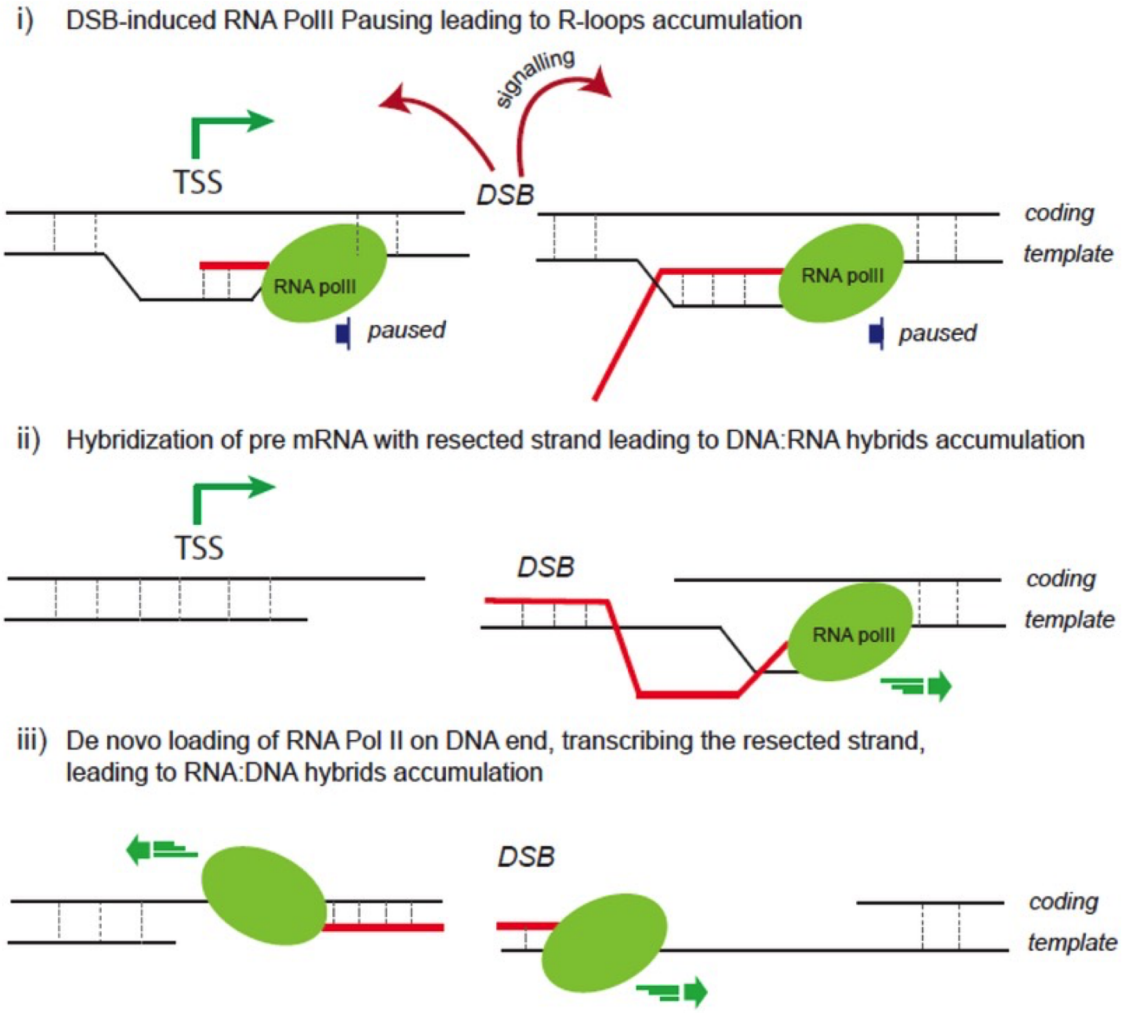

Figure 5.1 Current hypotheses of DNA-RNA hybrids accumulation at transcriptionally active DSBs.
i) DSBs trigger transcription repression at active transcriptional loci. **ii)** Pre-existing RNA before DSB induction can hybridize to the resected ssDNA. **iii)** Newly recruited RNA Pol II promotes transcription on the resected strand and DNA-RNA hybrid formation (from Puget *et al*., 2019).

5.3.2 Model of the putative roles of RNA in resection-dependent NHEJ repair

Collectively reconciling our findings and the reported mechanisms of DNA-RNA hybrid formation at DSBs, we propose a model involving RNA during resection-dependent NHEJ repair in G1 (Fig. 5.2). It is possible that both pre-existing transcription and DNA damage-induced transcription exist at resected DSBs in G1. Once can imagine that upon DSB induction, pre-existing RNA Pol II stalls at DSBs and promotes the recruitment of resection factors. This is in an agreement without observation that resection is impaired by transcription inhibition in G1-mESCs. The next step after resection may depend on whether pre-existing transcription occurred nearby resected breaks or not. If so, pre-existing RNA which is close to DSBs may be able to hybridize with ssDNA overhangs to form DNA-RNA

hybrids with the aid of RAD52. This hypothesis fits with other published data regarding RNA-templated DSB repair[127,156,165], and provides the possibility of error-free NHEJ repair in G1 by restoring the genetic information around DSBs.

However, another possibility is that resection may promote de novo transcription at DSBs, therefore leading to the generation of a damage-induced RNA (Fig. 5.2). This is consistent with our observations that resection inhibition causes a reduction in the DSB-induced EU foci. Since RAD52 deficiency in G1-mESCs also decreases the accumulation of damaged-induced DNA-RNA hybrids, this raises the prospect that DSB-induced RNA could bind to the resected ssDNA overhangs in a RAD52-dependent manner. Since damage-induced RNA can only restore the genetic information at resected sites, its repair fidelity will be poorer than utilizing pre-existing nascent RNA as a template, but still possibly a better option than other NHEJ repair outcomes leading to small deletions at breaks.

In addition, compelling evidence from the de Lange's lab suggests that the CST-Polα-primase complex counteracts resection to limit ssDNA at DSBs *via* fill-in synthesis in G1[166]. CST, a downstream effector of the 53BP1 pathway, has similar functions to RPA in assisting Polα-primases for enhancing fidelity of primer extension[167,168]. A small RNA primer is utilized in Polα-initiated DNA synthesis. Moreover, PhD candidate Emina Merdan also observed that combining inhibition of resection and Polα causes an epistatic repair defect in G1-MCF 10A cells after 2 Gy X-IR, suggesting that the resection and fill-in reactions are possibly occurring in the same pathway. She also observed no reduction of pRPA foci at DSBs when Polα was inhibited before DNA damage, indicating that Polα itself does not affect resection. Thus, an alternative repair pathway could be envisaged where DSB-induced RNA could serve as a primer for mediating Polα-dependent fill-in DNA synthesis at resected DSBs.

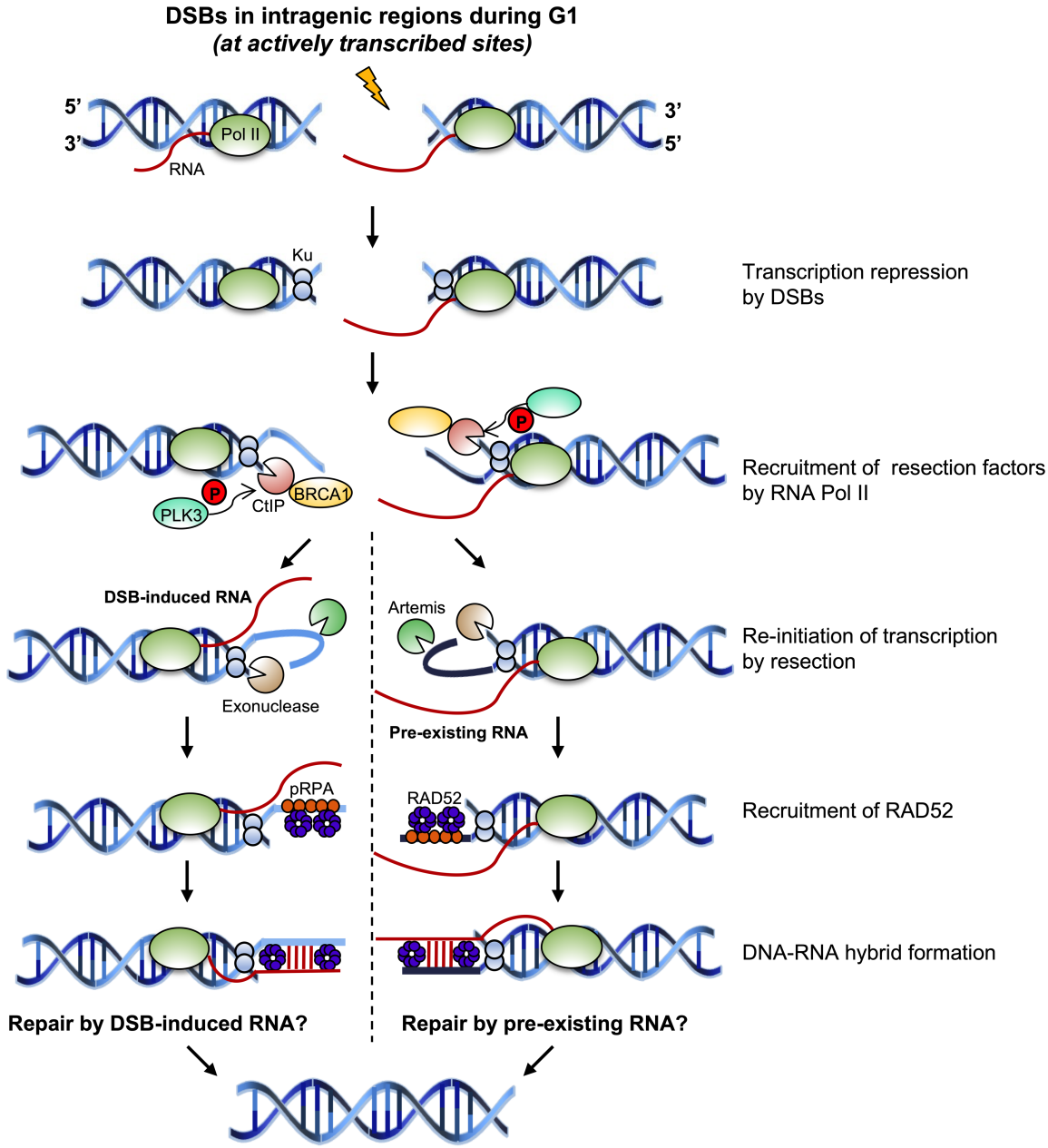

Figure 5.2 The hypothetic model for putative roles of RNA in resection-dependent NHEJ during G1.
Upon DSB induction during G1, transcriptional repression can be triggered at actively transcribed loci in genes. RNA Pol II may contribute to recruit resection factors, leading to the initiation of resection. Meanwhile, resection may also promote the re-initiation of transcription. Following the resection step, two different classes of RNA can arise at break sites: DSB-induced RNA and pre-existing RNA. Resection may facilitate de novo transcription, resulting in the generation of damage-induced RNA (shown in the left branch). The binding of DSB-induced RNA to resected ssDNA overhangs may be RAD52-dependent. Those DSBs may then be repaired utilizing damage-induced RNA which may partially recover the loss of genetic information. On the other hand, pre-existing RNA also possibly exists near DSBs, which can hybridize with ssDNA overhangs to form DNA-RNA hybrids with the aid of RAD52 (shown in the right branch). If so, pre-existing RNA could be employed as a template to precisely restore the missing genetic information, thereby improving repair fidelity in G1.

5.4 Concluding remarks and perspectives

Taken together, the findings in this work provide novel insights into the resection-dependent NHEJ pathway, showing that it may preferentially arise at intragenic loci and be regulated by transcription. Participation of RNA in the resection-dependent NHEJ may relatively enhance repair fidelity in G1 to maintain genomic stability. However, why resection-dependent NHEJ preferentially occurs in actives gene still needs to be further investigated. One possibility is that resection drives nucleosome disassembly, which may promote the re-initiation of transcription after DSBs and DNA-RNA hybrid formation. Meanwhile, transcription occurs more prominently in intragenic regions than in non-genic regions, thereby providing more accessibility to RNA templates for restoring the loss of sequences or contributing to fill-in DNA synthesis. Thus, RNA-dependent NHEJ at resected DSBs may minimize deletions/insertions during DSB repair in G1. Nonetheless, the repair fidelity of this pathway still needs to be further investigated through deletion analysis[50] or Next Generation Sequencing. Moreover, unravelling all these mechanisms will undoubtedly provide novel and essential perspectives to better understand DSB pathway choice in G1 phase.

6 Reference

1. De Bont R, van Larebeke N. Endogenous DNA damage in humans: A review of quantitative data. *Mutagenesis*. 2004;19(3):169-185. doi:10.1093/mutage/geh025
2. Hakem R. DNA-damage repair; the good, the bad, and the ugly. *EMBO J*. 2008;27(4):589-605. doi:10.1038/emboj.2008.15
3. Erdmann F, Ghantous A, Schüz J. Environmental Agents and Childhood Cancer. In: *Encyclopedia of Environmental Health*. Elsevier; 2019:347-359. doi:10.1016/B978-0-12-409548-9.11725-7
4. Zagórski ZP, Kornacka EM. Ionizing Radiation: Friend or Foe of the Origins of Life? *Orig Life Evol Biosph*. 2012;42(5):503-505. doi:10.1007/s11084-012-9314-1
5. Dunne-Daly CF. Principles of radiotherapy and radiobiology. *Semin Oncol Nurs*. 1999;15(4):250-259. doi:10.1016/S0749-2081(99)80054-0
6. Frenz MB. Diagnostic radiation exposure and cancer risk. *Gut*. 2005;54(6):889-890. doi:10.1136/gut.2005.066605
7. Lodish H, Berk A, Matsudaira P, Kaiser CA, Krieger M, Scott MP, Zipursky SL DJ. *Molecular Biology of the Cell (5th Ed.)*. Palgrave Macmillan; 2004.
8. Amente S, Scala G, Majello B, et al. Genome-wide mapping of genomic DNA damage: methods and implications. *Cell Mol Life Sci*. 2021;78(21-22):6745-6762. doi:10.1007/s00018-021-03923-6
9. Lans H, Hoeijmakers JHJ, Vermeulen W, Marteijn JA. The DNA damage response to transcription stress. *Nat Rev Mol Cell Biol*. 2019;20(12):766-784. doi:10.1038/s41580-019-0169-4
10. Goldstein M, Kastan MB. The DNA damage response: Implications for tumor responses to radiation and chemotherapy. *Annu Rev Med*. 2015;66:129-143. doi:10.1146/annurev-med-081313-121208
11. Jette N, Lees-Miller SP. The DNA-dependent protein kinase: A multifunctional protein kinase with roles in DNA double strand break repair and mitosis. *Prog Biophys Mol Biol*. 2015;117(2-3):194-205. doi:10.1016/j.pbiomolbio.2014.12.003
12. Ceccaldi R, Rondinelli B, D'Andrea AD. Repair Pathway Choices and Consequences at the Double-Strand Break. *Trends Cell Biol*. 2016;26(1):52-64. doi:10.1016/j.tcb.2015.07.009
13. Blackford AN, Jackson SP. ATM, ATR, and DNA-PK: The Trinity at the Heart of the DNA Damage Response. *Mol Cell*. 2017;66(6):801-817. doi:10.1016/j.molcel.2017.05.015
14. Paull TT. Mechanisms of ATM activation. *Annu Rev Biochem*. 2015;84:711-738. doi:10.1146/annurev-biochem-060614-034335

15. Marechal A, Zou L. DNA Damage Sensing by the ATM and ATR Kinases. *Cold Spring Harb Perspect Biol*. 2013;5(9):a012716-a012716. doi:10.1101/cshperspect.a012716
16. Cimprich KA, Cortez D. ATR: An essential regulator of genome integrity. *Nat Rev Mol Cell Biol*. 2008;9(8):616-627. doi:10.1038/nrm2450
17. Chang HHY, Pannunzio NR, Adachi N, Lieber MR. Non-homologous DNA end joining and alternative pathways to double-strand break repair. *Nat Rev Mol Cell Biol*. Published online 2017. doi:10.1038/nrm.2017.48
18. Johnson RD, Jasin M. Sister chromatid gene conversion is a prominent double-strand break repair pathway in mammalian cells. *EMBO J*. 2000;19(13):3398-3407. doi:10.1093/emboj/19.13.3398
19. Moynahan ME, Jasin M. Mitotic homologous recombination maintains genomic stability and suppresses tumorigenesis. *Nat Rev Mol Cell Biol*. 2010;11(3):196-207. doi:10.1038/nrm2851
20. Heyer W-D, Ehmsen KT, Liu J. Regulation of Homologous Recombination in Eukaryotes. *Annu Rev Genet*. 2010;44(1):113-139. doi:10.1146/annurev-genet-051710-150955
21. Chiruvella KK, Liang Z, Wilson TE. Repair of double-strand breaks by end joining. *Cold Spring Harb Perspect Biol*. 2013;5(5):1-22. doi:10.1101/cshperspect.a012757
22. Kent T, Chandramouly G, Mcdevitt SM, Ozdemir AY, Pomerantz RT. Mechanism of microhomology-mediated end-joining promoted by human DNA polymerase θ. *Nat Struct Mol Biol*. 2015;22(3):230-237. doi:10.1038/nsmb.2961
23. Iliakis G, Murmann T, Soni A. Alternative end-joining repair pathways are the ultimate backup for abrogated classical non-homologous end-joining and homologous recombination repair: Implications for the formation of chromosome translocations. *Mutat Res - Genet Toxicol Environ Mutagen*. 2015;793:166-175. doi:10.1016/j.mrgentox.2015.07.001
24. Löbrich M, Jeggo P. A Process of Resection-Dependent Nonhomologous End Joining Involving the Goddess Artemis. *Trends Biochem Sci*. 2017;42(9):690-701. doi:10.1016/j.tibs.2017.06.011
25. Shibata A, Jeggo PA. Roles for the DNA-PK complex and 53BP1 in protecting ends from resection during DNA double-strand break repair. *J Radiat Res*. 2020;61(5):718-726. doi:10.1093/jrr/rraa053
26. Riballo E, Kühne M, Rief N, et al. A pathway of double-strand break rejoining dependent upon ATM, Artemis, and proteins locating to γ-H2AX foci. *Mol Cell*. 2004;16(5):715-724. doi:10.1016/j.molcel.2004.10.029
27. Wang C, Lees-Miller SP. Detection and Repair of Ionizing Radiation-Induced DNA Double Strand Breaks: New Developments in Nonhomologous End Joining. *Int J Radiat Oncol*. 2013;86(3):440-449. doi:10.1016/j.ijrobp.2013.01.011
28. IMAMICHI S, SHARMA MK, KAMDAR RP, FUKUCHI M, MATSUMOTO Y. Ionizing

radiation-induced XRCC4 phosphorylation is mediated through ATM in addition to DNA-PK. *Proc Japan Acad Ser B*. 2014;90(9):365-372. doi:10.2183/pjab.90.365

29. Löbrich M, Jeggo P. A Process of Resection-Dependent Nonhomologous End Joining Involving the Goddess Artemis. *Trends Biochem Sci*. 2017;xx:1-12. doi:10.1016/j.tibs.2017.06.011
30. Barton O, Naumann SC, Diemer-Biehs R, et al. Polo-like kinase 3 regulates CtIP during DNA double-strand break repair in G1. *J Cell Biol*. 2014;206(7):877-894. doi:10.1083/jcb.201401146
31. Shibata A, Steinlage M, Barton O, et al. DNA Double-Strand Break Resection Occurs during Non-homologous End Joining in G1 but Is Distinct from Resection during Homologous Recombination. *Mol Cell*. 2017;65(4):671-684.e5. doi:10.1016/j.molcel.2016.12.016
32. Rass E, Grabarz A, Plo I, Gautier J, Bertrand P, Lopez BS. Role of Mre11 in chromosomal nonhomologous end joining in mammalian cells. *Nat Struct Mol Biol*. 2009;16(8):819-824. doi:10.1038/nsmb.1641
33. Guirouilh-Barbat J, Gelot C, Xie A, Dardillac E, Scully R, Lopez BS. 53BP1 Protects against CtIP-Dependent Capture of Ectopic Chromosomal Sequences at the Junction of Distant Double-Strand Breaks. *PLoS Genet*. 2016;12(10). doi:10.1371/JOURNAL.PGEN.1006230
34. Dynan WS, Yoo S. Interaction of Ku protein and DNA-dependent protein kinase catalytic subunit with nucleic acids. *Nucleic Acids Res*. 1998;26(7):1551-1559. doi:10.1093/nar/26.7.1551
35. Walker JR, Corpina RA, Goldberg J. Structure of the Ku heterodimer bound to DNA and its implications for double-strand break repair. *Nature*. 2001;412(6847):607-614. doi:10.1038/35088000
36. Symington LS, Gautier J. Double-Strand Break End Resection and Repair Pathway Choice. *Annu Rev Genet*. 2011;45(1):247-271. doi:10.1146/annurev-genet-110410-132435
37. Chanut P, Britton S, Coates J, Jackson SP, Calsou P. Coordinated nuclease activities counteract Ku at single-ended DNA double-strand breaks. *Nat Commun*. 2016;7. doi:10.1038/ncomms12889
38. Yun MH, Hiom K. CtIP-BRCA1 modulates the choice of DNA double-strand-break repair pathway throughout the cell cycle. *Nature*. 2009;459(7245):460-463. doi:10.1038/nature07955
39. Shibata A, Moiani D, Arvai AS, et al. DNA Double-Strand Break Repair Pathway Choice Is Directed by Distinct MRE11 Nuclease Activities. *Mol Cell*. 2014;53(1):7-18. doi:10.1016/j.molcel.2013.11.003
40. Biehs R, Steinlage M, Barton O, et al. DNA Double-Strand Break Resection Occurs during Non-homologous End Joining in G1 but Is Distinct from Resection during Homologous Recombination. *Mol Cell*. 2017;65(4):671-684.e5. doi:10.1016/j.molcel.2016.12.016

41. Berkovich E, Monnat RJ, Kastan MB. Roles of ATM and NBS1 in chromatin structure modulation and DNA double-strand break repair. *Nat Cell Biol*. 2007;9(6):683-690. doi:10.1038/ncb1599
42. Li X, Tyler JK. Nucleosome disassembly during human non-homologous end joining followed by concerted HIRA- and CAF-1-dependent reassembly. *Elife*. 2016;5(JUN2016):1-18. doi:10.7554/eLife.15129
43. Aymard F, Bugler B, Schmidt CK, et al. Transcriptionally active chromatin recruits homologous recombination at DNA double-strand breaks. 2014;21. doi:10.1038/nsmb.2796
44. Aymard F, Aguirrebengoa M, Guillou E, et al. Genome-wide mapping of long-range contacts unveils clustering of DNA double-strand breaks at damaged active genes. *Nat Struct Mol Biol*. 2017;24(4):353-361. doi:10.1038/nsmb.3387
45. Clouaire T, Rocher V, Lashgari A, et al. Comprehensive Mapping of Histone Modifications at DNA Double-Strand Breaks Deciphers Repair Pathway Chromatin Signatures. *Mol Cell*. 2018;72(2):250-262.e6. doi:10.1016/j.molcel.2018.08.020
46. Vítor AC, Huertas P, Legube G, de Almeida SF. Studying DNA Double-Strand Break Repair: An Ever-Growing Toolbox. *Front Mol Biosci*. 2020;7(February):1-16. doi:10.3389/fmolb.2020.00024
47. Iacovoni JS, Caron P, Lassadi I, et al. High-resolution profiling of γh2AX around DNA double strand breaks in the mammalian genome. *EMBO J*. 2010;29(8):1446-1457. doi:10.1038/emboj.2010.38
48. Massip L, Caron P, Iacovoni JS, Trouche D, Legube G. Deciphering the chromatin landscape induced around DNA double strand breaks. *Cell Cycle*. 2010;9(15):3035-3044. doi:10.4161/cc.9.15.12412
49. Yilmaz D, Furst A, Meaburn K, et al. Activation of homologous recombination in G1 preserves centromeric integrity. *Nature*. 2021;600(7890):748-753. doi:10.1038/s41586-021-04200-z
50. Yasuhara T, Kato R, Yamauchi M, et al. RAP80 suppresses the vulnerability of R-loops during DNA double-strand break repair. *Cell Rep*. 2022;38(5):110335. doi:10.1016/j.celrep.2022.110335
51. Adamson B, Smogorzewska A, Sigoillot FD, King RW, Elledge SJ. A genome-wide homologous recombination screen identifies the RNA-binding protein RBMX as a component of the DNA-damage response. *Nat Cell Biol*. 2012;14(3):318-328. doi:10.1038/ncb2426
52. Francia S, Michelini F, Saxena A, et al. Site-specific DICER and DROSHA RNA products control the DNA-damage response. *Nature*. 2012;488(7410):231-235. doi:10.1038/nature11179
53. Wei W, Ba Z, Gao M, et al. A role for small RNAs in DNA double-strand break repair. *Cell*.

2012;149(1):101-112. doi:10.1016/j.cell.2012.03.002

54. Yang YG, Qi Y. RNA-directed repair of DNA double-strand breaks. *DNA Repair (Amst)*. 2015;32:82-85. doi:10.1016/j.dnarep.2015.04.017

55. Michelini F, Pitchiaya S, Vitelli V, et al. Damage-induced lncRNAs control the DNA damage response through interaction with DDRNAs at individual double-strand breaks. *Nat Cell Biol*. 2017;19(12):1400-1411. doi:10.1038/ncb3643

56. D'Alessandro G, Whelan DR, Howard SM, et al. BRCA2 controls DNA:RNA hybrid level at DSBs by mediating RNase H2 recruitment. *Nat Commun*. 2018;9(1):5376. doi:10.1038/s41467-018-07799-2

57. Crick F. Central dogma of molecular biology. *Nature*. 1970;227(5258):561-563. doi:10.1038/227561a0

58. Baltimore D. Retroviruses and Retrotransposons: The role of reverse transcription in shaping the eukaryotic genome. *Cell*. 1985;40(3):481-482. doi:10.1016/0092-8674(85)90190-4

59. Autexier C, Lue NF. The structure and function of telomerase reverse transcriptase. *Annu Rev Biochem*. 2006;75:493-517. doi:10.1146/annurev.biochem.75.103004.142412

60. Meers C, Keskin H, Storici F. DNA repair by RNA: Templated, or not templated, that is the question. *DNA Repair (Amst)*. 2016;44:17-21. doi:10.1016/j.dnarep.2016.05.002

61. Keskin H, Shen Y, Huang F, et al. Transcript-RNA-templated DNA recombination and repair. *Nature*. 2014;515(7527):436-439. doi:10.1038/nature13682

62. Keskin H, Meers C, Storici F. Transcript RNA supports precise repair of its own DNA gene. *RNA Biol*. 2016;13(2):157-165. doi:10.1080/15476286.2015.1116676

63. Esnault C, Maestre J, Heidmann T. Human LINE retrotransposons generate processed pseudogenes. *Nat Genet*. 2000;24(4):363-367. doi:10.1038/74184

64. Morrish TA, Gilbert N, Myers JS, et al. DNA repair mediated by endonuclease-independent LINE-1 retrotransposition. *Nat Genet*. 2002;31(2):159-165. doi:10.1038/ng898

65. Chakraborty A, Tapryal N, Venkova T, et al. Classical non-homologous end-joining pathway utilizes nascent RNA for error-free double-strand break repair of transcribed genes. *Nat Commun*. 2016;7(May):1-12. doi:10.1038/ncomms13049

66. D'Adda di Fagagna F. A direct role for small non-coding RNAs in DNA damage response. *Trends Cell Biol*. 2014;24(3):171-178. doi:10.1016/j.tcb.2013.09.008

67. Yasuhara T, Kato R, Hagiwara Y, et al. Human Rad52 Promotes XPG-Mediated R-loop Processing to Initiate Transcription-Associated Homologous Recombination Repair. *Cell*. 2018;175(2):558-570.e11. doi:10.1016/j.cell.2018.08.056

68. Cohen S, Puget N, Lin YL, et al. Senataxin resolves RNA:DNA hybrids forming at DNA double-strand breaks to prevent translocations. *Nat Commun*. 2018;9(1). doi:10.1038/s41467-

018-02894-w

69. Lu WT, Hawley BR, Skalka GL, et al. Drosha drives the formation of DNA:RNA hybrids around DNA break sites to facilitate DNA repair. *Nat Commun*. 2018;9(1). doi:10.1038/s41467-018-02893-x
70. Hamperl S, Cimprich KA. The contribution of co-transcriptional RNA: DNA hybrid structures to DNA damage and genome instability. *DNA Repair (Amst)*. 2014;19:84-94. doi:10.1016/j.dnarep.2014.03.023
71. Ginno PA, Lott PL, Christensen HC, Korf I, Chédin F. R-Loop Formation Is a Distinctive Characteristic of Unmethylated Human CpG Island Promoters. *Mol Cell*. 2012;45(6):814-825. doi:10.1016/j.molcel.2012.01.017
72. Sanz LA, Hartono SR, Lim YW, et al. Prevalent, Dynamic, and Conserved R-Loop Structures Associate with Specific Epigenomic Signatures in Mammals. *Mol Cell*. 2016;63(1):167-178. doi:10.1016/j.molcel.2016.05.032
73. García-Muse T, Aguilera A. R Loops: From Physiological to Pathological Roles. *Cell*. 2019;179(3):604-618. doi:10.1016/J.CELL.2019.08.055
74. Costantino L, Koshland D. The Yin and Yang of R-loop biology. *Curr Opin Cell Biol*. 2015;34:39-45. doi:10.1016/J.CEB.2015.04.008
75. Wells JP, White J, Stirling PC. R Loops and Their Composite Cancer Connections. *Trends in Cancer*. 2019;5(10):619-631. doi:10.1016/j.trecan.2019.08.006
76. Rinaldi C, Pizzul P, Longhese MP, Bonetti D. Sensing R-Loop-Associated DNA Damage to Safeguard Genome Stability. *Front Cell Dev Biol*. 2021;8:1657. doi:10.3389/fcell.2020.618157
77. Beletskii A, Bhagwat AS. Transcription-induced mutations: Increase in C to T mutations in the nontranscribed strand during transcription in Escherichia coli. *Proc Natl Acad Sci U S A*. 1996;93(24):13919-13924. doi:10.1073/pnas.93.24.13919
78. Aguilera A, García-Muse T. R Loops: From Transcription Byproducts to Threats to Genome Stability. *Mol Cell*. 2012;46(2):115-124. doi:10.1016/J.MOLCEL.2012.04.009
79. Freudenreich CH. R-loops: targets for nuclease cleavage and repeat instability. *Curr Genet*. 2018;64(4):789-794. doi:10.1007/S00294-018-0806-Z/FIGURES/1
80. Hegazy YA, Fernando CM, Tran EJ. The balancing act of R-loop biology: The good, the bad, and the ugly. *J Biol Chem*. 2020;295(4):905-913. doi:10.1016/s0021-9258(17)49903-0
81. García-Muse T, Aguilera A. Transcription-replication conflicts: How they occur and how they are resolved. *Nat Rev Mol Cell Biol*. 2016;17(9):553-563. doi:10.1038/nrm.2016.88
82. Hamperl S, Bocek MJ, Saldivar JC, Swigut T, Cimprich KA. Transcription-Replication Conflict Orientation Modulates R-Loop Levels and Activates Distinct DNA Damage Responses. *Cell*. 2017;170(4):774-786.e19. doi:10.1016/J.CELL.2017.07.043

83. Promonet A, Padioleau I, Liu Y, et al. Topoisomerase 1 prevents replication stress at R-loop-enriched transcription termination sites. *Nat Commun*. 2020;11(1). doi:10.1038/s41467-020-17858-2
84. Crossley MP, Bocek M, Cimprich KA. R-Loops as Cellular Regulators and Genomic Threats. *Mol Cell*. 2019;73(3):398-411. doi:10.1016/j.molcel.2019.01.024
85. Niehrs C, Luke B. Regulatory R-loops as facilitators of gene expression and genome stability. *Nat Rev Mol Cell Biol 2020 213*. 2020;21(3):167-178. doi:10.1038/s41580-019-0206-3
86. Wang IX, Grunseich C, Fox J, et al. Human proteins that interact with RNA/DNA hybrids. *Genome Res*. 2018;28(9):1405-1414. doi:10.1101/gr.237362.118
87. Grunseich C, Wang IX, Watts JA, et al. Senataxin Mutation Reveals How R-Loops Promote Transcription by Blocking DNA Methylation at Gene Promoters. *Mol Cell*. 2018;69(3):426-437.e7. doi:10.1016/j.molcel.2017.12.030
88. Skourti-Stathaki K, Proudfoot NJ, Gromak N. Human Senataxin Resolves RNA/DNA Hybrids Formed at Transcriptional Pause Sites to Promote Xrn2-Dependent Termination. *Mol Cell*. 2011;42(6):794-805. doi:10.1016/J.MOLCEL.2011.04.026
89. Skourti-Stathaki K, Proudfoot NJ. A double-edged sword: R loops as threats to genome integrity and powerful regulators of gene expression. *Genes Dev*. 2014;28(13):1384-1396. doi:10.1101/gad.242990.114
90. Cristini A, Groh M, Kristiansen MS, Gromak N. RNA/DNA Hybrid Interactome Identifies DXH9 as a Molecular Player in Transcriptional Termination and R-Loop-Associated DNA Damage. *Cell Rep*. 2018;23(6):1891-1905. doi:10.1016/J.CELREP.2018.04.025
91. Ohle C, Tesorero R, Schermann G, Dobrev N, Sinning I, Fischer T. Transient RNA-DNA Hybrids Are Required for Efficient Double-Strand Break Repair. *Cell*. 2016;167(4):1001-1013.e7. doi:10.1016/j.cell.2016.10.001
92. Kato R, Miyagawa K, Yasuhara T. The role of R-loops in transcription-associated DNA double-strand break repair. *Mol Cell Oncol*. 2019;6(1). doi:10.1080/23723556.2018.1542244/FORMAT/EPUB
93. Daugaard M, Baude A, Fugger K, et al. LEDGF (p75) promotes DNA-end resection and homologous recombination. *Nat Struct Mol Biol*. 2012;19(8):803-810. doi:10.1038/nsmb.2314
94. Eidahl JO, Crowe BL, North JA, et al. Structural basis for high-affinity binding of LEDGF PWWP to mononucleosomes. *Nucleic Acids Res*. 2013;41(6):3924-3936. doi:10.1093/nar/gkt074
95. Ui A, Nagaura Y, Yasui A. Transcriptional Elongation Factor ENL Phosphorylated by ATM Recruits Polycomb and Switches Off Transcription for DSB Repair. *Mol Cell*. 2015;58(3):468-482. doi:10.1016/J.MOLCEL.2015.03.023

96. Capozzo I, Iannelli F, Francia S, d'Adda di Fagagna F. Express or repress? The transcriptional dilemma of damaged chromatin. *FEBS J*. 2017;284(14):2133-2147. doi:10.1111/febs.14048
97. Vítor AC, Sridhara SC, Sabino JC, et al. Single-molecule imaging of transcription at damaged chromatin. *Sci Adv*. 2019;5(1). doi:10.1126/SCIADV.AAU1249
98. Puget N, Miller KM, Legube G. Non-canonical DNA/RNA structures during Transcription-Coupled Double-Strand Break Repair: Roadblocks or Bona fide repair intermediates? *DNA Repair (Amst)*. 2019;81(July):102661. doi:10.1016/j.dnarep.2019.102661
99. Caron P, van der Linden J, van Attikum H. Bon voyage: A transcriptional journey around DNA breaks. *DNA Repair (Amst)*. 2019;82(March). doi:10.1016/j.dnarep.2019.102686
100. Machour FE, Ayoub N. Transcriptional Regulation at DSBs: Mechanisms and Consequences. *Trends Genet*. 2020;36(12):981-997. doi:10.1016/j.tig.2020.01.001
101. Long Q, Liu Z, Gullerova M. Sweet Melody or Jazz? Transcription Around DNA Double-Strand Breaks. *Front Mol Biosci*. 2021;8(April):1-14. doi:10.3389/fmolb.2021.655786
102. Marnef A, Legube G. R-loops as Janus-faced modulators of DNA repair. *Nat Cell Biol*. 2021;23(4):305-313. doi:10.1038/s41556-021-00663-4
103. Guha S, Bhaumik SR. Transcription-coupled DNA double-strand break repair. *DNA Repair (Amst)*. 2022;109. doi:10.1016/j.dnarep.2021.103211
104. Suzuki H, Okamoto-Katsuyama M, Suwa T, Maeda R, Tamura T aki, Yamaguchi Y. TLP-mediated global transcriptional repression after double-strand DNA breaks slows down DNA repair and induces apoptosis. *Sci Rep*. 2019;9(1). doi:10.1038/s41598-019-41057-9
105. Aygün O, Svejstrup J, Liu Y. A RECQ5-RNA polymerase II association identified by targeted proteomic analysis of human chromatin. *Proc Natl Acad Sci U S A*. 2008;105(25):8580-8584. doi:10.1073/pnas.0804424105
106. Saponaro M, Kantidakis T, Mitter R, et al. RECQL5 controls transcript elongation and suppresses genome instability associated with transcription stress. *Cell*. 2014;157(5):1037-1049. doi:10.1016/j.cell.2014.03.048
107. Williams LH, Fromm G, Gokey NG, et al. Pausing of RNA Polymerase II Regulates Mammalian Developmental Potential through Control of Signaling Networks. *Mol Cell*. 2015;58(2):311-322. doi:10.1016/j.molcel.2015.02.003
108. Gatti M, Pinato S, Maspero E, Soffientini P, Polo S, Penengo L. A novel ubiquitin mark at the N-terminal tail of histone H2As targeted by RNF168 ubiquitin ligase. *Cell Cycle*. 2012;11(13):2538-2544. doi:10.4161/cc.20919
109. Mattiroli F, Vissers JHA, van Dijk WJ, et al. RNF168 Ubiquitinates K13-15 on H2A/H2AX to Drive DNA Damage Signaling. *Cell*. 2012;150(6):1182-1195. doi:10.1016/j.cell.2012.08.005
110. Paul A, Wang B. RNF8- and Ube2S-Dependent Ubiquitin Lysine 11-Linkage Modification in

Response to DNA Damage. *Mol Cell*. 2017;66(4):458-472.e5. doi:10.1016/j.molcel.2017.04.013

111. Chou DM, Adamson B, Dephoure NE, et al. A chromatin localization screen reveals poly (ADP ribose)-regulated recruitment of the repressive polycomb and NuRD complexes to sites of DNA damage. *Proc Natl Acad Sci U S A*. 2010;107(43):18475-18480. doi:10.1073/pnas.1012946107
112. Polo SE, Kaidi A, Baskcomb L, Galanty Y, Jackson SP. Regulation of DNA-damage responses and cell-cycle progression by the chromatin remodelling factor CHD4. *EMBO J*. 2010;29(18):3130-3139. doi:10.1038/emboj.2010.188
113. Gong F, Clouaire T, Aguirrebengoa M, Legube G, Miller KM. Histone demethylase KDM5A regulates the ZMY ND8-NuRD chromatin remodeler to promote DNA repair. *J Cell Biol*. 2017;216(7):1959-1974. doi:10.1083/jcb.201611135
114. Pankotai T, Bonhomme C, Chen D, Soutoglou E. DNAPKcs-dependent arrest of RNA polymerase II transcription in the presence of DNA breaks. 2012;19(3). doi:10.1038/nsmb.2224
115. Caron P, Pankotai T, Wiegant WW, et al. WWP2 ubiquitylates RNA polymerase II for DNA-PK-dependent transcription arrest and repair at DNA breaks. *Genes Dev*. 2019;33(11-12):684-704. doi:10.1101/gad.321943.118
116. Kakarougkas A, Ismail A, Chambers AL, et al. Requirement for PBAF in Transcriptional Repression and Repair at DNA Breaks in Actively Transcribed Regions of Chromatin. *Mol Cell*. 2014;55(5):723-732. doi:10.1016/J.MOLCEL.2014.06.028
117. Marnef A, Cohen S, Legube G. Transcription-Coupled DNA Double-Strand Break Repair: Active Genes Need Special Care. *J Mol Biol*. 2017;429(9):1277-1288. doi:10.1016/j.jmb.2017.03.024
118. Chen L, Chen JY, Zhang X, et al. R-ChIP Using Inactive RNase H Reveals Dynamic Coupling of R-loops with Transcriptional Pausing at Gene Promoters. *Mol Cell*. 2017;68(4):745-757.e5. doi:10.1016/j.molcel.2017.10.008
119. Zhang X, Chiang HC, Wang Y, et al. Attenuation of RNA polymerase II pausing mitigates BRCA1-associated R-loop accumulation and tumorigenesis. *Nat Commun*. 2017;8. doi:10.1038/ncomms15908
120. Shivji MKK, Renaudin X, Williams ÇH, Venkitaraman AR. BRCA2 Regulates Transcription Elongation by RNA Polymerase II to Prevent R-Loop Accumulation. *Cell Rep*. 2018;22(4):1031-1039. doi:10.1016/j.celrep.2017.12.086
121. Edwards DS, Maganti R, Tanksley JP, et al. BRD4 Prevents R-Loop Formation and Transcription-Replication Conflicts by Ensuring Efficient Transcription Elongation. *Cell Rep*. 2020;32(12):108166. doi:10.1016/j.celrep.2020.108166
122. Shanbhag NM, Rafalska-Metcalf IU, Balane-Bolivar C, Janicki SM, Greenberg RA. ATM-

Dependent Chromatin Changes Silence Transcription In cis to DNA Double-Strand Breaks. *Cell*. 2010;141(6):970-981. doi:10.1016/J.CELL.2010.04.038

123. Ui A, Chiba N, Yasui A. Relationship among DNA double-strand break (DSB), DSB repair, and transcription prevents genome instability and cancer. *Cancer Sci*. 2020;111(5):1443-1451. doi:10.1111/cas.14404
124. Mazina OM, Keskin H, Hanamshet K, Storici F, Mazin A V. Rad52 Inverse Strand Exchange Drives RNA-Templated DNA Double-Strand Break Repair. *Mol Cell*. 2017;67(1):19-29.e3. doi:10.1016/j.molcel.2017.05.019
125. McDevitt S, Rusanov T, Kent T, Chandramouly G, Pomerantz RT. How RNA transcripts coordinate DNA recombination and repair. *Nat Commun*. 2018;9(1):1091. doi:10.1038/s41467-018-03483-7
126. Wei L, Nakajima S, Böhm S, et al. DNA damage during the G0/G1 phase triggers RNA-templated, Cockayne syndrome B-dependent homologous recombination. *Proc Natl Acad Sci U S A*. 2015;112(27):E3495-504. doi:10.1073/pnas.1507105112
127. Welty S, Teng Y, Liang Z, et al. RAD52 is required for RNA-templated recombination repair in post-mitotic neurons. *J Biol Chem*. 2018;293(4):1353-1362. doi:10.1074/jbc.M117.808402
128. Teng Y, Yadav T, Duan M, et al. ROS-induced R loops trigger a transcription-coupled but BRCA1/2-independent homologous recombination pathway through CSB. *Nat Commun*. 2018;9(1):4115. doi:10.1038/s41467-018-06586-3
129. Rogakou EP, Pilch DR, Orr AH, Ivanova VS, Bonner WM. DNA double-stranded breaks induce histone H2AX phosphorylation on serine 139. *J Biol Chem*. 1998;273(10):5858-5868. doi:10.1074/jbc.273.10.5858
130. Rothkamm K, Löbrich M. Evidence for a lack of DNA double-strand break repair in human cells exposed to very low x-ray doses. *Proc Natl Acad Sci U S A*. 2003;100(9):5057-5062. doi:10.1073/pnas.0830918100
131. Sedelnikova OA, Rogakou EP, Panyutin IG, Bonner WM. Quantitative detection of 125idU-induced DNA double-strand breaks with γ-H2AX antibody. *Radiat Res*. 2002;158(4):486-492. doi:10.1667/0033-7587(2002)158[0486:QDOIID]2.0.CO;2
132. Oslowski CM. Stress responses: Methods and protocols. *Stress Responses Methods Protoc*. 2015;1292:1-246. doi:10.1007/978-1-4939-2522-3
133. Choi EH, Yoon S, Kim KP. Combined Ectopic Expression of Homologous Recombination Factors Promotes Embryonic Stem Cell Differentiation. *Mol Ther*. 2018;26(4):1154-1165. doi:10.1016/j.ymthe.2018.02.003
134. Vitale I, Manic G, De Maria R, Kroemer G, Galluzzi L. DNA Damage in Stem Cells. *Mol Cell*. 2017;66(3):306-319. doi:10.1016/j.molcel.2017.04.006

135. Mandal PK, Blanpain C, Rossi DJ. DNA damage response in adult stem cells: Pathways and consequences. *Nat Rev Mol Cell Biol*. 2011;12(3):198-202. doi:10.1038/nrm3060
136. Choi EH, Yoon S, Koh YE, Seo YJ, Kim KP. Maintenance of genome integrity and active homologous recombination in embryonic stem cells. *Exp Mol Med*. 2020;52(8):1220-1229. doi:10.1038/s12276-020-0481-2
137. Bunting SF, Callén E, Wong N, et al. 53BP1 inhibits homologous recombination in Brca1-deficient cells by blocking resection of DNA breaks. *Cell*. 2010;141(2):243-254. doi:10.1016/j.cell.2010.03.012
138. Bunting SF, Callén E, Kozak ML, et al. BRCA1 Functions Independently of Homologous Recombination in DNA Interstrand Crosslink Repair. *Mol Cell*. 2012;46(2):125-135. doi:10.1016/j.molcel.2012.02.015
139. Li M, Cole F, Patel DS, et al. 53 BP 1 ablation rescues genomic instability in mice expressing ‘ RING -less’ BRCA 1 . *EMBO Rep*. 2016;17(11):1532-1541. doi:10.15252/embr.201642497
140. Nacson J, Krais JJ, Bernhardy AJ, et al. BRCA1 Mutation-Specific Responses to 53BP1 Loss-Induced Homologous Recombination and PARP Inhibitor Resistance. *Cell Rep*. 2018;25(5):1384. doi:10.1016/j.celrep.2018.10.009
141. Escribano-Díaz C, Orthwein A, Fradet-Turcotte A, et al. A Cell Cycle-Dependent Regulatory Circuit Composed of 53BP1-RIF1 and BRCA1-CtIP Controls DNA Repair Pathway Choice. *Mol Cell*. 2013;49(5):872-883. doi:10.1016/j.molcel.2013.01.001
142. Bader AS, Hawley BR, Wilczynska A, Bushell M. The roles of RNA in DNA double-strand break repair. *Br J Cancer*. 2020;122(5):613-623. doi:10.1038/s41416-019-0624-1
143. Plosky BS. The Good and Bad of RNA:DNA Hybrids in Double-Strand Break Repair. *Mol Cell*. 2016;64(4):643-644. doi:10.1016/j.molcel.2016.11.010
144. Marini F, Rawal CC, Liberi G, Pellicioli A. Regulation of DNA Double Strand Breaks Processing: Focus on Barriers. *Front Mol Biosci*. 2019;6(July):1-8. doi:10.3389/fmolb.2019.00055
145. Te Poele RH, Okorokov AL, Joel SP. RNA synthesis block by 5,6-dichloro-1-β-D-ribofuranosylbenzimidazole (DRB) triggers p53-dependent apoptosis in human colon carcinoma cells. *Oncogene*. 1999;18(42):5765-5772. doi:10.1038/sj.onc.1202961
146. Singh J, Padgett RA. Rates of in situ transcription and splicing in large human genes. *Nat Struct Mol Biol*. 2009;16(11):1128-1133. doi:10.1038/nsmb.1666
147. Bensaude O. Inhibiting eukaryotic transcription: Which compound to choose? How to evaluate its activity? *Transcription*. 2011;2(3):103-108. doi:10.4161/trns.2.3.16172
148. König F, Schubert T, Längst G. The monoclonal S9.6 antibody exhibits highly variable binding affinities towards different R-loop sequences. *PLoS One*. 2017;12(6).

doi:10.1371/journal.pone.0178875

149. Hartono SR, Malapert A, Legros P, Bernard P, Chédin F, Vanoosthuyse V. The Affinity of the S9.6 Antibody for Double-Stranded RNAs Impacts the Accurate Mapping of R-Loops in Fission Yeast. *J Mol Biol*. 2018;430(3):272-284. doi:10.1016/j.jmb.2017.12.016
150. Mazina OM, Keskin H, Hanamshet K, Storici F, Mazin A V. Rad52 Inverse Strand Exchange Drives RNA-Templated DNA Double-Strand Break Repair. *Mol Cell*. 2017;67(1):19-29.e3. doi:10.1016/j.molcel.2017.05.019
151. Iacovoni JS, Caron P, Lassadi I, et al. High-resolution profiling of γH2AX around DNA double strand breaks in the mammalian genome. *EMBO J*. 2010;29(8):1446-1457. doi:10.1038/emboj.2010.38
152. Baranovskiy AG, Babayeva ND, Suwa Y, Gu J, Pavlov YI, Tahirov TH. Structural basis for inhibition of DNA replication by aphidicolin. *Nucleic Acids Res*. 2014;42(22):14013-14021. doi:10.1093/nar/gku1209
153. Monnat RJ, Hackmann AFM, Cantrell MA. Generation of highly site-specific DNA double-strand breaks in human cells by the homing endonucleases I-PpoI and I-CreI. *Biochem Biophys Res Commun*. 1999;255(1):88-93. doi:10.1006/bbrc.1999.0152
154. Richardson C, Jasin M. Frequent chromosomal translocations induced by DNA double-strand breaks. *Nat 2000 4056787*. 2000;405(6787):697-700. doi:10.1038/35015097
155. Mao Z, Bozzella M, Seluanov A, Gorbunova V. Comparison of nonhomologous end joining and homologous recombination in human cells. *DNA Repair (Amst)*. 2008;7(10):1765-1771. doi:10.1016/J.DNAREP.2008.06.018
156. McDevitt S, Rusanov T, Kent T, Chandramouly G, Pomerantz RT. How RNA transcripts coordinate DNA recombination and repair. *Nat Commun*. 2018;9(1). doi:10.1038/s41467-018-03483-7
157. Hegazy YA, Fernando CM, Tran EJ. The balancing act of R-loop biology: The good, the bad, and the ugly. *J Biol Chem*. 2020;295(4):905-913. doi:10.1016/s0021-9258(17)49903-0
158. Li L, Germain DR, Poon H-Y, et al. DEAD Box 1 Facilitates Removal of RNA and Homologous Recombination at DNA Double-Strand Breaks. *Mol Cell Biol*. 2016;36(22):2794-2810. doi:10.1128/MCB.00415-16
159. Michelini F, Pitchiaya S, Vitelli V, et al. Damage-induced lncRNAs control the DNA damage response through interaction with DDRNAs at individual double-strand breaks. *Nat Cell Biol*. 2017;19(12):1400-1411. doi:10.1038/ncb3643
160. Bader AS, Bushell M. DNA:RNA hybrids form at DNA double-strand breaks in transcriptionally active loci. *Cell Death Dis*. 2020;11(4):1-7. doi:10.1038/s41419-020-2464-6
161. D'Alessandro G, d'Adda di Fagagna F. Transcription and DNA Damage: Holding Hands or

Crossing Swords? *J Mol Biol*. 2017;429(21):3215-3229. doi:10.1016/j.jmb.2016.11.002

162. Sharma S, Anand R, Zhang X, et al. MRE11-RAD50-NBS1 Complex Is Sufficient to Promote Transcription by RNA Polymerase II at Double-Strand Breaks by Melting DNA Ends. *Cell Rep*. 2021;34(1). doi:10.1016/j.celrep.2020.108565
163. Pessina F, Giavazzi F, Yin Y, et al. Functional transcription promoters at DNA double-strand breaks mediate RNA-driven phase separation of damage-response factors. *Nat Cell Biol*. 2019;21(10):1286-1299. doi:10.1038/s41556-019-0392-4
164. Jang Y, Elsayed Z, Eki R, et al. Intrinsically disordered protein RBM14 plays a role in generation of RNA:DNA hybrids at double-strand break sites. *Proc Natl Acad Sci U S A*. 2020;117(10):5329-5338. doi:10.1073/pnas.1913280117
165. Mazina OM, Keskin H, Hanamshet K, Storici F, Mazin A V. Rad52 Inverse Strand Exchange Drives RNA-Templated DNA Double-Strand Break Repair. *Mol Cell*. 2017;67(1):19-29.e3. doi:10.1016/j.molcel.2017.05.019
166. Mirman Z, Sasi NK, King A, Chapman JR, de Lange T. 53BP1–shieldin-dependent DSB processing in BRCA1-deficient cells requires CST–Polα–primase fill-in synthesis. *Nat Cell Biol*. 2022;24(1):51-61. doi:10.1038/s41556-021-00812-9
167. Mirman Z, Lottersberger F, Takai H, et al. 53BP1–RIF1–shieldin counteracts DSB resection through CST- and Polα-dependent fill-in. *Nature*. 2018;560(7716):112-116. doi:10.1038/s41586-018-0324-7
168. Casteel DE, Zhuang S, Zeng Y, et al. A DNA polymerase-α·primase cofactor with homology to replication protein A-32 regulates DNA replication in mammalian cells. *J Biol Chem*. 2009;284(9):5807-5818. doi:10.1074/jbc.M807593200

7 Appendix

7.1 Curriculum Vitae

PERSONAL INFORMATION

Name: Na Wei
Place of birth: Zhejiang, China
Nationality: Chinese

EDUCATION

04.2017 - 08.2022 Doctor of Philosophy, Radiation Biology and DNA Repair
Department of Biology, Technical University of Darmstadt, Germany
Thesis title: RNA involvement during non-homologous end joining of resected DNA double-strand breaks in G1
Supervisor: Prof. Dr. Markus Löbrich

08.2011 - 07.2012 Master of Science in Biomedical Engineering
School of Chemical and Biomedical Engineering
Nanyang Technical University, Singapore
Thesis title: Injectable formulation of a novel anti-breast cancer drug, acetyltanshinone IIA (ATA)
Supervisor: Prof. Kathy Qian Luo

09.2005 - 06.2009 Bachelor of Science in Biology,
Department of Life Science, Zhejiang Chinese Medical University, China
Thesis title: Anti-angiogenic effects of curcumin *in vitro* and *in vivo*
Supervisor: Prof. Zhishan Ding

09.2001 - 07.2004 Hangzhou No.4 High School, Zhejiang, China

AFFILIATION

10.2020 - 08.2022	Fellow, DFG-founded SFB 1361: Regulation of DNA Repair & Genome Stability at the Technical University of Darmstadt
04.2017 - 09.2020	Fellow, DFG-funded Graduate School (GrK) 1657: Molecular and Cellular Responses to Ionizing Radiation at the Technical University of Darmstadt

RESEARCH AND JOB EXPERIENCES

08.2014 - 03.2017	Research Associate Nanyang Technological University School of Chemical and Biomedical Engineering
07.2012 - 07.2014	Project Officer Nanyang Technological University, School of Chemical and Biomedical Engineering

POSTER PRESENTATIONS

- Na Wei, Marta Llorens Agost and Markus Löbrich. RNA involvement during non-homologous end joining of resected DNA double-strand breaks in G1. DGDR-Krupp 2022 Symposium on DNA Repair and Human Disease, April 2022, Jena, Germany.
- Na Wei, Marta Llorens Agost and Markus Löbrich. RNA involvement during non-homologous end joining of resected DNA double-strand breaks in G1. 5th German-French DNA Repair Meeting, November 2020, online.
- Na Wei, Marta Llorens Agost and Markus Löbrich. Mammalian RAD52 promotes RNA-mediated c-NHEJ of resected DNA double-strand breaks in G1. CNRS - Conférences Jacques Monod: Genome instability: when RNA meets chromatin, September 2019, Roscoff, France.
- Na Wei, Marta Llorens Agost and Markus Löbrich. Human RAD52 is involved in RNA-mediated DNA double-strand break repair in G1 phase. EMBO Workshop: RNA and genome maintenance: Cooperation and conflict management, October 2018, Mainz, Germany.

PUBLICATIONS

- Luo M, Fu AF, Wu R, Wei N, Song K, Lim S and Luo KQ (2022) High Expression of G6PD Increases Doxorubicin Resistance in Triple Negative Breast Cancer Cells by Maintaining GSH Level. Int. J. Biol. Sci. DOI: 10.7150/ijbs.65555
- Huang B, Yip WK, Wei N and Luo KQ (2020) Acetyltanshinone IIA is more potent than lapatinib in inhibiting cell growth and degrading HER2 protein in drug-resistant HER2-positive breast cancer cells. Cancer Lett. DOI: 10.1016/j.canlet.2020.06.010
- Wang Q, Luo M, Wei N, Chang A and Luo KQ (2019) Development of a Liposomal Formulation of Acetyltanshinone IIA for Breast Cancer Therapy. Mol. Pharm. DOI: 10.1021/acs.molpharmaceut.9b00493
- Fu AF, Peh YM, Ngan W, Wei N and Luo KQ (2018) Rapid identification of anti-micrometastases drugs using integrated model systems with 2D monolayer, 3D spheroids and zebrafish xenotransplantation tumors. Biotechnol. Bioeng. DOI: 10.1002/bit.26816
- Chiew GGY, Wei N, Sultania S, Lim S and Luo KQ (2017) Bioengineered three-dimensional co-culture of cancer cells and endothelial cells: A model system for dual analysis of tumor growth and angiogenesis. Biotechnol. Bioeng. DOI: 10.1002/bit.26297
- Wang Q, Wei N, Liu XF and Luo KQ (2017). Enhancement of the bioavailability of a novel anticancer compound (acetyltanshinone IIA) by encapsulation within mPEG-PLGA nanoparticles: a study of formulation optimization, toxicity, and pharmacokinetics. Oncotarget, DOI: 10.18632/oncotarget.14481.
- Qiu YB, Taichi M, Wei N, Yang H, Luo KQ and Tam JP (2016). An orally active bradykinin B1 receptor antagonist engineered as a bifunctional chimera of sunflower trypsin inhibitor. J. Med. Chem, DOI: 10.1021/acs.jmedchem.6b01011.
- Zhu HJ*, Fang Y*, Zhen X*, Wei N, Gao Y, Luo KQ, Xu CJ, Duan HW, Ding D*, Chen P* and Pu KY* (2016). Multilayered semiconducting polymer nanoparticles with enhanced NIR fluorescence for molecular imaging in cells, zebrafish and mice. Chemical Science, DOI: 10.1039/c6sc01251e. (*equal contribution)
- Fu AF, Ma SJ, Wei N, Tan BXX, Tan EY and Luo KQ (2016). High expression of MnSOD promotes survival of circulating breast cancer cells and increases their resistance to doxorubicin. Oncotarget. DOI: 10.18632/oncotarget.10360.

7.2 Acknowledgment

First and foremost, I would like to express my sincere gratitude to my principal supervisor Prof. Dr. Markus Löbrich, who gave me this great opportunity to conduct my PhD research, and provides me substantial support, insightful advice and continuous encouragement over these years. I would also like to appreciate my second supervisor, Prof. Dr. Alexander Löwer, for constant support and advice. Many thanks to Prof. Dr. Cristina Cardoso and Prof. Dr. Burkhard Jakob for being part of my examination committee. In addition, I would thank Prof. Dr. Cristina Cardoso for providing me many important equipment to continue my research work under the exceptional and global pandemic of COVID-19. My gratitude extends to all members of GrK 1657 for insightful discussions and good times during retreats and meetings. Special thanks to Ksenia Kolobynina, who provided me a lot of technical supports for the cell sorter.

I would like to thank all my colleagues in the AG Löbrich's group for helping me to grow more professionally and change my life. I am very thankful for Dr. Marta Llorens Agost and Dr. Ivana Josipovic who gave me lots of supervisions and discussions for my experiments, and insightful scientific comments. I would like to thank all excellent technicians in our lab (Ratna Nuria Weimer, Cornelia Schmidt, Christel Braun, Bettina Basso and Claudia Kastenholz) for giving me substantial technical supports throughout these years. Many thanks to all members in our lab for constantly motivating me to fulfill this work.

I would like to express my sincere appreciation to Dr. Marta Llorens Agost and Dr. Michael Ensminger for spending time to proofread and revise my thesis.

Last but not the least, my deepest appreciation and gratitude goes to all my friends: Geraldine Chiew, Fu Afu, Luo Man, Wang Qi, Ren Yanjun and everyone else who is always there for me. Your incredible help and encouragement made me more confident to start my PhD research and motivated me to reach the end. Without you, all this was impossible and just a dream.